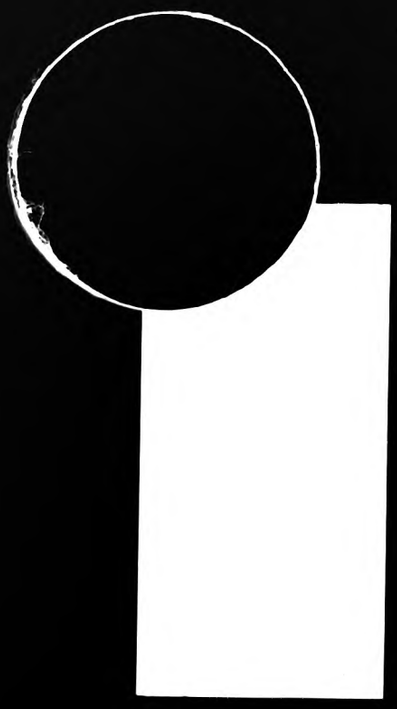

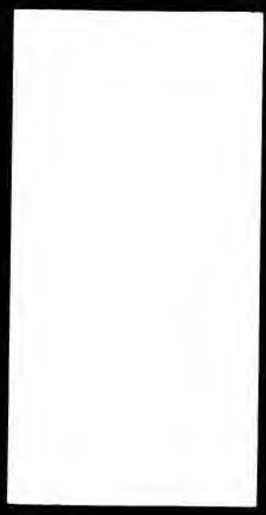

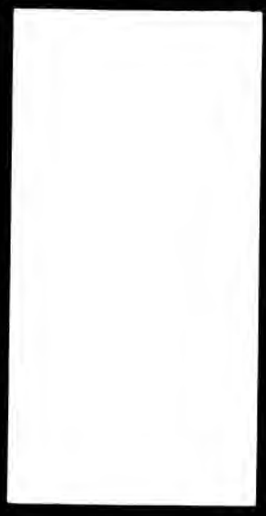

NUCLEAR MAGNETIC RESONANCE STUDIES OF ORGANOTIN AND RELATED SPECIES

A Thesis submitted to the Council for National Academic Awards in Partial Fulfilment of the Requirements for the Degree of Doctor of Philosophy

by

Nicholas Huw Rees, B.Sc.

Department of Chemistry,
Sir John Cass Faculty of Science and Technology,
City of London Polytechnic,
31 Jewry Street,
London EC3N 2EY.

NOVEMBER 1988.

ABSTRACT

Nuclear Magnetic Resonance Studies Of Organtin and Related Species

N. H. Rees

A selection of transition metal complexes including ligands of the type $R_3X_{n-3}M$ (X = halide: M = Sn,Pb: n = 0-3) were prepared and studied using multinuclear N.M.R. spectroscopy. The work concentrated on the signs of spin-spin coupling constants, and the techniques used to determine these were multiple resonance experiments of the type X-(Y,H) where X and Y were a wide range of magnetically active nuclei. In particular cases these experiments also yielded the magnitudes and the assignments of coupling constants. Variants in the INEPT pulse sequence were developed to overcome problems of insensitivity, and variable temperature N.M.R. was utilized in the study of fluxional molecules.

The pattern of reduced coupling constants between the magnetically active nuclei, in particular $^{119}Sn(^{117}Sn)$ and ^{207}Pb, was determined. The behaviour of these coupling constants (and their signs) is similar to that previously noted for ^{31}P in analagous transition metal-phosphine complexes. The geometrical dependance of the signs of the reduced coupling constants are discussed in terms of the dominance of the Fermi-contact mechanism. These results are tested against the predictions of both a) the Jameson and Gutowsky and b) the Pople and Santry theories of long range coupling interactions.

The signs of various coupling constants were also determined for bis-phosphine tin(IV) tetrahalide complexes. $^1K(SnP)$ and $^2K(PP)$ exhibited behaviour inconsistent with that previously observed in other tin-phosphorus and transition metal-phosphine compounds. These observations are discussed in terms of several molecular bonding models.

Acknowledgements

It is a privilege and a pleasure to be able to record my appreciation of the help and encouragement I have received throughout this study from my supervisor Professor William McFarlane, who suggested the initial line of work and who has been a constant source of guidance and inspiration ever since.

I would also like to thank Dr. I. Colquhoun for his helpful discussions on a range of topics. Dr. B. Wood for his help in recording some of the N.M.R. spectra and Lorraine Lacey for the typing of this thesis.

In addition I would like to thank the Inner London Education Authority for the award of a Research Assistantship.

Statement of Advanced Studies

The author has attended and contributed to many national and international meetings of the Royal Society of Chemistry, in particular those associated with N.M.R. spectroscopy and various aspects of group IV and transition metal chemistry. Throughout the study constant reference was made to relevant publications such as specialist Periodical Reports in Nuclear Magnetic Resonance, Journal of Magnetic Resonance etc., and the Dalton Transactions of the Journal of the Chemical Society, the Journal of Organometallic Chemistry and other journals were consulted regularly in order to keep abreast of the latest advances in chemistry in general.

CONTENTS

CHAPTER 1

INTRODUCTION

1.1 Introduction

Nuclear spin-spin coupling occurs when two neighbouring nuclei, which possess inherent angular momentum or spin, interact so that different combinations of allowed spin states differ in total energy.

Spin-spin coupling provides an important source of information about the nature of the bonding in molecules. Although chemical shifts show how many inequivalent chemical sites there are in a molecule; from spin-spin coupling data the sequence of atoms can often be deduced. A spin-spin coupling interaction generally indicates that the nuclei involved are connected via a number of chemical bonds. Empirical correlations have been established to show that certain orientations of bonds between two coupled nuclei lead to coupling constants of distinctive magnitude and sign. The phenomenon of spin-spin coupling is observed in N.M.R. spectra as line splittings. Depending on the natural abundance of the nuclei involved, the splitting patterns due to spin-spin coupling are an indication of the number of nuclei which occupy equivalent sites in a molecule.

Besides providing an insight into molecular structure, the way in which spin-spin coupling constants and splitting patterns vary with temperature can be used to study molecular dynamics. Also the effects of other changes in the molecular environment e.g. solvent polarity are often reflected by allied changes in the coupling constants and splitting patterns.

Finally spin-spin coupling constants, as an indicator of electronic distribution, provide a test for quantitative theories of chemical bonding and a barometer for changes in atomic hybridization and

effective nuclear charge. It is this aspect which is the prime concern of the present thesis.

The dominant mechanism is dipole-dipole coupling where the nuclear spins interact directly "through space". In isotropic fluids however, this is averaged to zero by rapid molecular motion reorientating the internuclear axes. There then remains a small isotropic interaction between the nuclear spins, which is transmitted via the (mainly valence) electrons of the molecule. The first nucleus perturbs the electrons and these in turn affect the magnetic field at the second nucleus. Spin-spin coupling constants can therefore be used to study the behaviour of bonding electrons.

The energy of the interaction is given by the equation.

$$E_{AB} = hJ_{AB}\, I_A \cdot I_B \qquad (1.1)$$

where J_{AB} is the spin-spin coupling constant between nucleus A and B, h is Planck's constant and I is the nuclear spin angular momentum. If the lowest energy configuration has the nuclear spins anti-parallel (i.e. the scalar product $I_A \cdot I_B$ is negative) to give a negative value of E_{AB}, J_{AB} must be positive.

The Dirac Vector model gives the simplest representation of a spin-spin coupling interaction. The nucleus-electron interactions in the HT molecule provide a basic example.

FIG. 1.1

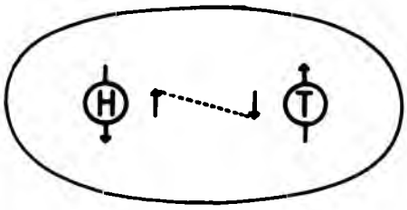

In FIG 1.I one electron is close to the proton, it being probable that the other will be close to the triton. The most stable configuration, given the Fermi contact interaction (see later), will be that in which the hydrogen nucleus and adjacent electron have anti-parallel spins. According to the Pauli exclusion principle, the two electrons in the molecular orbital will have opposite spins. Due to the Fermi-contact interaction, the tritium nucleus and its associated electron will also tend to have anti-parallel spins. Therefore the lowest energy configuration is where the nuclear spins are anti-parallel. The Dirac Vector model therefore predicts that all one bond coupling constants for nuclei with positive magnetogyric ratios are positive. The predictions of this simple model do not hold true for every case, as one bond coupling constants of negative sign are known.[1,2]

A complete general theory of coupling interactions was first given by Ramsey[3]. The theory shows that indirect spin-spin coupling, as seen in the high resolution N.M.R. of isotropic non-viscous fluids, is due to three types of nucleus-electron interaction:-

1) An interaction between the nuclear magnetic moment and the magnetic field produced by the orbital motion of the electrons (The Orbital Term).

2) The interaction between the nuclear magnetic moment and the spin magnetic moment of an extranuclear electron (The Spin-Dipolar Term).

3) The interaction between the spin magnetic moments of the nucleus and an electron in the region of the nucleus. This is similar to the spin-dipolar term, except it concerns the finite electron density in the region of the nucleus (The Fermi-Contact Term).

Theoretical expressions for all three contributions include a term $\gamma_X \gamma_Y$ (γ is the magnetogyric ratio and X and Y denote the coupled nuclei). γ can be either positive or negative depending on the nucleus. Hence $\gamma_X \gamma_Y$ can make a positive or negative contribution to the coupling constant. Pople and Santry[4] defined a reduced coupling constant K, which removes this term leaving the part due to the electronic environment of the coupled nuclei.

$$K_{(XY)} = \frac{4\pi}{h \gamma_X \gamma_Y} J_{(XY)} \qquad (1.2)$$

(Since $K_{(XY)}$ and $J_{(XY)}$ may be of different signs it should be noted that, in double resonance experiments to compare the signs of coupling constants, the relative signs of the K's are obtained. This is important for several nuclei dealt with in this thesis).

Pople and Santry[4] considered the three above contributions in terms of molecular orbital theory for coupling involving elements of the first row of the periodic table. They showed that generally the Fermi-Contact term makes the dominant contribution to the spin-spin coupling. The orbital term makes no contribution, except where π-bonding is involved. The orbital and spin-dipolar terms are both proportional to a term involving a combination of 2p bond orders and the product $\langle r^{-3}\rangle_A \langle r^{-3}\rangle_B$, where $\langle r^{-3}\rangle_A$ is the mean inverse cube of the nucleus-electron distance for a 2p orbital on atom A. Evaluation of these terms showed them to be negligible compared to the Fermi-contact term. A possible exception to this could be the molecule F_2, where the large value of $\langle r^{-3}\rangle_p$ may lead to a more significant contribution from the spin-dipolar term. Except in cases where multiple bonding is involved and for couplings involving fluorine, where the orbital and spin-dipolar

contributions can become significant, Pople and Santry's conclusion that the Fermi-contact term is dominant is usually assumed to apply even when heavier nuclei are involved.

Given the dominance of the Fermi-contact term and neglecting the other terms, the reduced coupling constant can be expressed as:-

$$K_{(XY)} = \frac{64\pi^2\beta^2}{9} \left|\Psi_{ns,X}(0)\right|^2 \left|\Psi_{ns,Y}(0)\right|^2 \Pi_{XY} \qquad (1.3)$$

where β is the Bohr magneton, $\left|\Psi_{ns,X}(0)\right|^2$ is the s electron density at the nucleus X for the ns valence orbital, and Π_{XY} is the mutual polarisability of the ns X and Y orbitals and is defined as:-

$$\Pi_{XY} = -4 \sum_{i}^{occ} \sum_{j}^{unocc} \frac{C_{is,X} C_{is,Y} C_{js,X} C_{js,Y}}{(E_j - E_i)} \qquad (1.4)$$

where $C_{s(X)}$ are the L.C.A.O. coefficients of the s type orbitals centered on X for molecular orbitals and $(E_j - E_i)$ is the triplet excitation energy from the i th occupied molecular orbital to the j th unoccupied molecular orbital. The physical interpretation of the mutual polarisability is that it represents the change in electron density in s_X when the energy of s_Y is changed and vice-versa. The sign of $K_{(XY)}$ resides in the mutual polarisability, since it is the only term which can be either positive or negative. It is a summation of a number of terms and the sign of each term depends on the product of the coefficients in equation (1.4).

For the isoelectronic tetrahedral species BH_4^-, CH_4, NH_4^+ only one excitation contributes to K. The product of the coefficients is positive and therefore $^1K_{(XH)}$ is predicted to be positive, increasing in value from B to N in line with the increasing s-electron densities at the nuclei for the valence shell atomic orbitals. For the molecule HF two excitations contribute to K. They are of opposite sign and given

that the energy difference between s and p orbitals is large, the negative term dominates Π_{FH} (it has a smaller excitation energy). Therefore $^1K_{(HF)}$ is predicted to be negative. With nuclei such as phosphorus the energy of the 3s orbital is such that $^1K(PC)$ and $^1K(PP)$ can be positive or negative.

An alternative approach to the rationalization of trends in the signs of coupling constants of directly bonded nuclei across the periodic table, is that of Jameson and Gutowsky[5]. They proposed, given the dominance of the Fermi-contact interaction, that the reduced coupling constant between two directly bonded nuclei, X and Y, could be represented by the product of the nucleus-electron contact interactions.

$$K_{(XY)} \propto S_X \, S_Y \qquad (1.5)$$

The sign of $K_{(XY)}$ is positive if both S_X and S_y are of the same sign, and negative if S_X and S_y have different signs. S_X and S_y are made up of two parts.

$$S_X = S_X(s) + S_X(\text{core pol}) \qquad (1.6)$$

where $S_X(s)$ is the direct Fermi-contact term caused by s-electron density of the bonding electrons at the nucleus. The second term is caused by spin polarisation of core s-electrons by an electron in a bonding orbital. $S_X(s)$ is positive and is the dominant term, if the atom employs orbitals with an appreciable s-character in bonding (e.g. carbon). In cases where orbitals of high p-character are used in bonding (e.g. fluorine) it is suggested that S_X (core pol) is dominant. In the case of fluorine S_p (core pol) is negative leading to an overall negative S_p. Jameson and Gutowsky suggest there is a change over between the two cases somewhere in the region of Group V and VI. For a nucleus such as phosphorus in an intermediate group, S_p may take either sign depending on such factors as the hybridization state (P^{III} or P^{V})

and the electronegativity of the elements to which it is bound. For example $^1K(PH)$ is invariably positive (P^{III} or P^V), whereas $^1K(PC)$ can be negative (P^{III}) or positive (P^V).[1]

An exception to the above rationalization is $Me_2P\text{-}PMe_2$ ($^1J(^{31}P^{31}P)$ = -179.7Hz) which has[2] a negative $^1K(PP)$. In this case S_p must be the same for both phosphorus nuclei in the molecule, and this would lead to a positive $^1K(PP)$, irrespective of the relative importance of $S_p(X)$ and S_X (core pol). In general the approach of Pople and Santry is used when rationalizing coupling constants of directly bonded nuclei[6], rather than that of Jameson and Gutowsky.

It is possible to simplify equation (1.4) by using an average energy approximation to remove the difficulties associated with the calculation of individual excitation energies. By assuming constant values of singlet excitation energies an average excitation energy ΔE, is introduced and Π_{XY} is replaced by

$$\Pi_{XY} = \Delta E^{-1} \; P^2_{S(X)\,S(Y)} \qquad (1.7)$$

where $P^2_{S(X)S(Y)}$ is the S(X) - S(Y) bond order. This corresponds to an earlier derivation by McConnell[7], and leads to values of $K_{(XY)}$ which are always positive and are linearly related to the s-character of the hybrid orbitals used by X and Y in bonding. General application of this simplification is not justified, since Π_{XY} may be positive or negative, but in a number of cases, such as for BH_4^-, CH_4, NH_4^+, it can be used to predict certain trends in the coupling constants.

1.2 Factors Affecting Spin-Spin Coupling Between Directly Bound Nuclei

1. Hybridisation

Although it is not generally valid to make the average energy approximation, the modified version of equation (1.3) shows the important influence of hybridization on coupling

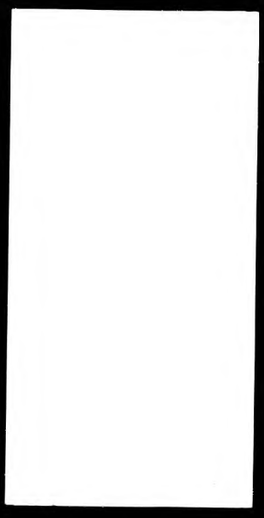

$$K_{(XY)} = \frac{64\pi^2 \beta^2}{9} \left|\Psi_{ns,X}(0)\right|^2 \left|\Psi_{ns,Y}(0)\right|^2 \Delta E^{-1} \alpha^2_X \alpha^2_Y \qquad (1.8)$$

$P^2_{S(X)\,S(Y)}$ has been replaced by $s^2_X \alpha^2_Y$ where α^2_X is the s-character of the hybrid orbital used by X in the X-Y bond, to emphasise the dependence on the s-character of the σ-bond between the nuclei, and therefore upon the hybridization. This is illustrated by values of $^1J(^{13}C^1H)$ and $^1J(^{119}Sn^{13}C)$ given in table 1.1 (N.B. $\gamma(^{119}Sn)$ is negative which accounts for the negative sign of $^1J(^{119}Sn^{13}C)$ in this table).

Table 1.1

Dependence of $^1J(^{13}CX)$ on Hybridization

Molecule	Hybridization	α^2C	X	$^1J(^{13}CX)$/Hz
Ethane	sp^3	1/4	^1H	124.9 (a)
Ethene	sp^2	1/3	^1H	156.4 (a)
Ethyne	sp	1/2	^1H	248.7 (a)
$H_3C\text{-}SnBr_3$	sp^3	1/4	^{119}Sn	-640.0 (b)
$HC{\equiv}C\text{-}SnBr_3$	sp	1/2	^{119}Sn	-1290.0 (b)

a) From ref. 8. b) from ref. 9.

The predictions of equations such as (1.8) are less successful where one or both nuclei have lone-pairs of electrons with appreciable s-character.

The s-character of a molecular orbital can be affected by changes in the hybridization of one of the atoms. If a substituent on an atom X is replaced by a more electronegative one, the hybridization of X is altered so that the orbital directed towards the substituent contains more p-character. This concentrates electron density at a greater distance from X (i.e. nearer to the substituent). This produces an increase in the s-character of orbitals directed towards the other

substituents (a lone pair will occupy an orbital of higher s-character), and therefore a variation in a^2_X. The electronic screening of atom X will also be affected by the electronegativity of its substituents. An increase in their electronegativity reduces the electron density around X, leading to a reduction in screening, giving an increase in the effective nuclear charge on X. This in turn leads to an increase in $|\Psi_{n,a_X}(0)|^2$. Both these effects act in the same direction, producing an increase in the coupling constant. Since it is not possible to tell which effect dominates, s-characters cannot be reliably derived from coupling constants except in special circumstances.

The hybridization of X is also altered by increasing the bulk of its substituents. This tends to increase the interbond angles between the substituents, which means that the bonds to the bulkier substituents will contain more s-character. The remaining bonds will have a reduced proportion of s-character.

To summarise, an increase in the electronegativity of substituents on X, will increase the s-orbital contribution from X to the X-Y bonding molecular orbital (a^2_X) and the s-electron density at the nucleus ($|\Psi_{ns,X}(0)|^2$); the net result being an increase in the coupling constant. Placing bulkier substituents on X will reduce the s-orbital contribution (a^2_X) to the X-Y coupling constant decreasing the coupling constant.

1.3 Coupling Constants Between Nuclei Over Two Or More Bonds.

When coupling constants $^2J(XMY)$, where another atom intervenes between the coupled nuclei are considered, the nature of the intervening atom (M) and the bond angle X-M-Y must be taken into consideration as well. This increase in the number of variables makes quantitative rationalization of trends very difficult.

The Dirac Vector model can be extended to cover coupling over two or more bonds, e.g. in the molecule HOT shown in FIG. 1.II.

FIG. 1.II

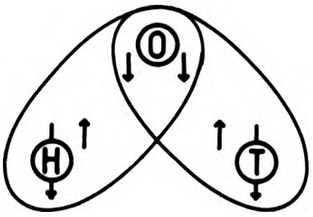

The same considerations apply to the electron-nucleus (Fermi-contact) and electron-electron (Pauli principle) interactions, in each two-electron molecular orbital. Where another atom intervenes, the interactions between electrons in different orbitals, in the region of the intervening nuclei must be considered. Hund's rule states that such electrons should have parallel spins, implying overall a negative coupling constant. By extending this argument it predicts that the sign of the reduced coupling constant will alternate as the number of bonds separating the coupled nuclei is increased. Since there must be a Hund-type interaction at each intervening atom for transmission of spin information, a rapid attenuation in the magnitude of J is predicted as the number of bonds separating the coupled nuclei increases. $^2J(^1H^1H)$ is indeed negative for CH_2 groups with an sp^3 hybridized carbon atom, but there are many compounds in which two-bond couplings are positive[10].

An attempt to account for geminal coupling constants was introduced by Jameson[11] as an extension of the rationale proposed for coupling between directly bonded nuclei by Jameson and Gutowsky[5], which was discussed earlier. The geminal coupling is considered in terms of the contact interaction, dividing the contributions to $^2K(XMY)$ into three parts. These describe the nature of the X-M bond (S_X) and the M-Y (S_Y)

bond with respect to transfer of nuclear spin information between the X nucleus and the Y nucleus. These are similar to the terms in equation (1.5). The third term F_{XMY}, is a function of one- and two-centre integrals, describing the transfer of electron spin information from the X bonding orbital in the X-M bond to the Y bonding orbital in the M-Y bond. These are related to the reduced coupling constant by:

$$^{2}K_{(XMY)} \propto S_X S_Y F_{XMY} \qquad (1.9)$$

Since S_X and S_Y represent interactions corresponding to coupling of directly bonded nuclei, the sign of $^{2}K_{(XMY)}$ can be predicted if the sign of F_{XMY} is known. In many cases it would appear that F_{XMY} is negative when the X-M-Y bond angle is between 90° and 110°. For tetrahedrally hybridized carbon $^{2}K_{(XCH)}$ is negative for X = H, C, Si, Sn, Pb, Cd, Hg, and also for X = $P^{(V)}$, the signs of S_X and S_H being positive, and in $(Me_3Sn)_3CH$, $^{2}K(SnSn)$ is negative[12], $^{1}K(SnC)$ being positive[13]. Exceptions to this may be found if X has an electron lone pair, e.g. $P^{(III)}$.

1.4 Factors Affecting Spin-Spin Coupling Between Nuclei Separated By Three Or More Bonds.

1. Dihedral angle Dependence

In saturated X-C-C-Y fragments the value of $^{3}J(XY)$ depends critically upon the dihedral angle ϕ, shown in Fig. 1.III.

FIG. 1.III

This dependence primarily results from variations in the interaction of

C-X and C-Y orbitals as the dihedral angle is changed[13]. This is described adequately by a Karplus equation of the general form:-

$$^{3}J(XY) = A \cos 2\phi + B \cos \phi + C \qquad (1.10)$$

where A,B and C are empirical constants, generally B is negative and $|A| > |B|$. Where X and Y are protons, A, B and C have the approximate values 4.0 Hz, -0.5 Hz and 4.5 Hz respectively. Fig. 1.IV shows the Karplus curve relating ϕ to $^{3}J(^{1}H^{1}H)$.

FIG. 1.IV

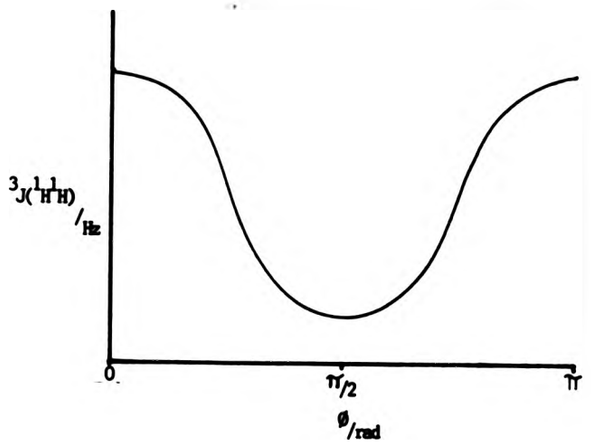

There are dangers in using this approach, since the Karplus model is only valid in the absence of electronegative substituents and departure from tetrahedral angles at carbon. The relative lack of data about three-bond coupling constants other than $^{3}J(^{1}H^{1}H)$ makes it difficult to prove the applicability of Karplus-type relationships. Therefore Karplus type equations are not general for nuclei other than hydrogen, although they have been developed for several other sets of nuclei including $^{3}J(^{31}P^{1}H)$, $^{3}J(^{31}P^{13}C)$[14], $^{3}J(^{13}C^{119}Sn)$[9] and $^{3}J(^{119}Sn^{2}D)$[15], and have been postulated for $^{3}J(^{119}Sn^{119}Sn)$[16].

2) Long Range Coupling

The term "long range" coupling is applied when the coupled nuclei are separated by more than three chemical bonds. In saturated compounds long range proton-proton coupling constants are generally small (often negligible) and often highly stereospecific. The optimum path for such coupling appears to be a planer zig-zag chain, see Fig. 1.V.

FIG. 1.V

e.g.

	positions of protons	J / Hz
$^4J(^1H^1H)$	2-equatorial-4 equatorial	1.0
	2-equatorial-4 axial	0.45
$^5J(^1H^1H)$	2-equatorial-5 equatorial	0.9
	2-equatorial-5 axial	< 0.3

$^4J(^1H^1H)$ two types of coupling paths should be considered (see FIG. 1.VI).

FIG. 1.VI

a)

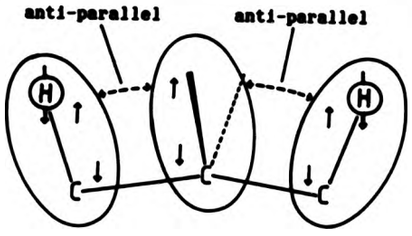

b)

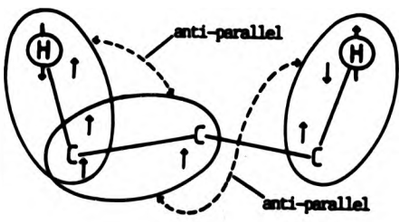

They may be described in terms of spin correlation between electrons in different bonds. Path a) consists of two vicinal orbital interactions, as in the description of the dihedral angle dependance, and leads to a negative contribution to $^4J(^1H^1H)$. Path b) consists of a geminal orbital interaction (see FIG. 1.II) and a vicinal orbital interaction leading to a positive contribution to $^4J(^1H^1H)$ which may be of either sign; path b) dominates for the zig-zag chain configuration giving a positive sign and maximum magnitude.

3) Coupling via Π-electrons

Π-electrons may be involved in nuclear spin-spin coupling in unsaturated systems. The observed coupling constant can be written as the sum of two parts J^{π} and J^{σ}. Since the Π-electron distributions have nodes at the nuclei they cannot contribute to the contact term. It is therefore necessary to introduce spin correlation between Π and σ electrons. This same interaction accounts for hyperfine coupling between protons and unpaired electrons in the E.S.R. of related free radicals. Three types of σ-Π exchange repulsion have to be considered.

a) Acetylenic - the σ electron on H is stabilized in the anti-parallel orientation to the Π-electron on C for a H-C≡ group.

b) Ethylenic - the anti-parallel orientation is stabilized for a  group.

c) Allylic - in this case the parallel orientation is stabilized.

For the case of propene (FIG. 1.VII), both allylic (c) and ethylenic (b) interactions must be considered and $^4J(^1H^1H)$ is predicted to be negative.

FIG. 1.VII

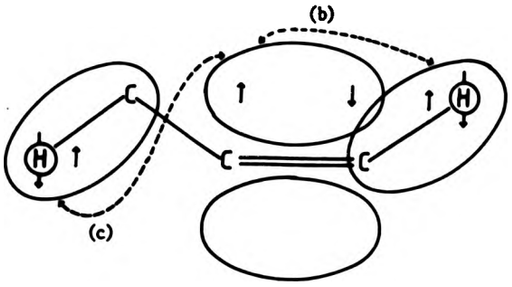

Since Π-electron systems are often delocalized, spin correlation may occur for electrons at atoms separated by many chemical bonds, making coupling via Π-electrons important in long range coupling. This is shown by the compound $CH_3C{\equiv}CC{\equiv}CC{\equiv}CCH_2OH$ which has a coupling over nine bonds of $^9J(^1H^1H) = 0.4$ Hz. Although 0.4 Hz is a small coupling, it is large when one considers that nine chemical bonds separate the coupled nuclei. Coupling via Π-electrons may be important for nuclei other than protons. Analogues have been drawn between $^5J(^1H^1H)$ in allenes and $^5J(^{119}Sn^1H)$ and $^5J(^{119}Sn^{119}Sn)$ in allenyl stannanes[17]. It has also been used to account for large values of $^4J(^{119}Sn^{13}C)$ in unsaturated species.[18]

4) Through-space coupling

This is most often invoked to account for (F,F) interactions where the nuclei are formally separated by several bonds. A semi-empirical approach is taken which best describes (H,H) interactions of this type.

$$K_{(AB)} = \text{constant} \propto s_A^2(0)\, s_B^2(0)\, (S_{SASB})^2 \qquad (1.11)$$

where S_{SASB} is the overlap integral between valence s orbitals of atoms A and B and the constant is determined experimentally[19]. For (F, F) interactions the through space contributions depend on the overlap of

lone pair p-orbitals[20]. There is little or no evidence for this type of mechanism involving tin[21] or other group IV elements, although it is quite likely that through-space Sn-F coupling could be important in certain situations.

The theoretical discussion of nuclear spin-spin coupling given in this chapter applies primarily to coupling interactions between lighter elements such as ^{1}H and ^{13}C, which belong to the first row of the periodic table. Although there is little theoretical and limited experimental evidence it is generally assumed that the Fermi-contact mechanism also dominates the spin-spin coupling of heavier elements and that many of the other factors discussed earlier may also apply. This is the approach that has been taken in this thesis. However for heavier elements relativistic effects become significant and it has been pointed out that the relativistic analogue of Ramsey's theory should be used[22]. In this situation it is useful to know the signs of coupling constants involving heavier elements, and in the case of this thesis the signs of various couplings, principally involving tin have been investigated.

1.5 Coupling Constants $^{n}J(MY)$ (M = ^{119}Sn, ^{207}Pb; Y = other magnetic nucleus; n ≥ 1)

In this review emphasis has been given to two-bond and longer-range couplings, as well as to couplings which involve nuclei other than ^{1}H and ^{13}C, except in the case of many-bond couplings which have novel intervening atoms.

A greater volume of information exists for ^{119}Sn compared to ^{207}Pb spin-spin coupling constants. This is reflected in the previous reviews of tin[9,23-29] and lead[28,29] N.M.R. and in the reports of spin-spin coupling constants given in Specialist Periodical Reports on N.M.R.[30] Of

these the review of ^{119}Sn-NMR parameters by Wrackmeyer[9] gives the most comprehensive coverage of ^{119}Sn coupling constants and as such forms a general starting point for the ^{119}Sn part of this review.

One-Bond Couplings

One-bond coupling constants are probably the best understood due to the absence of intervening atoms and have therefore generated the most interest concerning the theoretical prediction and experimental determination of their absolute signs. Both Kennedy and McFarlane,[29] and Jameson[31] have tabulated the known signs of group IV one-bond couplings.

In many cases the ratio $^{1}K(SnX):{}^{1}K(PbX)$ reflects the relative sizes of $\left|\Psi(0)\right|^{2}$. However this relationship breaks down for couplings to electronegative and polarisable elements where it is necessary to consider changes in the mutual polarisability, Π_{XY}.

$^{1}J(M^{1}H)$

For compounds of the type $R_{4-m}SnH_m$ (m = 1-4, R = aryl, alkyl), $^{1}J(^{119}Sn^{1}H)$ shows the expected trends concerning the number, bulk and electronegativity of R.[9,32] K(SnH) is positive for these couplings[33]. SnH_3^-, where $^{1}J(^{119}Sn^{1}H)$ = 109.4 Hz is an exception due to the electron lone-pair on tin[34].

Only two values of $^{1}J(^{207}Pb^{1}H)$ are known, one for Me_3PbH[35] (2379 Hz) and one for PbH_4 [33] (2456 Hz) which has a positive $^{1}K(PbH)$.

$^{1}J(M^{13}C)$

In general, good correlations between the coupling constant and the s-character and/or effective nuclear change of the central atom are found for $^{1}J(^{119}Sn^{13}C)$.[9,29] However the relationship with tin and carbon hybridizations can break down in unusual situations, for example in μ^{5}-C_5H_5 tin (II) compounds[9] or $R_3Sn^-Li^+$ (R = Me[36], Ph[37]). $^{1}K(SnC)$ is

generally positive [38-41] except in $Me_3Sn^-Li^+$ where $^1K(SnC)$ is negative[36] since most of the tin s-character resides in an electron lone-pair.

It would appear that $^1J(^{207}Pb^{13}C)$[40-48] generally follows the same pattern as $^1J(^{119}Sn^{13}C)$[29]. However due to the greater polarisability of lead anomalies are more likely to occur in unusual situations. For example $^1K(PbC)$ is also generally positive,[40,41,46-48] but may be negative for $K(Pb-C\equiv)$[40-44] whereas $^1K(Sn-C\equiv)$ is positive. Also $^1J(^{207}Pb^{13}C)$ is large and solvent-independant in $Ph_3Pb^-X^+$ (X = Li, K) whereas in $Ph_3Sn^-X^+$ $^1J(^{119}Sn^{13}C)$ is relatively small and solvent dependent.[37]

<u>^1J (M - M') (M' = ^{29}Si, ^{119}Sn, ^{207}Pb)</u>

Of these couplings most data is available for $^1J(^{119}Sn^{119}Sn)$[9, 50,51] (often $^1J(^{119}Sn^{117}Sn)$ is reported since this coupling can be measured where the coupled nuclei are in equivalent sites). $^1J(^{119}Sn^{119}Sn)$ generally depends on the tin hybridization when tin substituents are not bulky. In this situation $^1K(SnSn)$ is positive.[52, 53] However when the tin substituents are bulky[34] and steric hinderance becomes important or in anionic species where tin has an electron lone-pair, the tin-tin s-overlap is small and Π_{SnSn} may become negative leading to small[54] or negative[55] values of $^1K(SnSn)$.

Much larger values of $^1J(^{119}Sn^{119}Sn)$ have been reported for ditin compounds with five coordinate tin which have electronegative oxygen or sulphur atoms co-ordinated in the axial position (the geometry at tin is trigonal bipyramidal.[54,56] However smaller values of $^1J(^{119}Sn^{119}Sn)$, of the same magnitude as observed for four coordinate ditin compounds, can occur in five coordinate ditin compounds with long tin-tin bonds.[57]

$^1J(^{119}Sn^{119}Sn)$ has also been measured for a wide range of naked-metal tin cluster anions.[9,58,59] These can contain other atoms such as

Pb, Ge, Tl, Bi, Pt and Te as well as tin, and various systematic trends in $^1J(^{119}Sn^{119}Sn)$ are reported.[58]

$^1K(SnSi)$ is positive in $Me_3SnSiMe_3$[60] although very few values of $^1J(^{119}Sn^{29}Si)$ are known.[12]

Although $^1K(SnPb)$ is positive[52] in $Me_3PbSnMe_3$, its magnitude is small when compared to $^1K(SnSn)$ in $Me_3SnSnMe_3$. From this it would appear that $^1J(^{207}Pb^{119}Sn)$ is even more sensitive than $^1J(^{119}Sn^{119}Sn)$ to subtle changes in bonding. $^1J(^{207}Pb^{119}Sn)$ has also been reported for a series of naked-metal cluster anions.[9,58]

$^1K(PbPb)$ shows even more extreme behaviour than $^1K(SnPb)$. In $Me_3PbPbMe_3$, $^1K(PbPb)$, although positive, is extremely small.[61] Also a recent report shows that $^1J(^{207}Pb^{207}Pb)$ is extremely sensitive to the nature of the lead substituents and may change sign with certain phenyl and anisyl substituents.[62]

$^1J(M\ ^{11}B)$ and $^1J(M\ ^{205}Tl)$

$^1K(SnB)$ has been shown to be positive[52,60] and given the low polarity of Sn-B bond, changes in hybridization are well reflected by $^1J(^{119}Sn^{11}B)$.[9]

Besides $[(Me_3Sn)_4Tl]\ Li$[28] ($^1K(SnTl)$ positive) $^1J(^{119}Sn\ ^{205}Tl)$ has only been reported for naked-metal cluster anions.[38]

$^1K(PbB)$ is positive[52] in $Me_3PbB(NMeCH_2-)_2$ and appears to parallel $^1K(SnB)$ reflecting the change in $\left|\Psi_X(0)\right|^2$

$^1J(M\ ^{15}N)$ and $^1J(M\ ^{31}P)$

It is difficult to predict the sign of $^1K(SnN)$, for which both +ve and -ve values have been determined,[28,60,63] due to the polarisability of tin and the presence of an electron lone-pair on nitrogen. Although the available $^1J(^{119}Sn^{15}N)$ data are sparse,[9,60,63-68] changes in effective electronegativity have been used to account for $^1J(^{119}Sn^{15}N)$ in $Me_{4-n}Sn(NMePh)_n$ (n = 1-4).[63]

In contrast, the sign of $^{1}K(PbN)$ has been found to be negative [52,63] in all cases so far. This is due to the s-overlap integral S(PbN) being smaller than S(SnN), which leads to a large negative value for Π_{PbN}.[63,64] However insufficient data exists to establish any trends in $^{1}J(^{207}Pb^{15}N)$ [63-65,69-71]

In $(Me_3Sn)_nPh_{3-n}P$ (n = 1,3), $^{1}K(SnP)$ is negative.[63,72] Where the electron lone-pair on phosphorus is used in metal complexation $^{1}K(SnP)$ becomes less negative. Besides compounds of four coordinate tin (IV)[9], values of $^{1}J(^{119}Sn^{31}P)$ of unknown sign have been reported for tin (II)[9,73-76] and six coordinate tin (IV)[9,77] phosphine complexes; large values being reported for the latter.

$^{1}K(PbP)$ is also negative [52,63] in four coordinate lead (IV) compounds, though the effect of using the phosphorus in metal complexation is not reported. $^{1}J(^{207}Pb^{31}P)$ is also reported for lead (II) phosphine complexes.[73,74]

<u>$^{1}J(M^{77}Se)$ and $^{1}J(M^{125}Te)$</u>

Although the data available for these coupling constants is limited,[9,78] $^{1}K(SnSe)$ has been shown to be negative for tin (IV) compounds.[39,60,79] Variations in $^{1}J(^{119}Sn^{77}Se)$ have been accounted for by changes in effective nuclear charge.[79] $^{1}J(^{119}Sn^{77}Se)$ has been reported for a series of Zintl anions[80] of the type $SnTe_nSe_{4-n}^{4-}$ (n = 0-4) and $SnTe_nSe_{3-n}^{2-}$ (n = 0-3). Also $^{1}J(^{119}Sn^{77}Se)$ is generally smaller in cationic tin (II) than in tin (IV) compounds.

$^{1}K(SnTe)$ is also negative in tin(IV) species[39,60] and it has been demonstrated that $^{1}J(^{119}Sn^{125}Te)$ parallels $^{1}J(^{119}Sn^{77}Se)$[78]. $^{1}J(^{119}Sn^{125}Te)$ is reported for the same series of Zintl anions[80] as $^{1}J(^{119}Sn^{77}Se)$.

Only one value of $^{1}K(PbSe)$ has been reported, for $Me_3PbSeMe$ which

is negative[52].

$^{1}J(M\ ^{19}F)$

Besides substituted SnF_6^{2-} species,[9] only one value of $^{1}J(^{119}Sn^{19}F)$ for $(PhCMe_2CH_2)_3SnF$, is known. In this species $^{1}K(SnF)$ is negative[81].

$^{1}J(M\ M')$ (M' = transition metal)

These coupling constants are noted for often having very large magnitudes. The majority of values in the literature concern $^{1}J(^{119}Sn^{195}Pt)$[9], most of which are for complexes containing the Pt-$SnCl_3$ group.[9,82-86] $^{1}J(^{119}Sn^{195}Pt)$ is also reported for complexes containing organotin ligands[9,87] and for Pt-Sn-Pt complexes.[88]

The next largest data set is for $^{1}J(^{119}Sn^{103}Rh)$ which is reported for a range of Rh-$SnCl_3$ complexes.[9,89] $^{1}J(^{119}Sn^{99}Ru)$[9,90], $^{1}J(^{119}Sn^{187}Os)$[9,90], $^{1}J(^{119}Sn^{199}Hg)$[9], $^{1}J(^{119}Sn^{51}V)$[91] and $^{1}J(^{119}Sn^{183}W)$[9] have also been reported. Of all these couplings, only the sign of $^{1}K(SnW)$, which is positive[52], has been determined.

For lead only values of $^{1}J(^{195}Pt^{207}Pb)$ have been reported for organolead complexes[92,93] and naked metal cluster polyanions.[58]

Two-Bond Couplings

The same factors that determine one-bond coupling constants also apply to two-bond coupling constants. However the presence of an intervening atom introduces another source of variable which can effect their magnitude and sign.

$^{2}J(M\text{-}X\text{-}^{1}H)$

Where X is carbon, there is a wealth of data for $^{2}J(^{119}Sn\text{-}X\text{-}^{1}H)$ which is adequately dealt with elsewhere.[9,27]. Only a limited amount of information exists for $^{2}J(^{119}Sn\text{-}X\text{-}^{1}H)$ where X is any other element.

In $Me_3SnPHPh$, $^2K(Sn-P-H)$ has been found to be negative[94]. More information exists for $^2J(^{119}Sn-X-^1H)$ in transition metal complexes,[9] where X = Pt[9,29], Ir[89,95] or Rh[89]. The magnitude of $^2J(^{119}Sn^1H)$ is dependant on the geometrical relation, cis or trans, of the coupled nuclei.

$^2J(^{207}Pb-C-^1H)$ varies in a similar way to $^2J(^{119}Sn-C-^1H)$, $^1K(Pb-C-H)$ being generally negative.[46,52,63] Most values are for intervening sp^3 hybridized carbon,[29,42] though some exist for sp^2 hybridized carbon.[96].

$^2J(M-X-^{13}C)$

For $^2J(^{119}Sn-X-^{13}C)$ the majority of the data is for X = C[9,27]. Also $^2K(Sn-X-C)$ has been reported as positive for X = Sn and negative for X = N[9], and a single value has been reported for X = As.[12] A geometrical dependence has been found for $^2J(^{119}Sn-X-^{13}C)$ in some transition metal carbonyl complexes (X = transition metal, ^{13}C = $X-^{13}C{=}O$)[9,82].

Although there is less data for lead compared to tin, the vast majority of reported values of $^2J(^{207}Pb-X-^{13}C)$ are for X = C[37,42-45,49,96] A negative sign has been determined for $^2K(Pb-C{\equiv}C)$ compared to a positive sign for $^2K(Sn-C{\equiv}C)$ in analogous compounds.[49] For $Me_3PbPbMe_3$ $^2K(Pb-Pb-C)$ is positive.[46]

$^2J(M-X-M')$ (M' = ^{29}Si, ^{119}Sn, ^{207}Pb)

$^2J(^{119}Sn-X-^{119}Sn)$ covers a large range of values with a variety of intervening atoms.[9,50,51] Negative values of $^2K(Sn-X-Sn)$ have been determined for X = C[12], N and P [9] and a positive value for X = Sn [9]. Values have also been reported for X = S, O, Se, Te [9,97] and for a range of transition metals,[9,82,84,90] where $^2J(^{119}Sn^{119}Sn)$ parallels the behaviour of $^2J(^{31}P\ ^{31}P)$ in transition metal complexes.[9]

Only a few values of $^{2}J(^{119}Sn\text{-}X\text{-}^{29}Si)$ and $^{2}J(^{119}Sn\text{-}X\text{-}^{207}Pb)$ have been reported for X = C[98,111] and N.[12]

$^{2}J(^{207}Pb\text{-}X\text{-}^{29}Si)$ has been measured for $Pb[N(SiMe_3)_2]_2$[99]

$^{2}J(M\text{-}X\text{-}^{31}P)$

$^{2}J(^{119}Sn\text{-}X\text{-}^{31}P)$ has been reported with a variety of intervening atoms,[9] including X = C, O, S and a transition metal.[83-87,95] As with $^{2}J(^{119}Sn^{119}Sn)$, $^{2}J(^{119}Sn^{31}P)$ in transition metal complexes parallels the behaviour of $^{2}J(^{31}P\ ^{31}P)$.

A few values of $^{2}J(^{207}Pb\text{-}X\text{-}^{31}P)$ have been reported for compounds where X = O, S, Se[100] and in transition metal complexes where X = Pt[93] and W[101].

Other Two-Bond Couplings $^{2}J(M\text{-}X\text{-}Y)$

Two-bond couplings to other nuclei are much rarer. For tin[9] these include $^{2}J(^{119}Sn^{19}F)$ for various polyfluoroorganotin[9,21] compounds and $^{2}J(^{119}Sn\text{-}Sn\text{-}^{125}Te)$ in a tin-tellurium heterocycle.[97] Two values of $^{2}J(^{119}Sn\text{-}Pt\text{-}^{195}Pt)$ are reported for two different transition metal complexes;[9,82] one of which is remarkably large,[9] as is the reported value of $^{2}J(^{119}Sn\text{-}Ir^{199}Hg)$ in another transition metal complex.[9] $^{2}J(^{119}Sn\text{-}Pt\text{-}^{15}N)$ is also reported for a couple of square planar platinum complexes.[85]

Some values of $^{2}J(^{207}Pb^{19}F)$ are known for lead trifluorocarbon compounds.[102]

Three-Bond Couplings $^{3}J(M\text{-}X\text{-}Z\text{-}Y)$

For tin interest in three bond couplings has centered on coupling to ^{13}C, ^{1}H and to a lesser extent ^{119}Sn. As mentioned earlier a Karplus-type dependence has been claimed for $^{3}J(^{119}Sn^{13}C)$[14], $^{3}J(^{119}Sn^{2}D)$[15] and $^{3}J(^{119}Sn^{119}Sn)$[16]. A similar relationship has yet to be proved for $^{3}J(^{119}Sn^{1}H)$. Often $\left|^{3}J(^{119}Sn^{1}H)\right| > \left|^{2}J(^{119}Sn^{1}H)\right|$ and

$\left|{}^{3}J(^{119}Sn^{13}C)\right| > \left|{}^{2}J(^{119}Sn^{13}C)\right|$ where the intervening atoms are carbon. For $^{3}J(^{119}Sn^{1}H)$ examples also exist where an intervening carbon is replaced by an electropositive (e.g. Si, Sn, Pb) or an electronegative (e.g. N, S, Se) heteroatom.[9]

$^{2}J(^{119}Sn^{13}C)$ values have also been reported for systems where one or both intervening atoms are not carbon. For example $^{3}J(^{119}Sn\text{-}B\text{-}N\text{-}^{13}C)$, $^{3}J(^{119}Sn\text{-}X\text{-}Sn\text{-}^{13}C)$ X = O, S, Se, Te, C, Sn, Si,[9] and $^{3}J(^{119}Sn\text{-}Pt\text{-}Pt\text{-}^{13}C)$ where the coupled ^{13}C is a carbonyl[82].

Most of the reported values of $^{3}J(^{119}Sn^{119}Sn)$[9] are for compounds where the intervening atoms are both carbon. However a very large value of $^{3}J(^{119}Sn^{119}Sn)$ is reported for $[Pt_2(SnCl_3)_2(\mu\text{-dppm})_2]$[9] and a much smaller value for $[Pt_2(SnCl_3)_4(CO)_2]^{2-}$ [82] where the intervening atoms are two platinum atoms in both cases. Also $^{3}J(^{119}Sn^{119}Sn)$ has been reported where both intervening atoms are tin.[50,51] A positive sign has been determined for $^{3}K(Sn\text{-}N\text{-}N\text{-}Sn)$.[10]

Other $^{3}J(^{119}SnY)$ have been reported where the intervening atoms are carbon and Y = ^{31}P, ^{103} ^{11}B, ^{19}F, ^{207}Pb, ^{29}Si and ^{195}Pt.[9] $^{3}J(^{119}Sn\text{-}C\text{-}Pt\text{-}^{31}P)$ has been measured for a series platinum complexes.[104]

Three-bond lead couplings to ^{1}H and ^{13}C [42-45,96] show similar trends to tin couplings and often where the intervening atoms are carbon $\left|{}^{3}J(^{207}Pb^{1}H)\right| > \left|{}^{2}J(^{207}Pb^{1}H)\right|$ and $\left|{}^{3}J(^{207}Pb^{13}C)\right| > \left|{}^{2}J(^{207}Pb^{13}C)\right|$.[42]

As with tin, values of $^{3}J(^{207}Pb\text{-}X\text{-}C\text{-}^{1}H)$ exist where an intervening atom is other than carbon[52], where X = Pb, Sn (for which $^{3}K(PbH)$ is +ve) and X = Se, N (for which magnitudes only are reported).

For couplings to carbon $^{3}J(^{207}Pb\text{-}C\text{-}Pb\text{-}^{13}C)$ has been reported.[98]

Three-bond couplings between lead and other nuclei are extremely rare. $^{3}J(^{207}Pb\text{-}Pb\text{-}Pt\text{-}^{31}P)$ in <u>cis</u>-$[Pt(Ph)(PPh_3)_2(PbPh_2PbPh_3)]$ has observed for the phosphorus <u>trans</u> to the organolead ligand.[93]

Four-Bond and Longer Range Couplings

It is occasionally possible to observe very large range couplings for tin and lead.

Besides a few values of long range couplings to ^{1}H and ^{13}C from ^{119}Sn[9,51] and ^{207}Pb[43-45], four,[105,106] five,[17,107,108] six[107] and seven[107] bond $^{n}J(^{119}Sn^{119}Sn)$ have been reported. Couplings to other nuclei include four[21] and five [21,108] bond $^{n}J(^{119}Sn^{19}F)$ and $^{4}J(^{119}Sn^{31}P)$[109] and $^{5}J(^{119}Sn^{29}Si)$.[101]

For lead four[111,112] and five [112,113] bond $^{n}J(^{207}Pb^{19}F)$ have been observed.

1.6 REFERENCES

1) W. McFarlane, Chem. Comm., 58, (1967).

2) E. G. Finer, R. K. Harris, Mol. Phys. (1967), 13, 65.

3) N. F. Ramsey, Phys. Rev. 91, 303, (1953).

4) J. A. Pople, D. D. Santry, Mol. Phys., (1964), 8, 1.

5) C. J. Jameson, H. S. Gutowsky, J. Chem. Phys., 51, 2790 (1969).

6) W. McFarlane, Quart. Rev., 23, 187, (1969).

7) H. M. McConnell, J. Chem. Phys., 24, 460, (1965).

8) B. E. Mann, "NMR and the Periodic Table", R. K. Harris, B. E. Mann, Eds; Academic; New York, (1978), 95.

9) B. Wrackmeyer, Ann. Rep. NMR. Spectrosc., 16 (1985), 73.

10) B. Wrackmeyer, J. Magn. Reson., 59, (1984), 141.

11) C. J. Jameson, J.A.C.S., 91, 6232, (1969).

12) W. Biffar, T. Gasparis-Ebeling, H. Noth, W. Storch, B. Wrackmeyer, J. Magn. Reson., 44, (1981), 54.

13) M. Barfield, M. Karplus, J.A.C.S., 91, 1, (1969).

14) T. A. Albright, Org. Magn. Reson., 8, (1976), 489.

15) J. P. Quintard, M. Degueil-Castaing, B. Barbe, M. Petraud, J. Organomet. Chem., 234, (1982) 41.

16) T. N. Mitchell, W. Reimann, C. Nettelbeck, Organometallics, 1044, (1985).

17) B. Wrackmeyer, J. Organomet.Chem., 205, (1981), 1.

18) D. Dodrell, M. L. Bulpitt, C. J. Moore, C. W. Fong, W. Kitching, W. Adcock, B. D. Gupta, Tetrahedron Lett., 665, (1973).

19) A. D. Buckingham, J. E. Cordle, J. C. S. Faraday II, 994, (1974).

20) J. Hilton, L. H. Sutcliffe, J. C. S. Faraday II, 1395, (1975).

21) M. Barnard, P. J. Smith, R. F. M. White, J. Organomet. Chem., 77, (1974), 189.

22) P. Pyykko, L. Wiesenfeld, Mol. Phys., (1981), 43, 557.

23) P. J. Smith, L. Smith, Inorg. Chim. Acta. Rev., 7, (1973), 11.

24) P. J. Smith, A. Tupciauskas, Ann. Rep. NMR Spectrosc., 8, (1978), 291.

25) J. D. Kennedy, W. McFarlane, Rev. Silicon Germanium Tin Lead Compounds, 1, 235, (1974).

26) R. Hani, R. A. Geanangel, Coord. Chem. Rev., (1982), 44, 229.

27) V. S. Petrosyan, Prog. NMR Spectrosc., 11, (1977), 115.

28) J. D. Kennedy, W. McFarlane, "NMR and the Periodic Table", R. K. Harris, B. E. Mann, Eds: Academic; New York; (1978), 309.

29) J. D. Kennedy, W. McFarlane, "Multinuclear NMR", J. Mason, Ed ; Plenum; New York; (1987), 305.

30) "Specialist Periodical Reports, Nuclear Magnetic Resonance", The Royal Society of Chemistry, Alden Press, London.

31) C. J. Jameson, "Multinuclear NMR", J. Mason, Ed ; Plenum, New York, (1987), 89.

32) T. Birchall, V. Manivannan, J.C.S. Dalton., 2671, (1985).

33) C. Schumann, H. Dreeskamp, J. Magn. Reson., 3, (1970), 204.

34) T. Birchall, A. Pereira, Chem. Comm., 1150, (1972).

35) N. Flitcroft, H. D. Kaesz, J.A.C.S., 85, 1377, (1963).

36) J. D. Kennedy, W. McFarlane, J.C.S. Chem. Comm., 983, (1974).

37) U. Edlund, T. Lejon, P. Pyykko, T. K. Venkatachalam, E. Buncel, J.A.C.S., 109, 5982, (1987).

38) W. McFarlane, J. C. S. (A), 528, (1967).

39) J. D. Kennedy, W. McFarlane, J. Organomet. Chem., 94, (1975), 7.

40) B. Wrackmeyer, J. Organomet. Chem., 166, (1979), 353.

41) H. Dreeskamp, G. Stegmeier, Z. Naturforsch. A, (1967), 22, 1458.

42) D. de Vos, D. C. Van Beelen, J. Wolters, Bull. Soc. Chim. Belg., 89, 10, (1980), 791.

43) D. C. Van Beelen, A. E. J. Van Kamper, J. Wolters, J. Organomet. Chem., 187, (1980), 43.

44) D. de Vos, D. C. Van Beelen, J. Walters, J. Organomet. Chem., 172, (1979) 303.

45) R. H. Cox, J. Magn. Reson., 33, (1979), 61.

46) R. J. H. Clark, A. G. Davies, R. J. Puddephatt, W. McFarlane, J.A.C.S., 91, 1334, (1969).

47) W. McFarlane, Mol. Phys., (1967), 13, 587.

48) W. McFarlane, J. Organomet. Chem., 116, (1976), 315.

49) B. Wrackmeyer, J. Magn. Reson., 42, (1981), 287.

50) B. Jousseaume, E. Chanson, M. Bevilacqua, A. Saux, M. Pereyre, B. Barbe, M. Petraud, J. Organomet. Chem., 294, (1985), C41.

51) S. Adams, M. Drager, J. Organomet. Chem., 288, (1985), 295.

52) J. D. Kennedy, W. McFarlane, B. Wrackmeyer, Inorg. Chem., (1976), 15, 1299.

53) W. McFarlane, J.C.S.(A)., 1630, (1968).

54) T. N. Mitchell, G. J. Walter, J. C. S. Perkin Trans. II, 1842, (1977).

55) J. D. Kennedy, W. McFarlane, J. C. S. Dalton., 1219, (1976).

56) B. Mathiasch, T. N. Mitchell, J. Organomet. Chem., 185, (1980), 351.

57) K. Jurkschat, A. Tzschach, C. Mugge, J. Piret-Meunier, M. Van Meerssche, G. Van Binst, C. Wynants, M. Gielen, R. William, Organometallics, 593, (1988).

58) F. Teixidor, M. L. Luetkens, R. W. Rudolph, J.A.C.S., 105, 149, (1983).

59) W. L. Wilson, R. W. Rudolph, L. L. Lohr, R. Craig Taylor, P. Pyykko, Inorg. Chem., (1986), 25, 1535.

60) J. D. Kennedy, W. McFarlane, G. S. Pyne, B. Wrackmeyer, J.C.S. Dalton., 386, (1975).

61) J. D. Kennedy, W. McFarlane, J. Organomet. Chem., 80, (1974), C47.

62) P. Granger, C. Brevard, M. Devaud, J. Magn. Reson., 76, (1988), 232.

63) J. D. Kennedy, W. McFarlane, G. S. Pyne, B. Wrackmeyer, J. Organomet. Chem., 195, (1980), 285.

64) B. Wrackmeyer, J. Organomet. Chem., 297, (1985), 265.

65) C. Stader, B. Wrackmeyer, J. Magn. Reson., 72, (1987), 544.

66) S. J. Blunden, P. A. Cusack, J. Magn. Reson., 60, (1984), 114.

67) E. Kupce, E. Liepins, A. Lapsina, I. Urtane, G. Zelcans, E. Lukevics, J. Organomet. Chem., 279, (1985), 343.

68) K. C. Malloy, K. Quill, S. J. Blunden, R. Hill, J.C.S. Dalton., 875, (1986).

69) N. W. Alcock, N. Herron, P. Moore, J.C.S. Dalton., 1486, (1979).

70) E. H. Curzon, N. Herron, P. Moore, J.C.S. Dalton., 721, (1980).

71) B. Wrackmeyer, J. Magn. Reson., 61, (1985), 536.

72) W. McFarlane, D. S. Rycroft, J.C.S. Dalton., 1977, (1974).

73) P. A. W. Dean, D. D. Phillips, L. Polensek, Can. J. Chem., 59, 50, (1981).

74) P. A. W. Dean, Can. J. Chem., 61, 1765 (1983).

75) W. W. duMont, M. Grenz, Chem. Ber., 118, 1045, (1985).

76) H. H. Karsch., A. Appelt, G. Mueller, Angew. Chem. Int. Ed. Engl., (1985), 24, 402.

77) V. S. Petrosyan, N. S. Yashina, E. I. Gefel, Si. Ge. Sn. Pb. Compds, 9, 213, (1986).

78) P. A. W. Dean, R. S. Srivastava, Inorg. Chim. Acta, 105, (1985), 1.

79) J. D. Kennedy, W. McFarlane, J.C.S. Dalton., 2134, (1973).

80) R. C. Burns, L. A. Devereux, P. Granger, G. J. Schrobilgen, Inorg. Chem., (1985), 24, 2615.

81) W. McFarlane, R. J. Wood, J. Organomet. Chem., 40, (1972), C17.

82) I. R.Herbert, P. S. Pregosin, H. Ruegger, Inorg. Chim. Acta., 112, (1986), 29.

83) M. S. Holt, J. J. MacDougall, F. Mathey, J. H. Nelson, Inorg. Chem., (1984), 23, 449.

84) A. Albinati, P. S. Pregosin, H. Ruegger, Inorg. Chem., (1984), 23, 3223.

85) A. Albinati, H. Moriyama, H. Ruegger, P. S. Pregosin, A. Togni, Inorg. Chem., (1985), 24, 4430.

86) A. Albinati, U. Von Gunten, P. S. Pregosin, H. J. Ruegger, J. Organomet. Chem., 295, (1985), 239.

87) H. Weichmann, J. Organomet. Chem., 238, (1982), C49.

88) R. J. Goodfellow, I. R. Herbert, Inorg. Chim. Acta., 65, (1982), L161.

89) T. Yamakawa, S. Shinoda, Y. Saito, H. Moriyama, P. S. Pregosin, Magn. Reson. Chem., 23, (1985), 202.

90) H. Moriyama, P. S. Pregosin, Y. Saito, T. Yamakawa, J.C.S. Dalton, 2329, (1984).

91) M. Hoch, J. Organomet. Chem., 288, (1985), C25.

92) S. Carr, R. Colton, D. Dakternieks, J. Magn. Reson., 47, (1982), 156.

93) S. Carr, R. Colton, D. Dakternieks, J. Organomet. Chem. 240, (1982), 143.

94) P. G. Harrison, S. E. Ulrich, J. J. Zuckerman, Inorg. Nucl. Chem. Lett., (1971), 7, 865.

95) M. Kretschmer, P. S. Pregosin, A. Albinati, A. Togni, J. Organomet. Chem., 281, (1985), 365.

96) T. N. Mitchell, H. C. Marsmann, Org. Magn. Reson., 15, (1981), 263.

97) A. Blecher, B. Mathiasch, T. N. Mitchell, J. Organomet. Chem., 184, (1980) 175.

98) T. N. Mitchell, R. Wickenkamp, J. Organomet. Chem. 291, (1985), 179.

99) B. Wrackmeyer, J. Magn. Reson., 61, (1985), 536.

100) P. A. W. Dean, Can. J. Chem., 60, 2921, (1982).

101) T. A. George, C. D. Sterner, Inorg. Chem., (1976), 15, 165.

102) R. Eugen, R. J. Lagow, J. C. S. Dalton, 541, (1978).

103) H. Weichmann, C. Muegge, A. Grand, J. B. Robert, J. Organomet. Chem. 238, (1982), 343.

104) S. W. Carr, R. Colton, D. Dakternieks, B. F. Hoskins, R. J. Steen, Inorg. Chem., (1983), 22, 3700.

105) B. Wrackmeyer, J. Organomet. Chem., 190, (1980), 237.

106) B. Wrackmeyer, J. Magn. Reson., 39, 359, (1980).

107) B. Jousseaume, J. G. Duboudin, J. Organomet. Chem., 232, (1982), 171.

108) W. Adcock, G. B. Kok, A. N. Abeywickrema, W. Kitching, G. M. Drew, H. A. Olszowry, I. Schott, J.A.C.S., 105, 290, (1983).

109) B. Mathiasch. U. Kunze, Inorg. Chim. Acta, 75, (1983), 209.

110) B. Wrackmeyer, C. Bihlmayer, M. Schilling, Chem. Ber., 116, 3182, (1983).

111) R. J. Puddephatt, G. H. Thislethwaite, J. Organomet. Chem.,40, (1972), 143.

112) D. C. Van Beelen, H. O. Van der Kool, J. Walters, J. Organomet Chem., 179, (1979), 37.

113) M. J. Cooper, A. K. Holliday, P. H. Makin, R. J. Puddephatt, P. J. Smith, J. Organomet. Chem., 65, (1974), 377.

CHAPTER 2

MULTIPLE RESONANCE EXPERIMENTS

2.1 Introduction

In an ordinary (single resonance) N.M.R. experiment the sample is placed in a magnetic field and exposed to just one radio frequency. However, it is also possible to perform multiple resonance[1] experiments in which several radio frequencies are used, the most common type of which is double resonance[2] where one type of nucleus is irradiated at its resonance frequency, while another in the same molecule is observed. The coupling between the observed and irradiated nuclei then leads to different perturbation effects being observed, depending on the frequency and amplitude of the irradiating (also known as the "decoupling", "perturbing" or "tickling") radio frequency field. These experiments can be either homonuclear (i.e. among like nuclei which are chemically shifted) or heteronuclear (i.e. one species is observed while another is irradiated), each presenting different instrumental problems.

The uses of double resonance techniques are diverse and include the removal of unwanted spin-spin coupling[3] in ^{19}F and ^{1}H spectra; the elimination of nuclear quadrupolar broadening (e.g. due to ^{14}N [4]) in proton spectra; the determination of chemical shifts and coupling constants of other nuclei (e.g. ^{77}Se [5], ^{103}Rh [6], ^{195}Pt [7]); the determination of chemical shifts of protons whose resonances are concealed in the normal spectrum[8]; the determination of nuclear geometry from nuclear Overhauser effects[9]; the study of spin-population transfer effects[10]; and the determination of the relative signs of coupling constants[11].

2.2 Double Resonance Experiments

The success of many double resonance experiments depends on being able to irradiate the appropriate transition(s) without significantly

affecting others. This sets a major limitation on the power level of the irradiating radio frequency field and therefore upon the type of perturbation effects that can be achieved. It may also be necessary to reduce the power to minimise electronic interference effects. Finally limitations in the equipment used may dictate the power level of the irradiation field that can be used.

At high powers decoupling can be achieved, where irradiation at or near the resonant frequency of one nucleus removes the spin-spin coupling which it produces in the spectrum of another nucleus[2] (see Fig.2.I). A simple explanation of this effect is that rapid transitions are induced between the spin states associated with the irradiated transitions so that the lifetime of a particular state is short compared with $^1/J$ where J is the relevant coupling constant, thereby removing the coupling effect. At somewhat lower power levels <u>selective decoupling</u> is achieved, whereby the only coupling removed is that arising from irradiated nuclei lying in a particular (chosen) chemical shift range. Extending this effect to a three spin system (AMX), the A-M coupling can be selectively collapsed in part of the A spectrum corresponding to a particular spin state of X by irradiation of transitions in the M spectrum associated with the same spin state of X. An example is given in FIG. 2.II where A = ^{119}Sn, M = ^1H, X = ^{195}Pt. In such an experiment the general criterion for being able to achieve selective decoupling is that the coupling to be collapsed [J(A-M)] must be small compared with the other two coupling constants, J(A-X) and J(M-X).

Where the irradiating field is too weak to cause selective decoupling then "spin tickling" is said to occur. In such experiments, transitions which have an energy level in common with the irradiated transition are split into symmetrical doublets, where the size of

FIG.2.I ^{31}P Decoupling Of The ^{13}C Spectrum Of $(MeO)_3P$

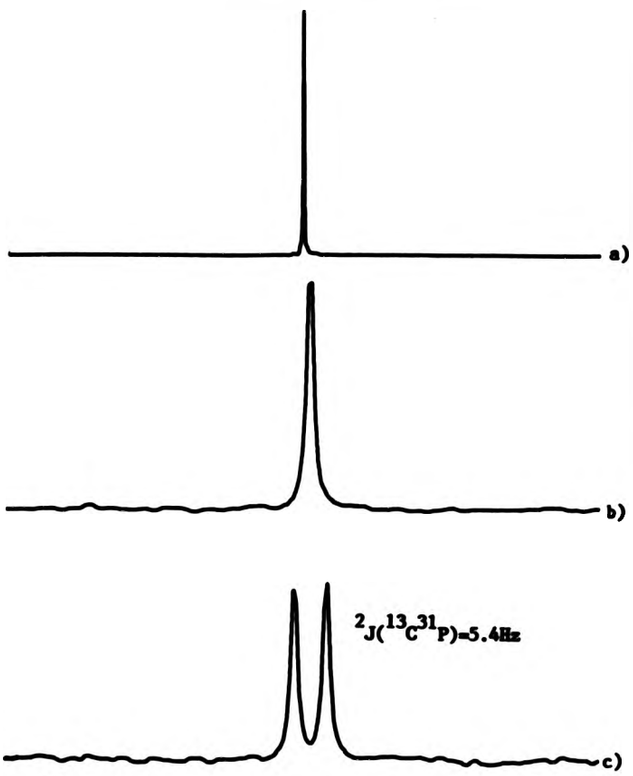

a) ^{31}P spectrum
b) ^{13}C spectrum with irradiation at $\nu^{31}P$
c) ^{13}C spectrum without ^{31}P irradiation

FIG.2.II Selective ^{1}H Decoupling Of The ^{119}Sn Spectrum Of Trans-[Pt($SnCl_3$)(PPh_3)$_2$H]

splitting depends on the power of the irradiating frequency[12]. An example is given in FIG. 2.III. If the irradiating frequency does not exactly coincide with the transition under consideration, the components of the doublet will not be of equal intensity, and will not be symmetrically spaced about the unperturbed position, the more intense component being closer to the unperturbed position[12]. As the irradiating frequency offset becomes larger the doublet produced becomes more distorted until no observable effect can be seen. The effects arise because irradiation of the transition causes some mixing of the wave functions of the associated energy levels, thus producing new levels, involving some previously forbidden transitions which become allowed. Hence an associated transition is replaced by two new transitions, which appear as the doublet components.

As the radio frequency power is further decreased spin population transfer effects begin to predominate with intensity changes being observed in associated transitions[13]. The advantage of population transfer experiments is that it is possible to recognise the progressively and regressively associated transitions. The changes in intensity seen are due to partial or complete saturation of the irradiated transition (A -> B, see FIG.2.IV).

FIG.2.III Line Splitting In The ^{119}Sn Spectrum Of $(Me_3Sn)_3P$ Caused By ^{31}P "Spin Tickling"

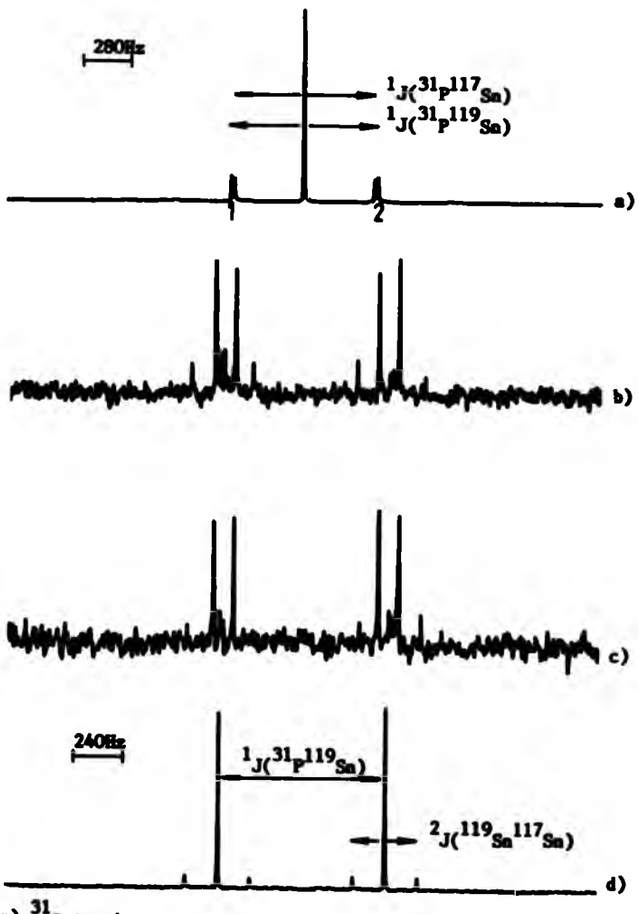

a) ^{31}P spectrum

b) ^{119}Sn spectrum with irradiation at line 2 $(\nu^{31}P-\frac{1}{2}{}^1J(^{31}P^{119}Sn))$

c) ^{119}Sn spectrum with irradiation at line 1 $(\nu^{31}P+\frac{1}{2}{}^1J(^{31}P^{119}Sn))$

d) ^{119}Sn spectrum with NO irradiation

FIG. 2.IV

Energy Level Diagram of Two Coupled Nuclei

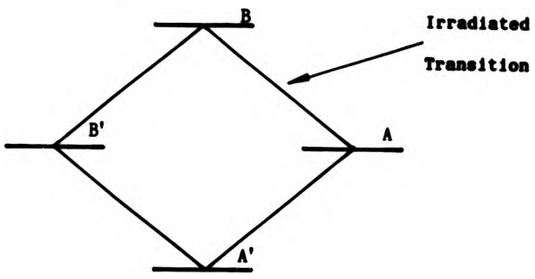

This leads to equalisation of the populations of the two energy levels connected by the transition (A -> B). Given two associated transitions; one progressively associated with the lower energy level (A) connecting it to another, lower energy level (A'), and one regressively associated with the higher energy level (B), connecting it to another, lower energy level (B'), the population of the higher level (B) will be increased reducing the population difference between it and the level (B'). Therefore the intensity of the regressive transition (B'-> B) will be reduced. The population of the lower energy level (A) is decreased, increasing the population difference between it and the level (A'). Therefore the intensity of the progressive transition (A'->A) will be increased. An example is given in FIG.2.V. The effect depends on the relaxation properties of the nuclei. For population transfer effects to be seen it is necessary that $T_{1X} < T_{1A}$ (where an X transition is irradiated and A transitions are perturbed).

The width of lines in a high resolution Fourier transform N.M.R. spectrum observed in a multiple resonance experiment, may differ from

FIG.2.V Population Transfer Effects In The ^{119}Sn Spectrum Of $(Me_3Sn)_3P$ Caused By ^{31}P "Spin Tickling"

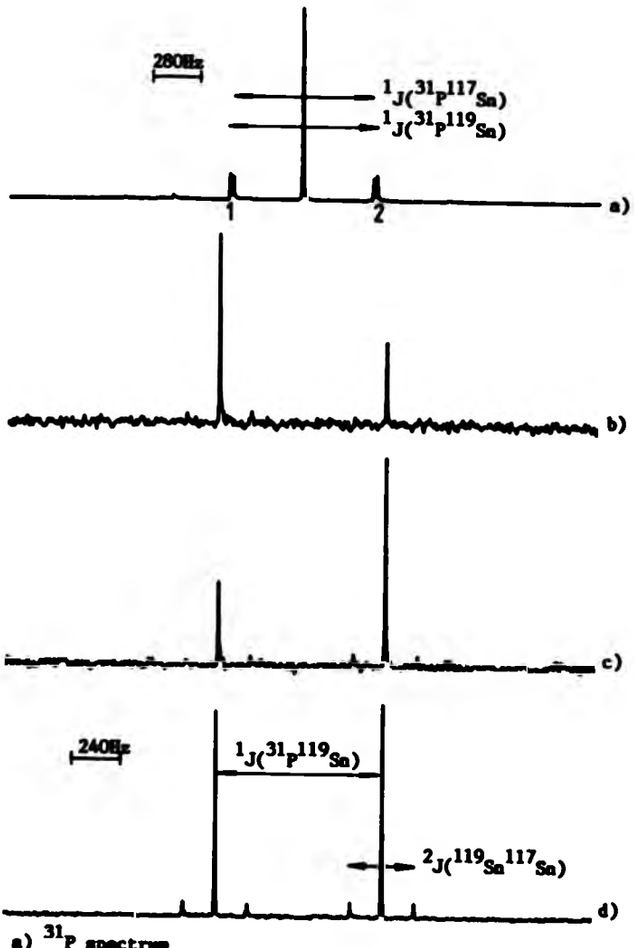

a) ^{31}P spectrum

b) ^{119}Sn spectrum with irradiation at line 2 ($\nu^{31}P - \frac{1}{2}{}^1J(^{31}P^{119}Sn)$)

c) ^{119}Sn spectrum with irradiation at line 1 ($\nu^{31}P + \frac{1}{2}{}^1J(^{31}P^{119}Sn)$)

d) ^{119}Sn spectrum with NO irradiation

those observed in a conventional single resonance experiment[12]. In general the magnetic field inhomogeneity determines the width of lines in a spectrum. Where a transition has been split into a doublet as the result of a multiple resonance experiment, the components of the doublet will be either narrower or sharper than the unperturbed lines. If the perturbed transition is progressively associated with the irradiated transition the lines will be broader, and if it is regressively associated, the lines will be sharper[12]. Also the extent to which the lines of a spectrum are broadened or sharpened depends on the ratio (r) of the magnetogyric ratios of the observed nucleus (γ_A) and the irradiated nucleus (γ_X) given in equation 2.1.

$$r = \gamma_A / \gamma_X \qquad (2.1)$$

If $r > 1$ then the affected lines will be sharper and if $r < 1$ the affected lines will be broader, than the unperturbed line[12].

There are no clearcut points where one type of perturbation effect takes over from another. It is possible to see both line splitting and population transfer effects together, which can lead to situations where loss of peak height, due to almost resolved line splitting can be counteracted by an increase in the intensity due to spin population transfer and line broadening. The resulting peak then merely appears slightly broader. In pulsed Fourier transform experiments it is possible to separate the line splitting and intensity effects by gating the irradiation. The line splitting effect is short lived compared to the spin population transfer effect. If the irradiation is switched on only during the accumulation of the F.I.D. the spin population transfer effect has insufficient time to build up, and only the line splitting is seen. The pulse delay used (i.e. the interval between successive accumulations) must be long enough to allow any population changes

caused during the previous accumulation to relax, before the next F.I.D. is accumulated. Conversely if the irradiation is applied before and not during the accumulation of the F.I.D., the line splitting effect will disappear leaving only the longer lived, relaxation-associated, spin population transfer effects.

2.3 Determination Of The Signs Of Coupling Constants

Information concerning the signs of coupling constants can be obtained in a number of ways:-

1) Studies of molecules which have been partially orientated in liquid crystals can yield the absolute signs of coupling constants[14]. The rotational motion of the molecule is sufficiently hindered, for the intermolecular dipole-dipole coupling to be still averaged to zero as in isotropic N.M.R., but the intramolecular dipole-dipole coupling is not and contributes to the observed splittings. By comparing this value to that which is obtained in an isotropic medium, the sign of the spin-spin coupling relative to the dipole-dipole coupling (which may be of known sign) is obtained.

2) In particular cases a strongly coupled spin-system (at the appropriate field strength) may exhibit 2nd order features, the analysis of which will give the relative signs of some of the coupling constants involved[13].

3) For certain compounds the magnitude of the observed coupling constant varies in response to a change in a property of the solvent[16]. If this change is known to be in an absolute direction, the coupling can be seen to increase or decrease relative to its sign. These solvent effects are not well understood and the behaviour of related coupling constants of known sign must be examined before valid conclusions can be drawn.

4) The observation of double quantum transitions can be used to determine the relative signs of coupling constants[17]. These are observed when the radio frequency field is increased to the point where the single quantum transitions are just saturated. The frequency of a double quantum transition is given by the sum of the

frequencies of two of the single quantum transitions (with respect to their signs), thereby yielding the relative signs of the two coupling constants.

5) By far the most generally applicable method for obtaining information about the signs of coupling constants is the use of double resonance experiments, the technique with which this study is primarily concerned[2].

The results of double resonance experiments, analysis of 2nd-order spectra and the frequencies of double quantum transitions can give the relative signs of coupling constants, which are invariant with respect to the reversal of all the signs of all coupling constants in a molecule. However it is desirable to know the absolute signs, and this can be achieved by determining the signs of coupling constants relative to one of a number of key coupling constants for which the absolute sign has been established. These key coupling constants appear always to have the same sign irrespective of the particular compound examined. They are generally determined by studies upon partially orientated molecules and some of these are listed in table 2.1.

Table 2.1

Coupling	Sign	Ref
^1J (^{13}C-^1H)	+	18
^1J (^{13}C-^{19}F)	-	19
^3J (^1H-^1H) in ethyl group	+	20
^3J (^1H-^1H) in aromatic ring	+	21
^3J (^{19}F-^{19}F)" " "	-	22

2.4 Sign Determination By Double Resonance Experiments[2]

Loosely coupled spin systems are comprised of a number of subspectra, each associated with a different spin orientation of a particular nucleus. It may be possible to determine which lines belong to a particular subspectrum by double resonance experiments, which perturb only lines belonging to that subspectrum. Which lines of a spectrum belong to a particular subspectrum determines the relative signs of the coupling constants.

For example consider the AMX spin system provided by the ^{31}P and ^{195}Pt nuclei of (1) in FIG.2.VI

FIG.2.VI Structure of cis-$[Pt(PPh_3)_2Ph(SnClPh_2)]$

(1)

(see Fig. 2.VII for ^{195}Pt and ^{31}P spectra)

The A, M and X spectra consist of four lines each, as marked in FIG.2.VII. The spin-states ((-) ones are of lower energy) of the two nuclei associated with a particular transition of the third are given for the cases of (a) all three coupling constants positive (b) J(AM) and J(MX) positive, and J(AX) negative. This is one way of interpreting sign determining double resonance experiments. Another is to construct a complete energy level diagram for the system. For a three spin system the energy levels can be represented by the vertices of a cube; edges corresponding to the single quantum transitions, with all those parallel belonging to a single nucleus. As in the previous method FIG. 2.VIII (a) represents a system where all the coupling constants are positive

J(AX) is negative.

FIG.2.VII Cis-$[Pt(Ph)(PPh_3)(SnPh_2Cl)]$
(See chapter 4 for coupling constants)

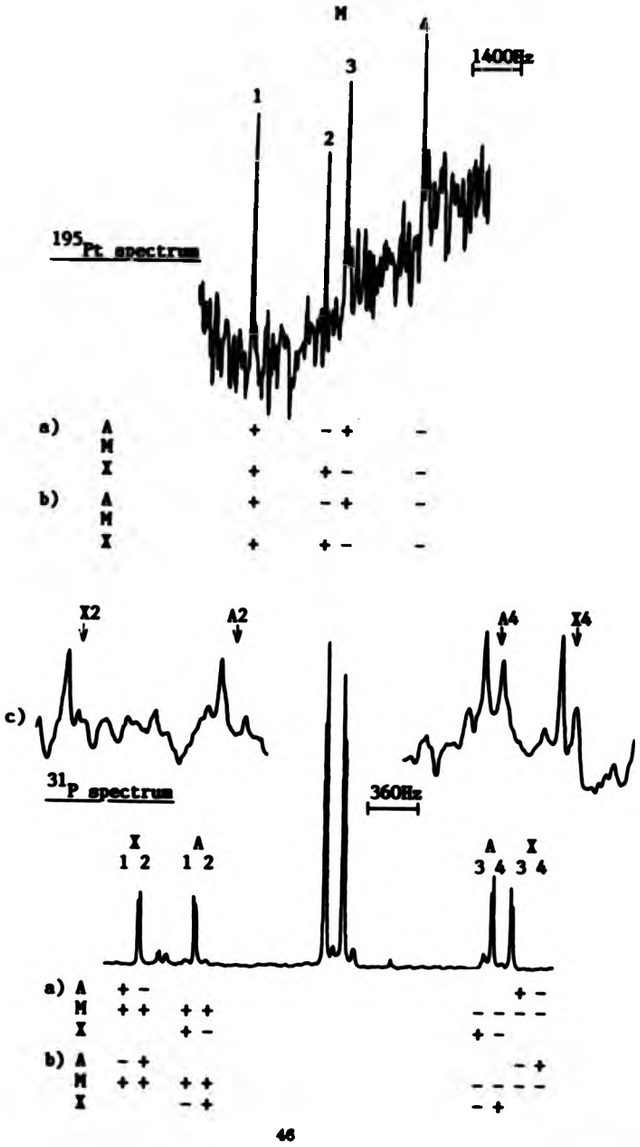

Fig.2.VIII Energy Level Diagram of an AMX spin system

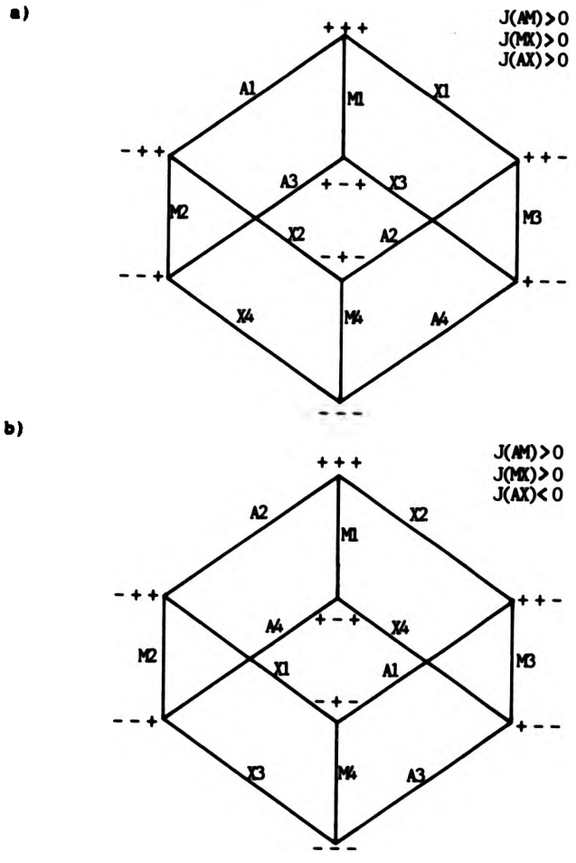

When a particular transition is irradiated, other transitions which share an energy level with it will be perturbed. Therefore when the M-1 transition is irradiated, (a) if all the coupling constants have the same sign, the A-1, A-3, X-1 and X-3 transitions will be perturbed or (b) if J(AX) is negative and J(AM) and J(MX) are positive, the A-2, A-4, X-2 and X-4 transitions will be perturbed. The result is shown on the

expansion of the A and X lines in FIG. 2.VII (c). The latter (b) is the case, and given that $^{1}J(^{31}P-^{195}Pt)$ is +ve, $^{1}J(^{195}Pt_{M}-^{31}P_{A})$ and $^{1}J(^{195}Pt_{M}-^{31}P_{X})$ are positive and $^{2}J(^{31}P_{A}-^{31}P_{X})$ is negative. It can be seen by examining the energy level diagram that to compare the signs of all the coupling constants in a system by double resonance experiments, each different nucleus must be either observed or have its transitions irradiated.

In the example above, all the nuclei involved have positive magnetogyric ratios. However, if one of nuclei has a negative magnetogyric ratio the situation is not as simple. The reason for this is that when the spectral parameters are defined in terms of J's and δ's, the magnetogyric ratio (γ) appears in the chemical shift part, and not the spin coupling part of the expression for an energy level. It is better to consider the experiment as comparing the signs of the K's (the reduced coupling constant), which is independent of γ and is defined in equation 1.2.

A simpler approach can be used to interpret a double resonance experiment of this type. The two coupling constants to be compared must arise from two different nuclei 'A' and'X' (or groups of equivalent nuclei) coupled to the same nucleus 'M' (or groups of equivalent nuclei). To compare the signs of the coupling constants $^{n}K(A-M)$ and $^{m}K(M-X)$, irradiation is applied at the frequency of a line in the A spectrum due to coupling to X and M. Simultaneously the X spectrum is observed. Lines in the X spectrum due to coupling to M and A will be perturbed. If a line containing the high (low) field component of the A-M coupling is irradiated, and the coupling constants are the same sign, lines in the X spectrum containing the high (low) field components of the M-X coupling will be perturbed. If the signs of the coupling

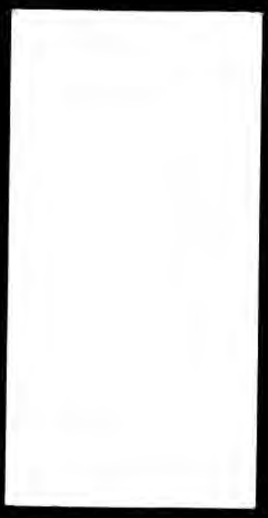

constants are opposite, then irradiating a high frequency component of the A spectrum will perturb a low frequency component in the X spectrum, and vice-versa.

The above discussion presupposes a previous knowledge of the line positions of the transitions to be irradiated. This is generally obtained by direct observation of the spectrum of the nucleus to be irradiated, but as mentioned earlier multiple resonance experiments can also be used to determine the chemical shifts and coupling constants (i.e. the line positions) of other nuclei. The multiple resonance experiment is performed in the same manner as for relative sign determination, except that since the required line positions are not known in advance, a number of experiments must be performed, sweeping the irradiating field in steps across the region containing the interesting transitions, until a perturbation occurs in the observed spectrum.

The initial sweep is carried out with relatively high power irradiation, to cover a large frequency region in each step. The position of each transition is then determined more accurately by reducing the irradiating power and homing in on the transition. In this way not only is the line position determined, but any sign-determining multiple resonance experiment which entails irradiation of that transition is also performed in the process.

For nuclei with low magnetogyric ratios (i.e. insensitive ones) the determination of chemical shifts and coupling constants by multiple resonance experiments can be easier, and often quicker than direct observation of the spectrum. For example, the rhodium chemical shifts in this thesis were determined in this way. However, where the spectrum consists of a large number of lines the determination of each line

position by multiple resonance becomes tedious and direct observation is preferable.

In the past, the majority of work of this type has involved ^{1}H-{X} or X-{^{1}H} experiments, and an important aspect of this thesis has been the extension of this approach to generalised X-{Y} experiments (X, Y = ^{31}P, ^{119}Sn, ^{195}Pt, etc.). In most cases these experiments were conducted under conditions of complete proton decoupling, and a range of instrumental problems had to be solved for their successful implementation.

2.5 References

1) W. McFarlane, D. S. Rycroft, Ann . Rep. NMR. Spectrosc., 16, (1985), 293; 9, (1979), 319; 5, (1973), 356.

2) W. McFarlane, Determination Org. Struct. Phys. Methods, 4, 139, (1971).

3) R. O. Hutchins, B. E. Maryanoff, J. P. Albrand, A. Cogne, D. Gagnaire, J. B. Robert, J.A.C.S., 94, 9151, (1972).

4) T. Wamsler, J. T. Nielsen, E. J. Pedersen, K. Schaumberg, J. Magn. Reson., 43, (1981), 387.

5) R. Keat, D. S. Rycroft, D. G. Thompson, Org. Magn. Reson., 12, (1979), 391.

6) I. J. Colquhoun, W. McFarlane, J. Magn. Reson., 46, (1982), 525.

7) J. Browning, P. L. Goggin, R. J. Goodfellow, J. Chem. Res. Synop., 328, (1978), J. Chem. Res. Miniprint, 4201, (1978).

8) N. S. Bhacca, M. E. Wolff, R. Kwok, J.A.C.S., 84, 4976 (1962).

9) J. H. Noggle, R. E. Schirmer, "The Nuclear Overhauser Effect: Chemical Applications", Academic Press, New York, (1971).

10) I. D. Campbell, R. Freeman, J. Magn. Reson., 11, (1973), 143.

11) I. J. Colquhoun, W. McFarlane, R. L. Keiter, J. C. S. Dalton Trans., 455, (1984).

12) R. Freeman, W. A. Anderson, J. Chem. Phys., 37, 2053 (1962).

13) R. Kaiser, J. Chem. Phys., 39, 2435, (1963).

14) N. Zumbulyadis, B. P. Dailey, Mol. Phys., (1974), 27, 633.

15) P. J. Narasimhan, M. T. Rogers, J. Chem. Phys., 33, 727 (1960).

16) P. A. W. Dean, D. F. Evans, J.C.S.(A), 698, (1967).

17) J.I. Musher, J. Chem. Phys., 40, 983 (1964).

18) G. Englert, A. Saupe, Mol. Cryst., 1, 503, (1966).

19) G. V. D. Tiers, J.A.C.S., 84, 3972 (1962).

20) G. M. Woodman, Mol. Phys., (1967), 13, 365.

21) L. C. Snyder, E. W. Anderson, J.A.C.S., 86, 5023, (1964).

22) L. C. Snyder, E. W. Anderson, J. Chem. Phys., 42, 3336, (1965).

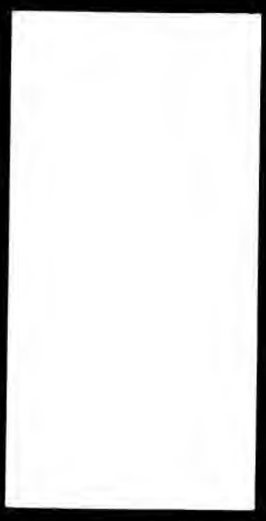

CHAPTER 3

BIS-PHOSPHINE TIN (IV) TETRAHALIDES

3.1 Introduction

There has been considerable interest in transition metal-phosphine complexes and ^{31}P N.M.R. has proved to be an extremely useful tool in their study. This has produced a considerable body of data on $^{1}J(M^{31}P)$[22] and $^{2}J(^{31}PM^{31}P)$[11] (M = transition metal). Bis-phosphine complexes of tin (IV) tetrahalides allows these coupling constants and other spectroscopic data to be compared to analogous main group metal complexes, in order to ascertain if established trends can be extended from transition metal-phosphine to main group metal-phosphine complexes.

Also previous studies on $^{1}J(^{119}Sn^{31}P)$ have mainly centred on compounds of the type $(R_3Sn)_nR_{3-n}PX$ (n = 1-3; R = alkyl, aryl group; X = electron lone-pair, transition metal)[4], where the tin is in a tetrahedral environment and is formally sp^3 hybridized. However in $[(PR_3)_2SnX_4]$ (R = alkyl, aryl group; X = halide) type complexes, the tin is in an octahedral environment and will have a different hybridization state. This may lead to a significant difference in the nature of the tin-phosphorus bond, which will be reflected in the magnitude and sign of $^{1}J(^{119}Sn^{31}P)$ and $^{2}J(^{31}PSn^{31}P)$.

In this chapter a number of multiple resonance experiments to determine the magnitudes and signs of various coupling constants in bis-phosphine tin (IV) tetrahalide complexes, including $^{1}J(^{119}Sn^{31}P)$ and $^{2}J(^{31}PSn^{31}P)$, are described. Each experiment presents different problems, which are overcome in a variety of ways.

3.2 Possible Multiple Resonance Experiments

When multiple resonance experiments are used to determine the relative signs of spin-spin coupling constants, three different spins or

groups of equivalent spins are considered. Where a large number of different types of spins are involved in the molecule under investigation, they can be grouped into sets of three in a number of different ways. Therefore there are a number of possible combinations of multiple resonance experiments by which the signs of the various spin-spin coupling constants can be mutually related.

In the present case, for the multiple resonance experiments the compound Bis(triethylphosphine) tin (IV) tetrachloride was chosen, due to its good solubility in dichloromethane, its stability in solution, and the relatively simple alkyl group attached to phosphorus.

The object of these experiments is to place the signs of the coupling constants on an absolute basis by relating them to a coupling of known sign. In the case of this compound the signs of $^{1}J(^{13}C\text{-}^{1}H)$ and $^{3}J(^{31}P\text{-}^{1}H)^{2}$ can be taken as positive.

A number of approaches to the multiple resonance experiments can be considered.

1) $^{13}C\text{-}\{^{119}Sn\}$ experiments on a proton-decoupled three-spin system (^{13}C, ^{31}P, ^{119}Sn) (see FIG. 3.I) would allow the signs of $J(^{31}P\text{-}^{119}Sn)$ and $J(^{13}C\text{-}^{31}P)$ to be related.

FIG. 3.I Possible Three Spin Systems (^{13}C, ^{31}P, ^{119}Sn)

a) $\left[(H_3C\text{-}H_2C)_2(H_3{}^{13}C\text{-}H_2C)^{31}P\right]$ $^{119}SnCl_4$ $\left[P(CH_2\text{-}CH_3)_3\right]$

b) $\left[(H_3C\text{-}H_2C)_2(H_3C\text{-}H_2{}^{13}C)^{31}P\right]$ $^{119}SnCl_4$ $\left[P(CH_2\text{-}Ch_3)_3\right]$

Then considering a spin system (^{13}C, ^{31}P, ^{1}H, see FIG. 3.II) the signs of $J(^{13}C\text{-}^{31}P)$ could then be related to $J(^{13}C\text{-}^{1}H)$ by $^{31}P\text{-}\{^{1}H\}$ experiments or to $J(^{1}H\text{-}^{31}P)$ by $^{13}C\text{-}\{^{1}H\}$ experiments.

FIG. 3.II Possible Three Spin Systems (^{13}C, ^{31}P, ^{1}H)

a) $[(H_3C\text{-}H_2C)_2(H_3C\text{-}{}^{1}H_2{}^{13}C){}^{31}P]\ SnCl_4\ [P(CH_2\text{-}CH_3)_3]$

b) $[(H_3C\text{-}H_2C)_2({}^{1}H_3C\text{-}H_2{}^{13}C){}^{31}P]\ SnCl_4\ [P(CH_2\text{-}CH_3)_3]$

c) $[(H_3C\text{-}H_2C)_2(H_3{}^{13}C\text{-}{}^{1}H_2C){}^{31}P]\ SnCl_4\ [P(CH_2\text{-}CH_3)_3]$

d) $[(H_3C\text{-}H_2C)_2({}^{1}H_3{}^{13}C\text{-}H_2C){}^{31}P]\ SnCl_4\ [P(CH_2\text{-}CH_3)_3]$

This approach was rejected for a number of reasons. ^{119}Sn is of 8.6% natural abundance and ^{13}C is of 1.11% natural abundance; therefore in order to perform the required experiments, lines from a 0.095% abundant species (^{31}P is 100% abundant) need to be detected. Due to the low abundance of ^{13}C, the lines in the ^{13}C spectrum are almost entirely due to molecules containing one ^{13}C nucleus per molecule. The presence of one ^{13}C nucleus at a particular site makes the two ^{31}P nuclei in the molecule magnetically inequivalent (see FIG. 3.III) and therefore introduces second order effects into the ^{13}C spectrum. This makes detection of lines due to coupling between ^{119}Sn and ^{13}C virtually impossible even if such a low abundant species could be detected anyway.

FIG. 3.III Magnetic equivalence of ^{31}P nuclei removed by presence of ^{13}C

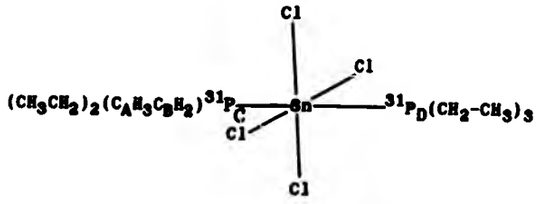

C_A experiences a $^2J(^{31}P_C-^{13}C_A)$ and a $^4J(^{31}P_D-^{13}C_A)$ and C_B experiences a $^2J(^{31}P_C-^{13}C_B)$ and a $^3J(^{31}P_D-^{13}C_B)$; therefore ^{13}C at either C_A or C_B makes $^{31}P_C$ and $^{31}P_D$ magnetically inequivalent.

2) $^{119}Sn-\{^1H\}$ experiments on a three spin system (^{119}Sn, ^{31}P, ^1H) (see FIG.3.IV) would relate the signs of $J(^{119}Sn-^{31}P)$ and $J(^{31}P-^1H)$ to one another. This has the advantage that the required species is more abundant than the species required under option (1), shown in FIG. 3.III.

FIG 3.IV Possible three spin systems (^{119}Sn, ^{31}P, ^1H)

a) $[(^1H_3C - H_2C)\ ^{31}P]_2{}^{119}SnCl_4$ b) $[(H_3C-^1H_2C)^{31}P]_2{}^{119}SnCl_4$

However there are two types of protons in the molecule so that coupling between them leads to a complex second order spectrum, and the proton spectrum due to protons coupled to ^{119}Sn, as well as ^{31}P, is obscured beneath the more intense second order spectrum due to molecules

without ^{119}Sn.

3). Thus a more circuitous route is needed in order to relate the signs of the various spin-spin coupling constants to one another. As mentioned in (1), when a molecule contains one ^{13}C nucleus, the two ^{31}P nuclei become magnetically inequivalent. There are two different types of carbon atom in the molecule as shown in Fig. 3.III. The proton-decoupled ^{13}C spectrum of each carbon forms the X part of an AA'X spin system where X = C_A or C_B and A,A' = ^{31}P. By performing ^{13}C - $\{^{31}P\}$ experiments on these AA'X spin systems the signs of the $(^{31}P\text{-}^{31}P)$ and $(^{31}P\text{-}^{13}C)$ couplings can be related. The signs of the $(^{31}P\text{-}^{13}C)$ couplings can then be related to the signs of $J(^{13}C\text{-}^{1}H)$ or $J(^{1}H\text{-}^{31}P)$ as in (1). The next problem is to determine the sign of $^{1}J(^{31}P\text{-}^{119}Sn)$ relative to that of one of the above coupling constants. In fact a chemical solution to this problem was adopted by to making a Bis-phosphine tin (IV) tetrahalide with two different tertiary phosphines co-ordinated to the tin. The proton-decoupled ^{31}P spectrum of this compound is then an AB spectrum with ^{119}Sn and ^{117}Sn satellites. Therefore the signs of the $(^{119}Sn\text{-}^{31}P)$ coupling constants can be related to the sign of $^{2}J(^{31}P\text{-}^{31}P)$ by $^{31}P\text{-}\{^{119}Sn\}$ experiments on this compound.

3.3 Spectral Analysis And Interpretation Of Multiple Resonance Experiments

In determining the relative signs of the spin-spin coupling constants, multiple resonance experiments were carried out on three different types of spin systems. The experiments on each type of spin system will be considered in turn.

3.4 ABX Spin System (A, B = ^{31}P, X = ^{119}Sn)

By reacting the appropriate quantity of $SnCl_4$ with an equimolar

mixture of PEt_3 and PBu^n_3 in CH_2Cl_2, a mixture of three different Bis-phosphine tin (IV) tetrachlorides was produced in solution; $(PEt_3)_2SnCl_4$, $(PBu^n_3)_2SnCl_4$ and $(PEt_3)(PBu^n_3)SnCl_4$. The multiple resonance experiments were carried out on the last species. The proton-decoupled ^{31}P (FIG. 3.V) and ^{119}Sn (FIG. 3.VI) spectra of a ^{119}Sn-containing molecule are described by an ABX spin system with A, B = ^{31}P and X = ^{119}Sn. The analysis of an AMX spin system, with respect to relative sign determining multiple resonance experiments, given in the previous chapter can be used when interpreting the experiments carried out on this spin system. The sign of $^1J(^{119}Sn\text{-}^{31}P)$ was compared with the sign of $^2J(^{31}P\text{-}^{31}P)$ by $^{31}P\text{-}\{^{119}Sn\}$ experiments as shown in FIG. 3.VII. By examining the energy level diagram for the ABX spin system, it can be seen that when an X (^{119}Sn) transition is irradiated, two A (^{31}P) and two B (^{31}P) transitions will be perturbed. Also the information concerning the relative signs of two coupling constants, X-A and A-B, is obtained from which B transitions are affected. Irradiation of line 1 (FIG. 3.VI) of the ^{119}Sn spectrum perturbs lines 2, 4, 6, 8 (FIG. 3.VII) in the ^{31}P spectrum and irradiation of line 3 (FIG. 3.VI) in the ^{119}Sn spectrum perturbs lines 1, 3, 5, 7 (FIG. 3.VII) in the ^{31}P spectrum of both the triethyl- and tri-n-butyl-phosphine parts of the spectrum. Therefore both $^1K(^{119}Sn\text{-}^{31}P_{Bu^n})$ and $^1K(^{119}Sn\text{-}^{31}P_{Et})$ are of opposite sign to $^2K(^{31}P_{Bu}\text{-}^{31}P_{Et})$ [$^1J(^{119}Sn\text{-}^{31}P_{Bu^n})$ and $^1J(^{119}Sn\text{-}^{31}P_{Et})$ have the same sign as $^2J(^{31}P\text{-}^{3}P)$].

3.5 AA'X Spin System (A, A' = ^{31}P, X = ^{13}C)

The two different types of carbon in the molecule both give ^{13}C spectra which are the X parts of AA'X spin systems. Although both systems can be described using the same energy level diagram, the

FIG. 3.V ^{31}P Spectrum Of $SnCl_4(PEt_3)_{2-n}(PBu^n_3)_n$ (n=0-2)

FIG.3.VI ^{119}Sn Spectrum Of $SnCl_4(PEt_3)_n(PBu^n_3)_{n-2}$ (n=0-2)

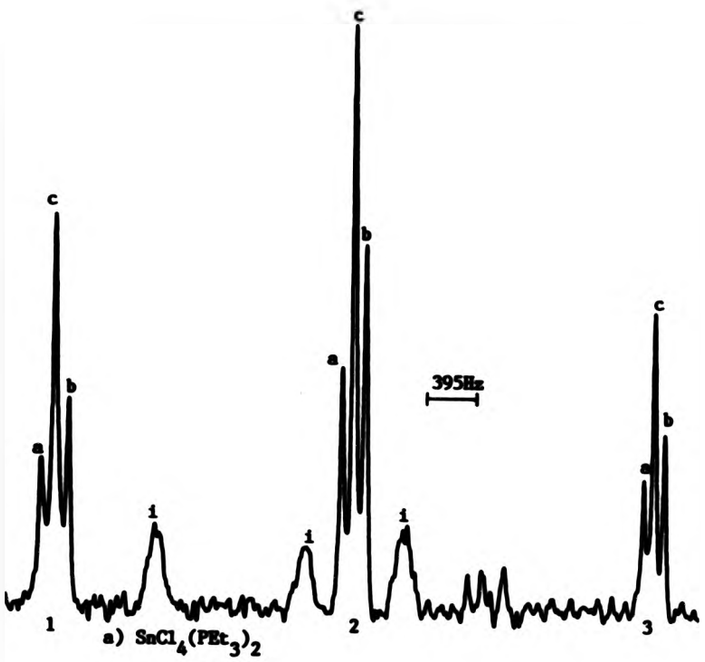

a) $SnCl_4(PEt_3)_2$

b) $SnCl_4(PBu^n_3)_2$

c) $SnCl_4(PEt_3)(PBu^n_3)$

i) impurity

FIG.3.VII Comparison Of The Signs Of $^{2}K(PP)$ And $^{1}K(PSn)$

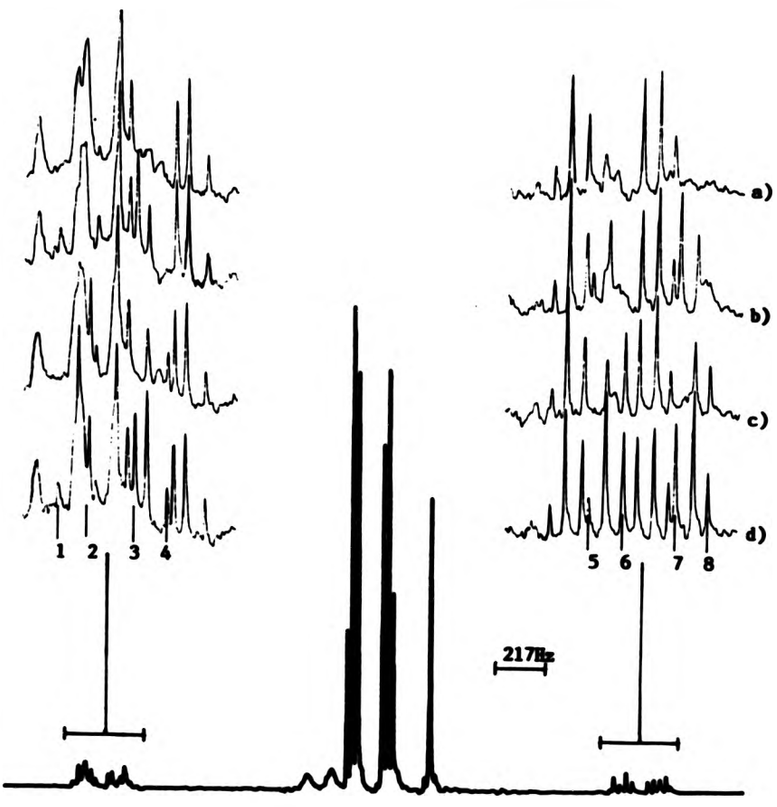

See FIG.3.V for labelling of lines

a) Irradiation at ^{119}Sn line 2 (See FIG.3.VI)

b) Irradiation at ^{119}Sn line 1 (See FIG.3.VI)

c) Irradiation at ^{119}Sn line 3 (See FIG.3.VI)

d) NO ^{119}Sn irradiation

magnitudes (and possibly the signs) of the coupling constants involved in each case will be different. The exception is the coupling J(AA') [$^2J(^{31}P\text{-}^{31}P)$] the interaction between the two phosphorus nuclei in the molecule.

For an AA'X spin system it is convenient to define the parameters N,L and J (equation 3.1-3.3).

$$N = J_{AX} + J_{A'X} \qquad (3.1)$$

$$L = J_{AX} - J_{A'X} \qquad (3.2)$$

$$J = J_{AA'} \qquad (3.3)$$

In the multiple resonance experiments performed on this type of spin system, it is the relative signs of N and J which are determined. The AA'X spin system is a special case of the ABX spin system and can be analysed in essentially the same way, except it has the simplification that ν_A ($\nu_{A'}$) = ν_B[23] (i.e. in this case both phosphorus nuclei have the same chemical shift). The X part of an AA'X spectrum consists of six lines, two of which (the N lines) are of equal intensity, are separated by N, have a combined intensity equal to half the total intensity of the X spectrum and are symmetrically placed about ν_X. Positioned centrally between the two lines are two <u>degenerate</u> transitions. The remaining two lines are placed symmetrically about the central degenerate pair of lines and may occur either inside or outside (or underneath) the N lines. Their separation is given by S as in equation (3.4).

$$S = (L^2 + 4J^2)^{\frac{1}{2}} \qquad (3.4)$$

FIG. 3.VIII shows the ^{13}C spectrum of $(Et_3P)_2\ SnCl_4$. The methylene lines are a typical example of the X part of an AA'X spectrum in which all five lines are resolved. For the methyl carbon only three lines are seen, the outer S lines being too weak to be detected.

The AA' part of an AA'X spectrum consists of two identical <u>ab</u> (or

FIG.3.VIII ^{13}C Spectrum Of $SnCl_4(PEt_3)_2$

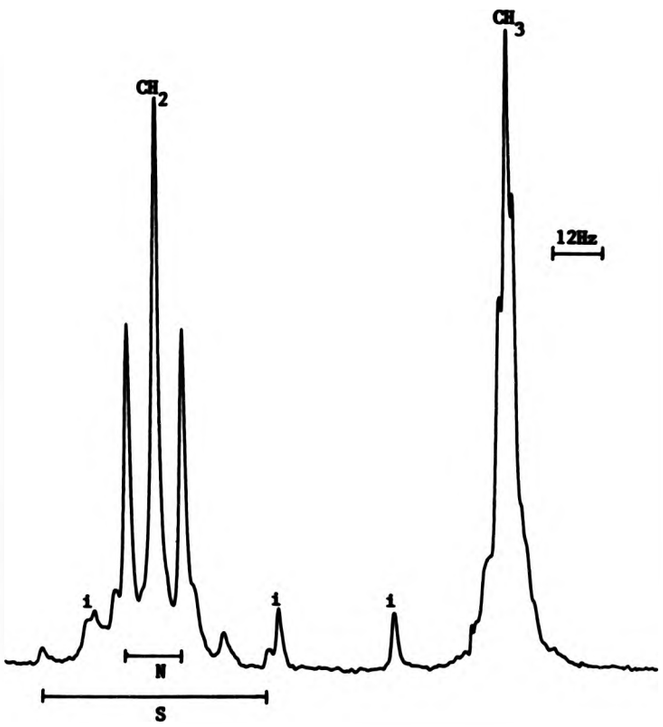

i) impurity

aa') subspectra, which are arranged symmetrically about point ν_A as shown schematically in FIG. 3.IX.

FIG.3.IX Schematic of the AA' part of an AA'X spectrum

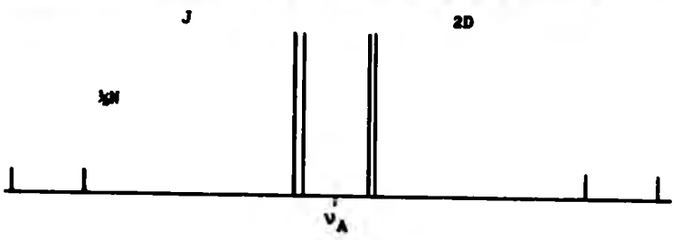

Black lines represent A transitions.

Red lines represent A' transitions.

The first step in analysing this part of the spectrum is to pick out these two quartets. The spacings in the quartets are given by J and N. As can be seen from the list of transition energies in FIG. 3.X, the two other variables, D+ and D-, also determine the position of the lines in the AA' spectrum. These are defined in equation (3.5)

$$D\pm = \tfrac{1}{2}\left([\nu_A - \nu_{A'} \pm \tfrac{1}{2}(J_{AX} - J_{A'X})]^2 + (J_{AA'})^2\right)^{\frac{1}{2}} \qquad (3.5)$$

Since in the AA'X spectrum $\nu_A = \nu_{A'}$ D+ is equal to D-, and the separation between the two aa' quartets is given by 2D as marked in FIG. 3.IX. As the relative magnitudes of the three variables J, N and D are altered, the appearance and ordering of the lines in the spectrum may change. However by cross checking with the X spectrum it should be possible to correctly assign N, J and D.

Due to the low natural abundance of ^{13}C the AA' parts of the spectrum, in the present case, occur as weak satellite peaks of the main ^{31}P resonance, and attempts to identify the aa' subspectra from the ^{31}P

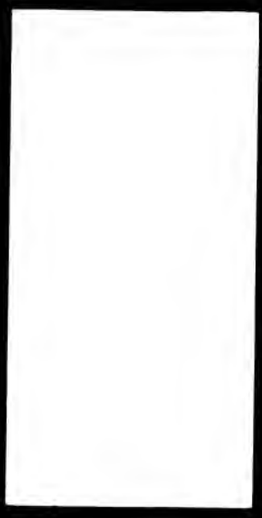

spectrum were unsuccessful. However in the course of ^{13}C - (^{31}P) multiple resonance tickling experiments the positions of these satellites were determined.

As stated previously, the appearance of any spectrum is invariant upon the reversal of all the signs of the coupling constants involved. In the case of an AA'X spectrum, it is also true that the appearance is invariant upon the reversal of the signs of N and J (i.e. the spectrum will have the same appearance with any of the following combinations of signs for N and J; N(+ve)/J(+ve), N(+ve)/J(-ve), N(-ve)/J(+ve), N(-ve)/J(-ve). The double resonance experiments can be described with the aid of the AA'X energy level diagram. There are four possible numbering schemes for the diagram, depending on the signs of N and J. However it is only possible to determine the relative signs of N and J by double resonance experiments. Therefore only two cases need be considered a) where N and J have the same sign, and b) where N and J have opposite signs. FIG. 3.X depicts the energy level diagram in the case that both N and J are positive and FIG.3.XI N positive and J negative. From these energy level diagrams, it can be seen that when lines in the AA' spectrum are irradiated the perturbations caused in the X spectrum will depend on the relative signs of N and J. The schematic spectra given above each energy level diagram relates to the case where X is the methylene carbon and all lines in the X spectrum can be resolved. There are two possible appropriate (^{13}C-$\{^{31}P\}$) experiments that can be performed on this system; either 1) the outer lines of the AA' spectrum (lines 1, 2, 7, 8) can be irradiated, the results of which are shown by the way the N lines in the X spectrum are perturbed; or 2) the inner lines of the AA' spectrum (lines 3, 4, 5, 6) can be irradiated, the

results of which are shown by the way the S lines in the X spectrum are perturbed.

1) If line 1 in the ^{31}P spectrum is irradiated and N and J are of like sign (FIG. 3.X applies), then energy levels 8 and 6 are involved. This will result in the low frequency N line (line b) and lines c or d being perturbed. However if N and J are of opposite sign (FIG. 3.XI applies) then energy levels 5 and 2 are affected. This will result in the high frequency N line (line e) and lines c or d, being perturbed. One of the two degenerate X transitions (lines c and d) is perturbed, no matter what the relative signs of N and J, since energy level 6 is affected in the first case and energy level 5 in the second case. By examining the two energy level diagrams it can be seen that irradiation of either low frequency outer AA' lines will perturb the same N line (the same being true of the high frequency lines). However one line will be regressively associated to the N line (e.g. line 2 and line b in FIG. 3.X and line 1 and line 3 in FIG. 3.XI) and the other progressively associated (e.g. line 1 and line b in FIG. 3.X and line 2 and line e in FIG. 3.XI). At low power irradiation levels this will lead to there being different perturbation effects on the N line, as described in the previous chapter, depending on which of the two A or A' lines is irradiated. This can be seen in FIG. 3.XII which shows the results of these experiments. Irradiation of lines 1 and 2 perturbed line e, and irradiation of lines 7 and 8 perturbed line b. Therefore N and J are of opposite sign. Also it can be seen that irradiation of lines 2 and 8 cause only apparent line broadening in the perturbed lines. This is because the irradiated and perturbed transitions are progressively associated and line splitting is accompanied by an increase in intensity due to spin population transfer and line broadening.

FIG. 3.X

N>0
J>0

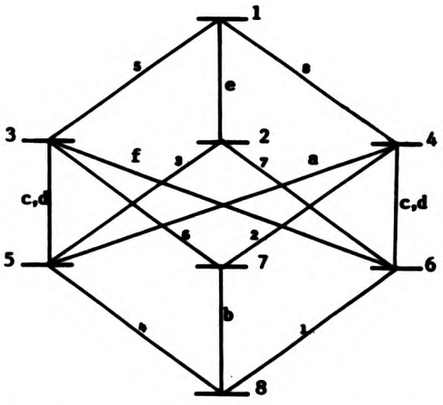

Transition	Origin	Energy	Line Number
8–6	A'	$\nu_A - \frac{1}{2}J - \frac{1}{2}N - D-$	1
7–4	A'	$\nu_A - \frac{1}{2}J + \frac{1}{2}N - D+$	2
8–2	A'	$\nu_A + \frac{1}{2}J - \frac{1}{2}N - D-$	3
3–1	A'	$\nu_A + \frac{1}{2}J + \frac{1}{2}N - D+$	5
8–5	A	$\nu_A - \frac{1}{2}J - \frac{1}{2}N + D-$	4
7–3	A	$\nu_A - \frac{1}{2}J + \frac{1}{2}N + D+$	6
6–2	A	$\nu_A + \frac{1}{2}J - \frac{1}{2}N + D-$	7
4–1	A	$\nu_A + \frac{1}{2}J + \frac{1}{2}N + D+$	8
8–7	X	$\nu_X - \frac{1}{2}N$	b
8–3	X	ν_X	} c, d
6–4	X	ν_X	
2–1	X	$\nu_X + \frac{1}{2}N$	e
5–4	X	$\nu_X - D+ - D-$	a
6–3	X	$\nu_X + D+ - D-$	f
7–2	X	$2\nu_A - D_X$ [intensity 0]	

FIG. 3.XI

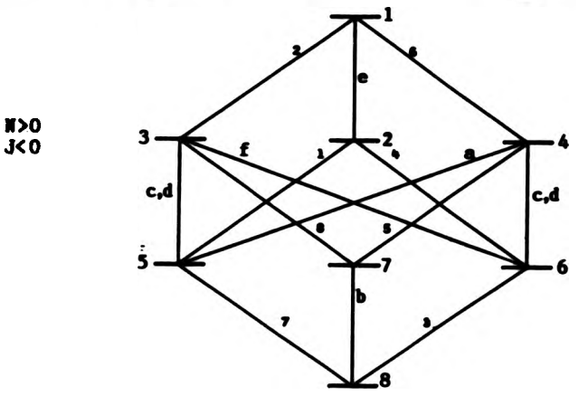

Transition	Origin	Energy	Line Number
8-6	A'	$\nu_A - \frac{1}{2}J - \frac{1}{2}N - D-$	3
7-4	A'	$\nu_A - \frac{1}{2}J + \frac{1}{2}N - D+$	5
5-2	A'	$\nu_A + \frac{1}{2}J + \frac{1}{2}N - D-$	1
3-1	A'	$\nu_A + \frac{1}{2}J + \frac{1}{2}N - D+$	2
8-5	A	$\nu_A - \frac{1}{2}J - \frac{1}{2}N + D-$	7
7-3	A	$\nu_A - \frac{1}{2}J + \frac{1}{2}N + D+$	8
6-2	A	$\nu_A + \frac{1}{2}J - \frac{1}{2}N + D-$	4
4-1	A	$\nu_A + \frac{1}{2}J + \frac{1}{2}N + D+$	6
8-7	X	$\nu_X - \frac{1}{2}N$	b
5-3	X	ν_X	) c, d
6-4	X	ν_X	
2-1	X	$\nu_X + \frac{1}{2}N$	e
5-4	X	$\nu_X - D+ - D-$	a
6-3	X	$\nu_X + D+ + D-$	b

FIG.3.XII Comparison Of The Signs Of J And N(CH_2)

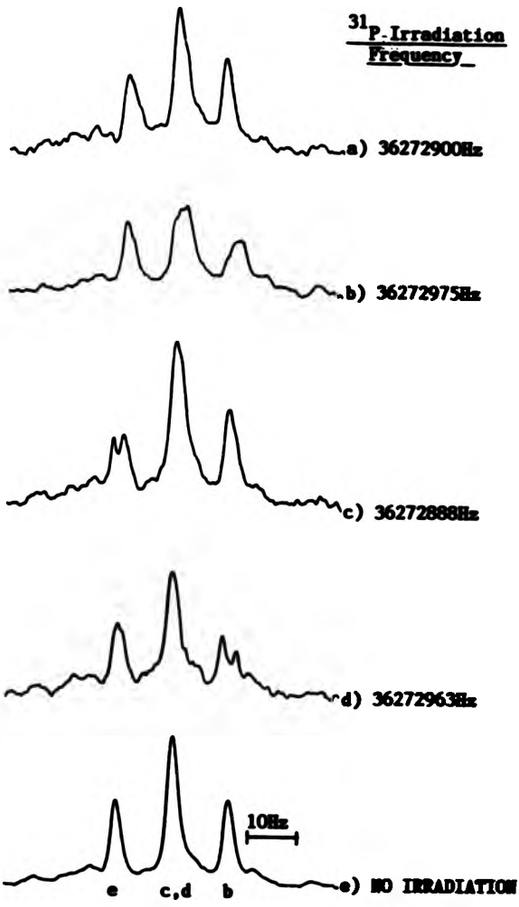

a) Irradiation at ^{31}P line 2 (See FIG.3.XI)] Line Broadening
b) Irradiation at ^{31}P line 8 (See FIG.3.XI)]
c) Irradiation at ^{31}P line 1 (See FIG.3.XI)] Line Splitting
d) Irradiation at ^{31}P line 7 (See FIG.3.XI)]
e) NO ^{31}P Irradiation

2) The inner lines of the AA' spectrum have the aa' quartets overlapping closely. Lines 3 and 4, and lines 5 and 6 are only separated by at most a few Hertz. It is not possible to irradiate one line without affecting the adjacent line in either pair. In fact the maximum perturbation of the X spectrum is achieved when irradiating at the average frequency of either pair of lines. From the energy level diagrams in FIG. 3.X and 3.XI it can be seen that all four lines; 3, 4, 5 and 6 share energy levels with the N lines b and e. However, no statement about the relative signs of N and J can be made from the way these lines are perturbed. Since lines 3 and 4 are irradiated simultaneously, energy levels 8 and 2 are affected, no matter what the relative signs of N and J, and the same population transfer effects (i.e. increase in intensity of line e and decrease of intensity of line b) are seen. When lines 5 and 6 are irradiated the opposite effects occur to lines b and e to those obtained by irradiating lines 3 and 4. Also, when lines 3 and 4 are irradiated either energy level 5 or level 6 is affected, depending on the relative signs of N and J. This will cause one of the S lines to be perturbed, and from this the required result can be deduced. This is shown in FIG. 3.XIII, which agrees with the result from method 1) which is that N and J have opposite signs, where X is the methylene carbon.

In the case of the methyl carbon the S lines cannot be resolved in the X spectrum. This eliminates the possibility of using method 2) to compare the signs of N and J for this spin system. Also since N is only 6.2 Hz (measured from ^{13}C spectrum) the separation between each pair of outer lines is only 3.1 Hz ($^{N}/_{2}$) and the maximum perturbation effect will be achieved when irradiation is applied at the average frequency of the two lines. The energy level diagrams in FIG. 3.X and 3.XI show that

FIG.3.XIII Comparison Of The Signs Of J And N(CH_2)

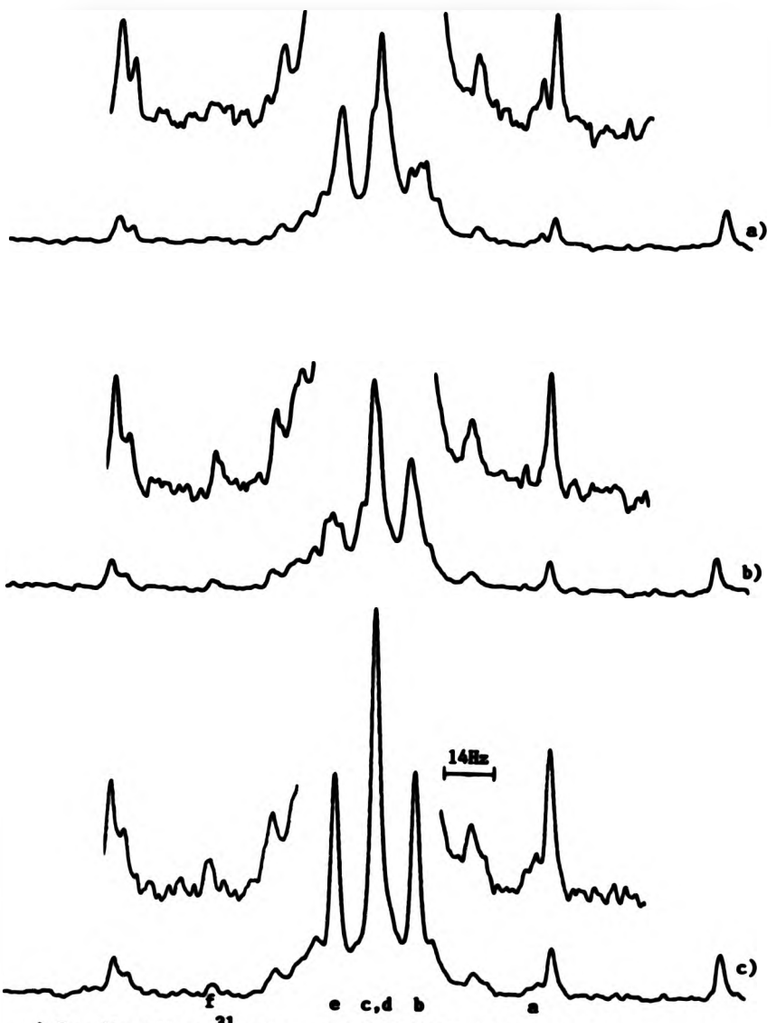

a) Irradiation at ^{31}P lines 3,4 (36272920Hz)(See FIG.3.XI)
b) Irradiation at ^{31}P lines 5,6 (36272931Hz)(See FIG.3.XI)
c) NO Irradiation

both lower frequency outer lines (line 1 and 2) in the AA' spectrum are associated with the same N line in the X spectrum, and so irradiation of both lines 1 and 2 simultaneously will perturb only one N line. This is line b, as shown in FIG. 3.XIV, and therefore J and N are of like sign, where X is the methyl carbon. This is the opposite result to that obtained for the methylene carbon. Therefore $N(CH_2)$ is of opposite sign, and $N(CH_3)$ is the same sign, as $^{2}J(^{31}P\text{-}^{31}P)$.

FIG.3.XIV Comparison Of The Signs Of J And N(CH_3)

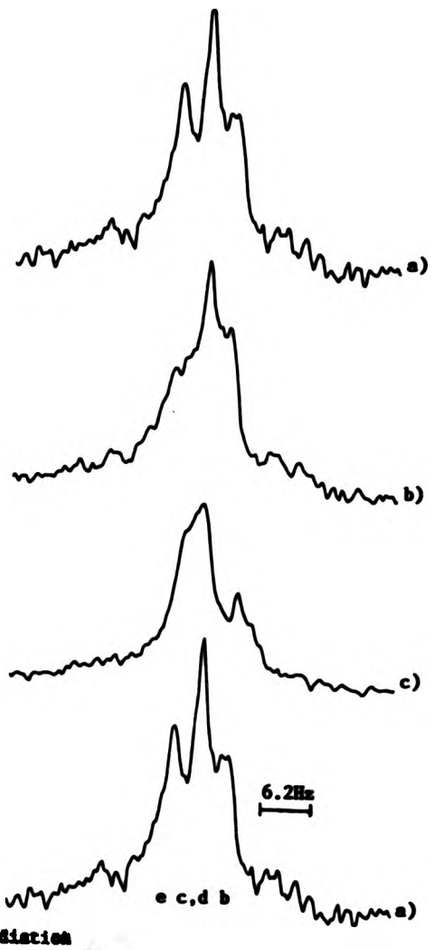

a) NO Irradiation

b) Irradiation at ^{31}P lines 7,8 (36272949Hz)(See FIG.3.X)

c) Irradiation at ^{31}P lines 1,2 (36272876Hz)(See FIG.3.X)

3.6 $AA'M_3M'_3M_2M'_2X$ Spin System (A, A' = ^{31}P; M, M', M, M' = ^{1}H; X = ^{13}C)

The previous experiments yielded the relative signs of the coupling constants $^{2}J(^{31}P\text{-}^{31}P)$, $^{1}J(^{119}Sn\text{-}^{31}P)$, $^{1}J(^{31}P\text{-}^{13}CH_2)$ and $^{3}J(^{31}P\text{-}^{13}CH_2)$ [combined in the form of the variable N_{CH_2}] and $^{2}J(^{31}P\text{-}^{13}CH_3)$ and $^{4}J(^{31}P\text{-}^{13}CH_3)$ [combined in the form of the variable N_{CH_3}]. The next step is to place the signs of the above coupling constants on an absolute basis. This requires that the sign of one of these coupling constants be compared with the sign of a coupling constant for which the absolute sign is known.

It has been shown that in organophosphorus compounds, for the molecular fragment P-C-C-H, the coupling $^{3}J(^{31}P\text{-}^{1}H)$ is positive[1] irrespective of the phosphorus oxidation state provided there are not serious steric distortions. The sign of N_{CH_3} can be compared to that of $^{3}J(^{31}P\text{-}^{1}H)$ (in the experiments described in this section, the sign of N_{CH_3} is actually compared to $[^{3}J(^{31}P\text{-}^{1}H) + {}^{5}J(^{31}P\text{-}^{1}H)]$, however $^{5}J(^{31}P\text{-}^{1}H)$ may be considered to be negligible) by performing selective proton decoupling experiments on the proton-coupled ^{13}C spectrum of the methyl carbon. Irradiating the appropriate part of the methyl proton multiplet will cause the selective decoupling of parts of the methyl carbon multiplet. Depending on the relative signs of the couplings being compared the decoupled ^{13}C lines will be the central line (line c, d in FIG. 3.X) and one of the M lines (line b or e in FIG. 3.X).

This proposed selective decoupling experiment involves a very complex spin system, which is defined as $AA'M'_3M_3M'_2M_2X$ where A,A' = ^{31}P, M',M = methyl protons, M',M = methylene protons and X = ^{13}C. Therefore there is some difficulty in locating the appropriate transitions in the proton spectrum to irradiate. An alternative method

of obtaining the same information is to perform a two-dimensional broad-band decoupled carbon/proton correlation experiment[3] on the molecule. This correlates the chemical shifts of directly bound carbons and protons. In this case the desired correlation is between the methyl proton and methyl carbon chemical shifts. The next section therefore gives a general description of two-dimensional N.M.R. and proton/carbon chemical shift correlation in particular.

3.7 Two-Dimensional N.M.R.[3]

In normal one-dimensional Fourier transform spectroscopy, a time-domain signal (the Free Induction Decay), excited by a short radio frequency pulse, is converted by Fourier transformation into a frequency-domain signal (the spectrum). Only one time variable (transforming to one frequency variable) is involved.

In two-dimensional N.M.R. two time variables (transforming to two frequency variables) are involved. The first time variable (t_1) relates to the evolution period, immediately prior to the period during which the Free Induction Decay is detected as a function of the second time variable (t_2). If a series of experiments are performed with regular increments of t_1, the N.M.R. signal can be represented by a matrix $S(t_1, t_2)$. Two Fourier transformations are performed, first with respect to t_2 and then with respect to t_1, to yield a spectrum which is a function of two orthogonal frequency dimensions $S(F_1,F_2)$. The spectrum can be thought of as a surface in three-dimensional space, with certain vertical sections through the surface corresponding to the conventional concept of a one-dimensional spectrum. A two-dimensional experiment relates the behaviour of the nuclear spins during t_1, to their behaviour during t_2. Each spectral component processes at its characteristic frequency during t_1, passing on information (usually in the form of

phase or amplitude) to the appropriate spectral component during the detection period. The experiment correlates information about the evolution period, when the receiver is inactive, with information about the detection period, when the N.M.R. response is acquired. By arranging for different experimental conditions to prevail during t_1 and t_2, it is possible to separate different N.M.R. parameters, for example chemical shifts and spin couplings constants, into the two frequency domains F_1 and F_2. There are three main categories of two-dimensional experiments:

a) Shift Correlation Spectroscopy; in which the chemical shifts of coupled nuclei, exchanging nuclei or nuclei which have a cross-relaxation interaction, are correlated.

b) J-spectroscopy; in which the chemical shifts of different nuclei and the scalar coupling are separated and then correlated.

c) Multiple Quantum Spectroscopy, which facilitates the detection of multiple quantum transitions.

The two-dimensional experiment performed on $(PEt_3)_2SnCl_4$ was of the shift correlation type, where the correlated nuclei were spin-coupled and effective chemical shifts were correlated (since coupling to a third nucleus was present).

3.8 Proton-Carbon Chemical Shift Correlation

Two-dimensional correlation N.M.R. experiments show a relationship between two different resonances, the chemical shift of each type of resonance is displayed along one of the two frequency axes. If in a two-dimensional spectrum, a cross-peak occurs at (δA, δB), this means that the nuclei A and B have a mutual interaction. Nucleus A and B can be either of the same (homonuclear) or different (heteronuclear shift correlation) species. Depending on the type of experiment, different

types of interaction can be shown. These include homonuclear scalar coupling, heteronuclear scalar coupling, cross-relaxation and chemical exchange.

The proton-carbon chemical shift correlation experiment relates the chemical shifts of directly bound carbon atoms and protons, via the heteronuclear scalar (usually one-bond) coupling.

Consider a ^{13}C nucleus directly bound to a proton. The ^{1}H and ^{13}C spectra will each consist of two lines separated by $^{1}J(^{13}C-^{1}H)$. FIG. 3.XV a) gives the appropriate energy level diagram at Boltzmann equilibrium. The deviation from the mean population given for each level reflects the fact that ^{1}H signals are inherently four times as strong as ^{13}C signals, due to the relative magnetogyric ratios.

FIG. 3.XV Energy Level Diagrams for a proton coupled to a carbon Nucleus

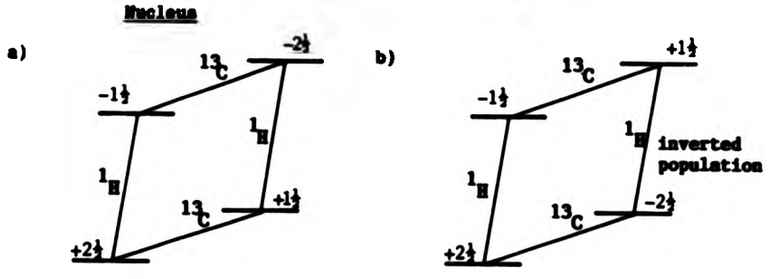

If a 180° pulse is selectively applied to only one of the proton transitions, the population will be inverted across the transition as shown in FIG. 3.XV b), which gives the new deviations from the mean population for each energy level. Since the ^{13}C transitions share energy levels with the proton transitions, the intensities of the ^{13}C signals are affected. One ^{13}C transition shows an increase in intensity of five times and the other of three times and is inverted. The ^{13}C signals are four times as strong as the equilibrium signals.

In the two-dimensional experiment selectivity of population inversion is achieved by exciting the proton transitions with two 90° pulses separated by t_1. The extent of nuclear precession during t_1 is given by equation (3.6).

$$\phi = 2\pi\,(\delta^1H \pm \tfrac{1}{2}J)t_1. \qquad (3.6)$$

When $\phi = 2n\pi$ the two 90° pulses behave like a single 180° pulse and invert the spin populations. When $\phi = (2n+1)\pi$ the two 90° pulses cancel each other out leading to unchanged Boltzmann equilibrium populations. For intermediate angles ϕ, population inversion is incomplete. This gives a cosine modulation of the spin populations as a function of t_1. Since the ^{13}C transitions share energy levels with the proton transitions, the intensities of the ^{13}C signals are also modulated according to equation (3.6) if a ^{13}C read pulse is applied immediately after the two 90° proton pulses.

The pulse sequence actually used is given in FIG. 3.XVI.

FIG. 3.XVI

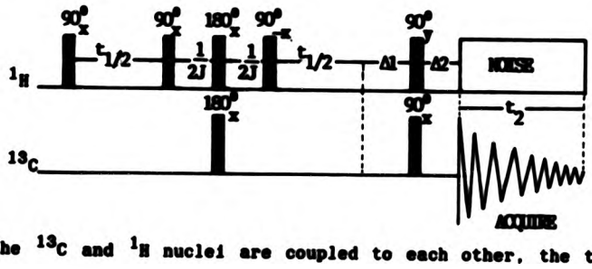

Since the ^{13}C and ^{1}H nuclei are coupled to each other, the two-dimensional Fourier transform of the experiment will yield four lines because coupling between the nuclei appears in both the ^{13}C and ^{1}H dimensions. For chemical shift correlation, this multiplet structure is unnecessary and is removed from both chemical shift dimensions leaving the protons and ^{13}C nuclei effectively decoupled.

This is achieved during t_1 by a 180°-pulse applied to ^{13}C half way

through t_1, which causes the two diverging magnetization vectors to refocus at the end of t_1. During t_2, noise decoupling is used. To prevent the mutual cancellation of the two anti-phase signals when these doublets collapse, the two delays Δ_1 and Δ_2 are introduced. The values $\Delta_1 = \frac{1}{2}J$ and $\Delta_2 \approx \frac{1}{2}\Delta_1$ allow 180° relative precession of these vectors before they are combined. Also since J is the one bond ^{13}C-^{1}H coupling, signals originating from magnetization transfer via long range ^{13}C-^{1}H couplings are minimized, since the corresponding vectors have insufficient time to precess from the anti-phase conditions, and they cancel each other out. Also included in the pulse sequence is a set of pulses applied to $^{1}H(90^{\circ}_{x} - (\frac{1}{2}J) - 180^{\circ}_{x} - (\frac{1}{2}J) - 90^{\circ}_{y})$ at the same time as the 180° ^{13}C refocussing pulse. This has the result of effectively decoupling from one another all protons except inequivalent ones attached to the same carbon atom (i.e. fine structure due ^{1}H-^{1}H coupling is removed from the ^{1}H dimension). The result of all these modifications to the basic experiment is a spectrum that has one peak per pair of coupled nuclei, the coordinates of which are given by the appropriate ^{13}C and ^{1}H chemical shifts. Another modification to the pulse sequence is to cycle the phases of the radio frequency pulses and the receiver. This has the effect of eliminating any small axial peaks, due to pulses not having ideal lengths.

3.9 Determination Of The Relative Signs Of Spin-Spin Coupling Constants Via Two-Dimensional Shift Correlation N.M.R.

As mentioned in the previous section, carbon-to-proton couplings are removed from both carbon and proton dimensions of the two-dimensional shift correlation spectrum. However in Bis(triethylphosphine) tin (IV) tetrachloride, the carbons and protons are coupled to a third nuclear species namely phosphorus. The spin

states of phosphorus are unaffected during the two-dimensional experiment and the coupling to phosphorus appears in each dimension of the spectrum. The different lines in the proton and carbon dimensions, due to coupling to phosphorus, are associated with the different spin states of the phosphorus nuclei. There are two phosphorus nuclei in the molecule under consideration. Therefore there are four possible combinations of phosphorus spin states as shown in FIG. 3.XVII.

FIG. 3.XVII

Spin ^{31}P 1st	State ^{31}P 2nd	
+½	+½	
+½	-½	} These spin states are mixed and
-½	+½	} cannot be assigned straight
-½	-½	} forwardly.

The methyl signal in the proton dimension and in the carbon dimension appears as three lines, each associated with different combinations of phosphorus spin states. Since the spectra are 2nd order, not all the lines can be exclusively assigned to one combination of spin states. However the outer lines of each triplet can be assigned to either the (+½, +½) or the (-½, -½) state exclusively and it is from the behaviour of these lines in the 2D experiment that the required result is obtained. Each of the lines in the triplet is treated by the two-dimensional correlation experiment as an effective chemical shift and a cross-peak appears in the two-dimensional spectrum, relating the effective chemical shifts of the directly bonded carbon and proton nuclei associated with the same combinaton of phosphorus spin states. For example a cross-peak will appear for the methyl proton line

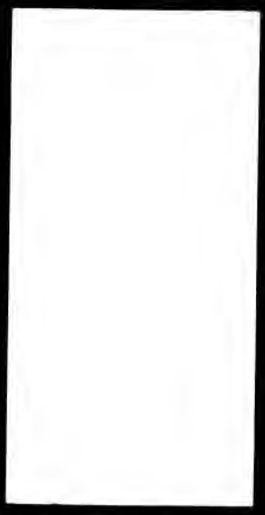

associated with the (+½, +½) combination of phosphorus spin states and the methyl carbon line associated with the (+½, +½) combination of phosphorus spin states. For an observed nucleus X coupled to a nucleus Y, the sign of the X-Y coupling determines which lines in the X multiplet are associated with the different spin states of Y. Therefore, since the experiment shows which carbon and proton lines are associated with the same combination of phosphorus states, it is possible to derive the relative signs of the carbon-to-phosphorus and proton-to-phosphorus couplings. For example, a particular combination of phosphorus spin states (either +½, +½ or -½, -½) is associated with the high frequency line in the methyl carbon dimension of the two-dimensional spectrum. If the phosphorus-to-carbon coupling is of the same sign as the phosphorus-to-proton coupling, the high frequency line of the methyl proton dimension will be associated with that same particular combination of phosphorus spin states, giving the appropriate cross-peak in the two-dimensional spectrum. However if the two couplings are of opposite sign, the low frequency line in the proton dimension will be associated with that particular combination of phosphorus spin states, giving a different cross-peak in the two-dimensional spectrum. As can be seen from FIG. 3.XVIII, which shows the contour plot of the two-dimensional spectrum, the second case applies and the phosphorus-to-carbon coupling is therefore of opposite sign to the phosphorus-to-proton coupling. Another advantage over the selective decoupling experiment is that the two-dimensional experiment also yields the relative signs of the phosphorus to carbon and phosphorus to proton couplings for the methylene carbon and protons. As can be seen from FIG. 3.XVIII these are also of opposite sign.

For both the methyl and methylene signals the carbon and protons

FIG.3.XVIII Contour Plot Of The C-H Chemical Shift Correlation Spectrum Of $SnCl_4(PEt_3)_2$

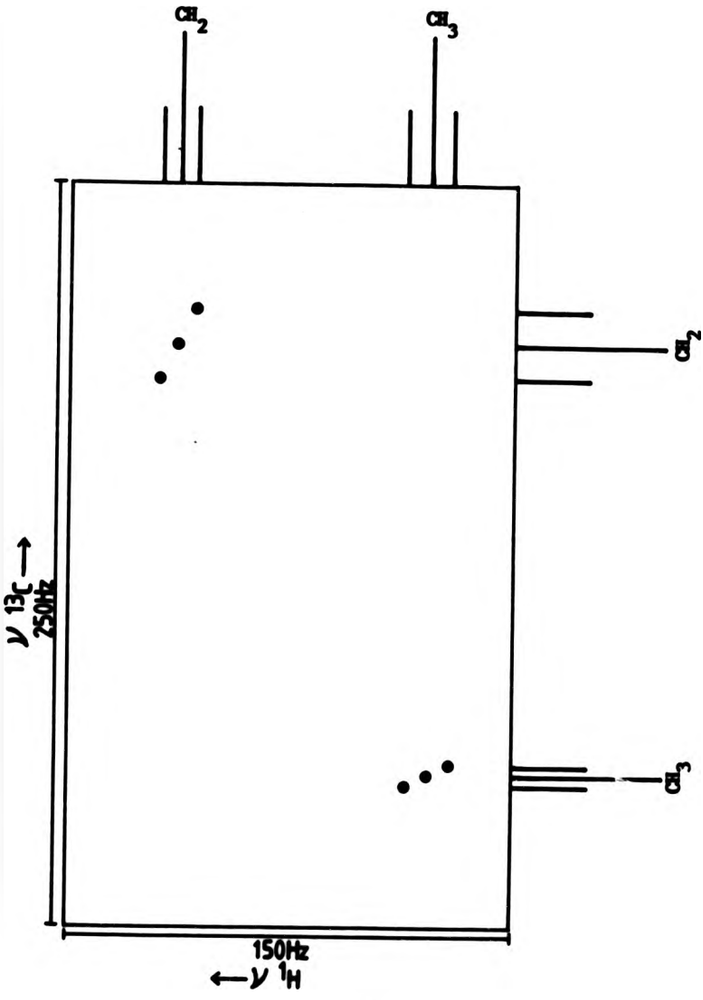

give second order spectra, and consist of pseudo-triplets in both dimensions. These can be described as the X parts of AA'X spectra where A,A' = ^{31}P and X = ^{13}C or ^{1}H appropriately. This type of spin system is discussed in the previous section of this chapter and the projection of the whole two-dimensional spectrum on to the carbon axis gives the proton decoupled ^{13}C spectrum as in FIG. 3.VIII. For both types of carbon, the outer S lines are too weak to be detected, and only the central and N lines are present in the carbon dimension. Therefore the carbon-to-phosphorus coupling present in the two-dimensional spectrum is given by N_{CH_2} and N_{CH_3} which are defined by equation (3.1). Similarly for the proton dimension the proton-to-phosphorus coupling can be described by equation (3.1) with the outer lines in the two proton pseudo-triplets being the N lines of AA'X spectra. Thus as stated earlier the sign of N_{CH_3} is actually compared with the sign of [$^{3}J(^{31}P-^{1}H)$ + $^{5}J(^{31}P-^{1}H)$] and the sign of N_{CH_2} is compared to the sign [$^{2}J(^{31}P-^{1}H)$ + $^{4}J(^{31}P-^{1}H)$]. $^{5}J(^{31}P-^{1}H)$ will be negligible compared to $^{3}J(^{31}P-^{1}H)$ and so can be discounted for the purpose of determining the relative signs of coupling constants. Since $^{3}J(^{31}P-^{1}H)$ is known to be positive,[2] this places all the other signs of the various coupling constants on an absolute basis, as shown in table (3.1).

Table 3.1

^{31}P and ^{119}Sn N.M.R. data

Compound (a)	$\delta(^{119}Sn)$ /ppm	$\delta(^{31}P)$ /ppm	$^1J(^{119}Sn^{31}P)$ /Hz (b)	$^2J(^{31}P^{31}P$ /Hz (c)
$SnCl_4(PEt_3)_2$	-572	20.9	-2391	-44.9
$SnCl_3Br(PEt_3)_2$	-671	17.5	-2278	
trans-$SnCl_2Br_2(PEt_3)_2$(d)	-771	14.0	-2170	
cis -$SnCl_2Br_2(PEt_3)_2$(d)		13.0	-2164	
$SnClBr_3(PEt_3)_2$	-867	8.3	-2056	
$SnBr_4(PEt_3)_2$	-910	2.4	-1947	
$SnCl_4(PBu^n_3)_2$	-576	16.7	-2437	
$SnCl_4(PEt_3)(PBu^n_3)$ (e)	-575	20.5	-2419	-44.7
(f)		16.0	-2430	

^1H and ^{13}C N.M.R. data

$SnCl_4(PEt_3)_2$ (a)	$\delta(^{13}C)$ /ppm	$\delta(^1H)$ /ppm	$^1J(^{13}C^{31}P)$ /Hz (g)	$^2J(^{13}C^{31}P)$ /Hz (h)	$^3J(^{13}C^{31}P)$ /Hz (i)
CH_2 (j)	19.5	2.1	22.3		0.6
CH_3 (k)	7.0	1.2		-6.2	

(a) run in CH_2Cl_2 at room temperature.

(b) $^1K(SnP)$ + ve

(c) $^2K(PP)$ -ve

(d) Smaller intensity peak assigned to cis species since steric hinderance will favour having the two bromine atoms trans.

(e) PEt_3

(f) PBu^n_3

(g) $^1K(CP)$ + ve

(h) $^2K(CP)$ - ve

(i) $^3K(CP)$ + ve

(j) $^2J(^1H^{31}P)+^4J(^1H^{31}P)$ = -11.8 Hz

(k) $^3J(^1H^{31}P)+^5J(^1H^{31}P)$ = +15.8 Hz

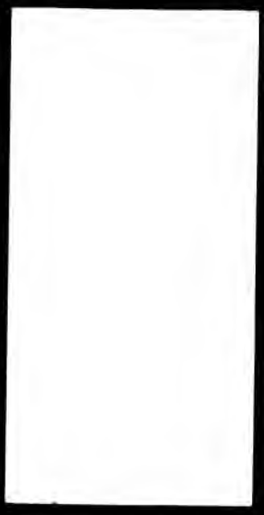

3.10 Discussion

The $^1K(Sn-P)$ coupling in $[(PEt_3)_2\ SnCl_4]$ is the first such coupling for which a positive sign has been determined. All other previous Sn-P reduced couplings for which the signs are known are negative[4]. Also the negative $^2K(P-P)$ coupling via tin is only the second such coupling for which the sign has been determined. The previous positive coupling was reported for $(CH_3)_2Sn[P(C_6H_5)_2]_2$[5].

Previous studies where the signs of $^1K(Sn-P)$ couplings have been determined have concerned triorganostannylphosphines and their complexes[4]. In the uncoordinated compounds, where the phosphorus has an electron lone pair, $^1K(Sn-P)$ is large and negative. When the lone pair is used in complexation, $^1K(Sn-P)$ decreases in magnitude, becoming less negative. This behaviour parallels that of $^1K(P-C)$ in analogous phosphine compounds [2]. However upon complexation $^1K(P-C)$ becomes positive. This can be explained by a large negative contribution in the tin-containing compounds due to a larger energy gap between the phosphorus and tin valence orbitals. In such compounds where the tin is four-coordinate and the bonds are tetrahedrally arranged, the tin is approximately sp^3 hybridized.

The compound under consideration here is six-coordinated, with the bonds arranged octahedrally around the tin atom to which the phosphorus is complexed. At first glance it would appear that the tin is acting more like a transition metal and any analogy to the behaviour of carbon in phosphines is inappropriate. However on closer examination, there are serious drawbacks to drawing too close a comparison with P-M couplings in transition metal complexes.

Before considering the type of bonding involved in bis-phosphino tin(IV) tetrahalides, the available evidence should be considered.

$^1K(Sn-P)$ is large and positive indicating large 5s and 3s contributions from tin and phosphorus, respectively, to the bond between them. The existence of the phosphorus 3s contribution is supported by the magnitude and sign of the P-C and P-H couplings in the coordinated, compared to the uncoordinated phosphine[2]. These follow the expected trends, with $^2K(P-C)$ and $^2K(P-H)$ becoming more positive, indicating the hybridization of phosphorus goes from being near p^3 to being near sp^3 when complexed. This is also supported by the X-ray structure of $(PEt_3)_2SnCl_4$[6], where the average C-P-C inter bond angles (107.1°) are less than the tetrahedral angle (109.5°), and the average C-P-Sn bond angles (111.8°) are greater, indicating that the bonds to phosphorus form a distorted tetrahedron, with the bond to tin including a greater proportion of s character than the bonds to carbon.

It has been demonstrated that $^1J(^{119}Sn-^{31}P)$ decreases with increased phenyl substitution of the phosphine[7]. This parallels the behaviour of $^1J(M-P)$ in other group B metal complexes where M is Hg^{II} [8] or Cd^{II}. [9] However in complexes of Pt^{II}, W^0 and Rh^I, [10] $^1J(M-P)$ increases with phenyl substitution of the phosphine. This increase has been explained by invoking $d\pi - d\pi$ bonding.[11] The phenyl groups increase the π-acceptor ability of the phosphine, and the synergic effect, where metal back donation of π-electrons increases the phosphine σ-donor ability leading to an increase in $^1J(M-P)$. More recent discussions[12] have ascribed this increase in $^1J(M-P)$ to changes in the s wavefunction at phosphorus and the s-character of the phosphorus lone pair. In the group B metal complexes, which show the opposite trend, analysis of the X-ray structures indicates that the metal-phosphorus bonds are relatively weak.[6] In such cases the steric effects of the

phenyl groups on phosphorus may outweigh any changes in the d-orbitals on the phosphorus, leading to an increase in the M-P bond length and a decrease in ^{1}J(M-P). The relatively long P-M bond length is also consistent with the absence of dπ -dπ bonding; the filled d-orbitals on the metal being strongly bound and of too low energy to participate in π-electron back-donation to the phosphorus d-orbitals. In this case the steric effects of the phenyl groups will also be dominant.

In mixed halide, bis-phosphine tin(IV) tetrahalides, the magnitude of $^{1}J(^{119}Sn-^{31}P)$ depends on the identity of the four halides cis to the phosphine. In the mixture of compounds resulting from the reaction of triethylphosphine with an equimolar mixture of tin(IV) tetrabromide and tin(IV) tetrachloride, the products are consistent with the two phosphorus ligands being trans to one another. This confirms the result given by the X-ray structure[6] for the solid state and inferred from Raman and infrared results.[13] The assignment of the different components of the mixture, is based on the expected statistical abundances of the different combinations of halides, compared to the relative intensities of the peaks in the ^{31}P spectrum (see FIG. 3.XIVa). This was confirmed by examining a similar mixture where tin(IV) tetrabromide was present in a 2:1 ratio to tin(IV) tetrachloride (see FIG. 3.XIVb). The dependence of $^{1}J(^{119}Sn-^{31}P)$ on the halides cis to phosphorus has also been found in Tri-n-butylphosphine tin(IV) pentahalides.[14] In these compounds however the identity of the halide (Br or Cl) trans to the phosphine has a negligible effect on $^{1}J(^{119}Sn-^{31}P)$. Also, an increase in $^{1}J(^{119}Sn-^{31}P)$ occurs when the halide trans to the phosphine is replaced by tri-n-butylphosphine[14] and a further increase occurs when the tri-n-butylphosphine is replaced by a methyl group.[15] A plot of $^{1}J(^{119}Sn-^{31}P)$ against n(where n = 0-4 in

FIG.3.XIVa ^{31}P Spectrum Of $SnCl_nBr_{4-n}(PEt_3)_2$ (n=0-4,ratio Cl:Br=1:1)

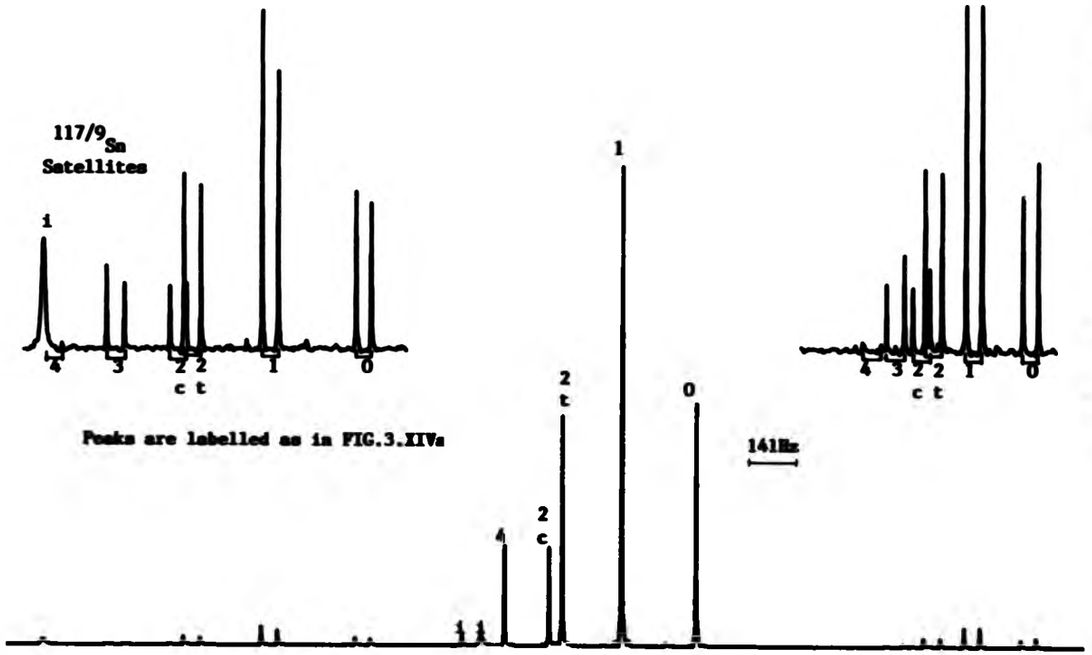

FIG.3.XIVb ^{31}P Spectrum Of $SnCl_{4-n}(PEt_3)_n$ (n=0-4, ratio Cl:Et=1:2)

$(PEt_3)_2SnCl_nBr_{4-n}$) is linear (see FIG. 3.XV) showing that the effect of exchanging a bromide for a chloride ligand is additive. If the change in $^1J(^{119}Sn-^{31}P)$ was due to the greater electronegativity of chloride compared to bromide, the nature of the halide trans to the phosphine would produce a similar effect on the coupling constant in $[(Bu^n_3P)SnCl_nBr_{5-n}]^-$. [14] However the effect may be caused by steric hindrance, with the greater bulk of bromide causing the weak Sn-P bond to be longer the more bromide ligands there are on the tin. This would lead to $^1J(^{119}Sn-^{31}P)$ decreasing as the number of bromides on tin increases. The X-ray structure of $(PEt_3)_2SnCl_4$ shows that the geometry at tin is not perfectly octahedral[6]; with the bond angles and bond lengths for the chloride ligands not all being equal. Replacement with bulkier bromide ligands may increase this distortion, leading to a change in the hybridization of tin, thereby increasing the s-character of the tin-halide bonds, with a concomitant decrease in the s-character of the Sn-P bonds and a resultant decrease in $^1J(^{119}Sn-^{31}P)$. Both or either of these effects may be responsible for the changes in the magnitude of $^1J(^{119}Sn-^{31}P)$, when the nature of the halide cis to phosphorus is changed.

As the ligand trans to the phosphorus is changed, $^1J(^{119}Sn-^{31}P)$ increases in the order $Br \sim Cl < PR_3 < CH_3$.[14, 15] If, in the compound under consideration, $^1K(Sn-P)$ had been negative (as in all previous sign determinations), then the change in magnitude of $^1J(^{119}Sn-^{31}P)$ (i.e. $^1K(Sn-P)$ becoming more negative) would be as predicted by the "trans-influence",[12] as manifested in many transition metal complexes. The "trans-influence" of a ligand in a metal complex is defined as the extent to which that ligand weakens the bond trans to itself in the equilibrium state of a complex. In a metal-phosphine complex containing

FIG.3.XV

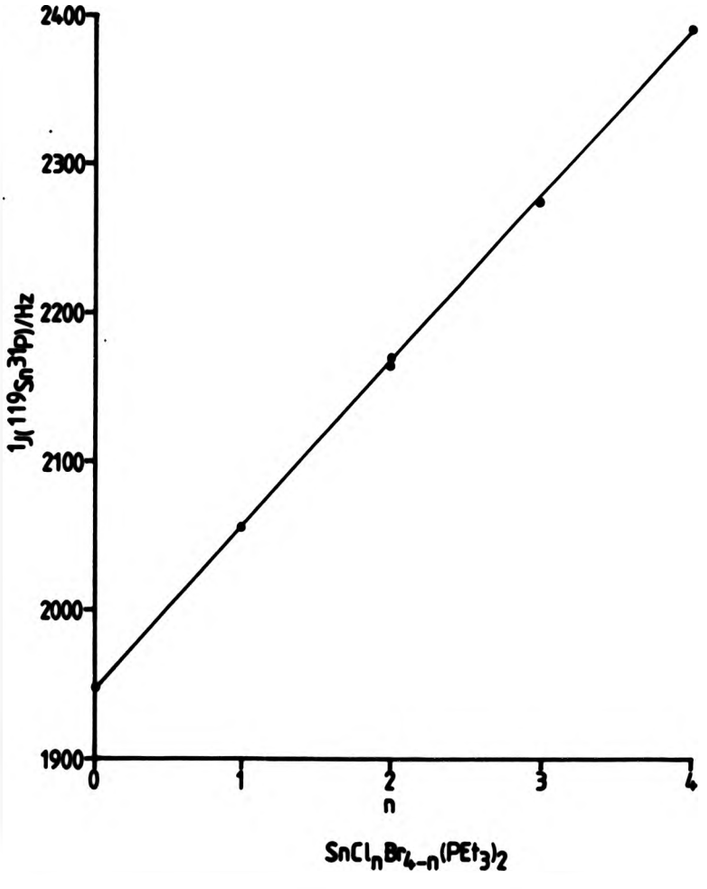
2400
2300
2200
2100
2000
1900
$^1J(^{119}Sn^{31}P)/Hz$
0
1
2
3
4
n
$SnCl_nBr_{4-n}(PEt_3)_2$

a ligand *trans* to the phosphine, an increase in that ligand's *trans*-influence causes a decrease in the size of $^{1}J(P\text{-}M)$ (i.e. the coupling becomes more negative) and generally the order of "*trans*-influence" for the ligands under consideration is $CN_3 > PR_3 > Cl \sim Br$. Since $^{1}K(Sn\text{-}P)$ is positive, the trend in the coupling constant goes counter to that expected.

However the "*trans*-influence" has been mainly studied in relation to transition metal complexes. The trends observed in these compounds have been rationalized in terms of changes in the metal hybridization. The best ligand-metal orbital overlap occurs when the hybrid orbitals on the metal and the ligand orbital, used in bonding, are of approximately the same energy. Thus the metal hybridization changes, so that the metal hybrid orbital is nearer the required energy of the ligand. This affects the hybridization of the other metal hybrid orbitals used in bonding to other ligands. The transition metal orbitals available for bonding are the (n-1)*d*, n*s* and n*p*, and any changes in *p*- and *d*-orbital character of a hybrid orbital, will most effect the hybrid orbital *trans* to it. The difference between transition metals and tin is that on tin the (n-1)*d* (i.e. the 4*d*) orbitals are filled and are unavailable for bonding. Therefore if *d*-orbitals are to be used by tin in forming octahedral complexes the hybridization will be sp^3d^2 and the n*d* -(i.e. 5*d*) orbitals will be used in bonding. The energy of a hybrid orbital is determined by the different amounts of *s*, *p* and *d*-orbitals from which it is constructed and the energy of those *s*, *p* and *d* orbitals. In bonding in octahedral complexes, the *d*-orbitals used in transition metal complexes are of lower energy than the *s* and *p* orbitals, whereas in tin complexes they are of higher energy than the *s* and *p* orbitals. Therefore, if in order to achieve a better orbital overlap, a ligand

requires the energy of the bonding metal-hybrid orbital to be lowered, a transition metal will increase the d-character (i.e. reduce the s and p-character) of the hybrid orbital, whereas tin will increase the s-character (i.e. reduce the p and d-character) of the hybrid orbital. Thus by changing the relative ordering of the energies of the s, p and d orbitals available for hybridization, a change in the relative *trans*-influence of different ligands will result in different changes in the s-character of the hybrid orbitals *trans* to the ligand. An increase in *trans*-influence will cause an increase in the s-character in the case of tin and a decrease in the s-character in the case of a transition metal.

Possibly the most striking evidence that bonding in phosphine complexes of tin(IV) halides differs significantly from that in analogous transition metal complexes is given by the negative sign and small magnitude of the phosphorus-to-phosphorus coupling. In an analogous transition metal complex a $^{2}J(^{31}P^{M}{}^{31}P)$ coupling of a similar magnitude (44.7-37.5 Hz) and sign would be consistent with the two phosphorus atoms being in a *cis* arrangement,[11a] whereas *trans* couplings are generally positive and greater in magnitude than *cis* couplings.[11b]

The phosphorus-to-phosphorus coupling constant is also an exception to Jamesons's explanation of two-bond couplings,[16] discussed in Chapter 1 and given in equation (1.9). Since $^{1}K(Sn\text{-}P)$ is positive, so are the terms S_X and S_Y in the equation. Therefore in order to achieve a negative $^{2}K(PP)$, the third term, F_{XMY} must be negative. However since the two phosphorus atoms are *trans* to each other the X-M-Y bond angle is greater than 110° and normally this would lead to F_{XMY} being positive. Previously, exceptions have occurred only when the intervening atom X has had an electron lone pair, for example $^{2}K(PC)$ via selenium.[17]

An alternative rationale, following Pople and Santry's molecular

orbital approach, has been proposed to explain the signs of $^{2}J(^{31}P_{M}{}^{31}P)$ in certain octahedral transition metal complexes.[11,18] Assuming that the Fermi-contact term dominates the coupling, the sign and magnitude of $^{2}J(^{31}P^{31}P)$ are determined by the symmetries and energies, respectively, of the dominant electronic transition(s), which appear in the mutual polarisability given by equation (1.4). An excitation from one orbital to another, where the phosphorus p-orbital contributions to the molecular orbital have the same symmetry (i.e. sym -> sym or antisym -> antisym) gives a negative contribution to the coupling constant, whereas a transition from one orbital to another of different symmetry, gives a positive contribution. Only excitations between occupied and unoccupied molecular orbitals where both coupled phosphorus nuclei contribute p-character to both the orbitals involved make any contribution at all. FIG. 3.XVI shows a simplified molecular orbital diagram for a transition metal d^{6} system.

For a coupling between two phosphorus nuclei cis to each other only transitions involving occupied and unoccupied a_{1g} and e_{g} orbitals make contributions.

FIG. 3.XVI

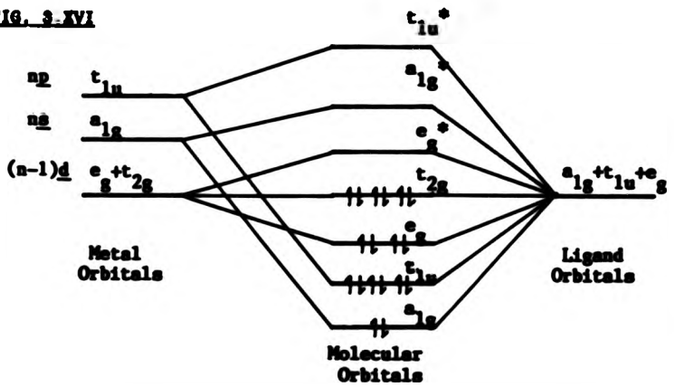

The transitions e_g -> e_g^* and a_{1g} -> a_{1g}^* make negative contributions and the transitions e_g -> a_{1g}^* and a_{1g} -> e_g^* make positive contributions. Since the contribution from a particular transition is proportional to the inverse of the energy difference between the occupied and unoccupied molecular orbitals, the e_g -> e_g^* transition dominates and cis $^2J(^{31}P^{31}P)$ is negative.

For a coupling between two phosphorus nuclei trans to each other, transitions between a_{1g}, e_g and t_{1u} orbitals are involved and the contributions from each transition, with the appropriate numerical weightings, to allow for the number of degenerate levels in each molecular orbital, relative signs and coefficients are given in table (3.2)

Table 3.2

Contributions to $^2J(^{31}P_M{}^{31}P)$			
Transition	Contribution	Transition	Contribution
a_{1g} -> a_{1g}^*	$-1/\Delta a_{1g}a_{1g}^*$	t_{1u} -> a_{1g}^*	$+3/\Delta t_{1u}a_{1g}^*$
a_{1g} -> e_g^*	$-2/\Delta a_{1g}e_g^*$	e_g -> e_g^*	$-4/\Delta e_g e_g^*$
a_{1g} -> t_{1u}^*	$+3/\Delta a_{1g}t_{1u}^*$	e_g -> t_{1u}^*	$+6/\Delta e_g t_{1u}^*$
t_{1u} -> e_g^*	$+6/\Delta t_{1u}e_g^*$	e_g -> a_{1g}^*	$-2/\Delta e_g a_{1g}^*$
t_{1u} -> t_{1u}^*	$-9/\Delta t_{1u}t_{1u}^*$		

It follows that $^2J(^{31}P^{31}P)$ is positive since the dominant contributions are from the positive t_{1u} -> e_g^* and e_g -> t_{1u}^* transitions, which have large numerical weightings and in the case of t_{1u} -> e_g^* a relatively small energy difference. In Verkade's treatment[18], the effect is also considered of changing the relative energy of the phosphorus ligands σ-orbital compared to that of the other ligands (specifically-CO) on the transition metal. As the relative energy of the carbonyl σ- and the phosphorus σ-orbitals changes, so does

the dominant transition, due to changes in the phosphorus s-orbital coefficients of the different molecular orbitals. Generally the energy of the carbonyl σ-orbitals is higher than that of the phosphorus σ-orbitals and the t_{1u} -> e_g^* transition dominates, but as the energy of the phosphorus σ-orbital reaches parity with the carbonyl σ-orbital the negative e_g -> e_g^* transition dominates and finally if the energy of the phosphorus σ-orbital exceeds that of the carbonyl σ-orbital the e_g -> a_{1g}^* may come to dominate giving a negative contribution to trans-$^2J(^{31}PW^{31}P)$. For the cis coupling the dominant transition is always negative even though changes in the relative energies of the phosphorus and carbonyl σ-orbitals causes different transitions to dominate cis $^2J(^{31}PW^{31}P)$.

Since tin will use nd rather than (n-1)d-orbitals, for bonding in octahedral complexes, as indicated earlier, the molecular orbital diagram changes and the relative ordering of the molecular orbitals is different as shown in FIG. 3.XVII.

FIG. 3.XVII

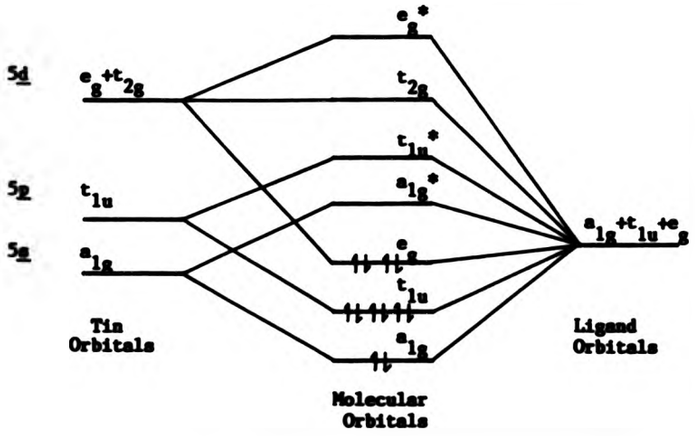

The symmetries of the different molecular orbitals remain the same as in FIG. 3.XV, so that the numerical weightings and relative signs of the different transitions which contribute to trans $^2J(^{31}P_M{}^{31}P)$ given in table (3.2) still apply. However since the ordering of the excited states has changed, the energy difference between occupied and unoccupied molecular orbitals for each transition is different. The t_{1u} -> e_g^* transition is no longer dominant, due to the large increase in the energy difference between the molecular orbitals. The transition with the lowest energy difference is e_g -> a_{1g}^*, which contributes negatively to $^2J(^{31}P_M{}^{31}P)$. However the two transitions with the next lowest energy difference are e_g -> t_{1u}^* and t_{1u} -> a_{1g}^* which make positive contributions. If there is significant tin 5p-character in the tin-phosphorus bond, there will be large phosphorus p-orbital coefficients for the t_{1u} molecular orbital and these two transitions become dominant. However this effect will be counteracted by the negative contribution from the t_{1u} -> t_{1u}^* transition which although it has a larger energy difference, also has a large numerical weighting. In the compound under consideration $^2J(^{31}P_{Sn}{}^{31}P)$, is small and negative, indicating a balance between these contributions with the negative contribution from e_g -> a_{1g}^*, and possibly t_{1u} -> t_{1u}^*, being dominant. Small changes in the p-orbital coefficients of the different molecular orbitals can cause relatively large changes in $^2J(^{31}P{}^{31}P)$ under these conditions.

The geometries of six-coordinate tin(IV) compounds, of similar type to the ones under consideration here, have been successfully predicted by the valence shell electron pair repulsion theory.[10] However this theory does not provide any information about hybridization of the tin orbitals. The ^{119}Sn Mossbauer data[6,13] for $[(PR_3)_2SnCl_4]$ has been

interpreted to indicate that there is little participation by tin 5*d*-orbitals in σ-bonding, and that in the absence of significant tin-phosphorus *d*Π-*d*Π bonding, a large proportion of tin 5*s*-character is concentrated in the tin-phosphorus bond. From this interpretation a bonding model has been suggested where the atom use the 5*s*- and one 5*p*-orbital in bonding to phosphorus and the remaining two 5*p*-orbitals are used to form "three-centre" bonds with two chlorines[20]. This model adequately predicts the sign and magnitude of $^{1}J(^{119}Sn^{31}P)$. However with this model, $^{2}J(^{31}P^{31}P)$ would be expected to be positive and probably of larger magnitude than is actually found.

This model was originally used with reference to compounds without electronegative substituents[21], where the *d*-orbitals could be rather diffuse. The presence of four electronegative chlorine ligands attached to the tin may mean that the total exclusion of the tin 5 *d*-orbitals from bonding is not justified in the complexes under consideration. However, the conventional sp^3d^2 hybridization description for octahedral complexes does not account for the high tin 5 *s*-orbital character of the tin-phosphorus bond. A compromise between the two descriptions is probably more appropriate, with the hybridization being a distortion of sp^3d^2 with more *s*-character concentrated in the hybrid orbitals directed towards phosphorus.

3.11 References

1) E. L. Mackor, C. McLean, J. Chem. Phys., 44, 64, (1966).

2) W. McFarlane, Proc. Roy. Soc. A, 306, 185 (1968).

3) R. Freeman, Proc. R. Soc. A., 373, 149 (1980).

4) W. McFarlane, D. S. Rycroft, J. C. S. Dalton, 1977, (1974).

5) J. D. Kennedy, W. McFarlane, G. S. Pyne, B. Wrackmeyer, J. Organomet. Chem., 186, (1980) 285.

6) G. G. Mather, G. McLaughlin, A. Pidcock, J. C. S. Dalton, 1823, (1973).

7) J. F. Malone, B. E. Mann, Inorg. Nucl. Chem. Lett., 8, 819, (1972).

8) R. L. Keiter, S. O. Grim, Chem. Comm., 521, (1968).

9) B. E. Mann, Inorg. Nucl. Chem. Lett., 7, 595, (1971).

10) B. E. Mann, C. Masters, J. C. S. (A), 1104, (1971); S. O. Grim, D.A. Wheatland, W. McFarlane, J. A. C. S, 89, 5573 (1967); S. O. Grim, D. A. Wheatland,. Inorg. Nucl. Chem. Lett., 4, 187 (1968); B. E. Mann, C. Masters, B. L. Shaw, J. C. S. Dalton, 704, (1972); S. O. Grim, R. L. Keiter, W. McFarlane, Inorg. Chem., (1967), 6, 1133.

11) a) R. M. Lynden-Bell, J. F. Nixon, J. Roberts, J. R. Swain, W. McFarlane, Inorg. Nucl. Chem. Lett., 7, 1187, (1971).

b) A. Pidcock, J. F. Nixon, Ann. Rep. N.M.R. Spectrosc, 2, (1969), 345.

12) T. G. Appleton, H. C. Clark, L. E. Manger, Coord. Chem. Rev., 10, (1973), 335.

13) A. J. Carty, T. Hinsperger, L. Mihichuk, N. D. Sharma, Inorg. Chem., (1970), 9, 2573.

14) R. Colton, D. Dakternieks, C. Harvey, Inorg. Chim. Acta, 61, (1982), 1.

15) V. S. Petrosyan, N. S. Yashina, E. I. Gefel, Si. Ge. Sn. and Pb. Compounds, 9, 213, (1986).

16) C. J. Jameson, J.A.C.S., 91, 6232, (1969).

17) W. McFarlane, J. A. Nash, Chem. Comm., 913, (1969).

18) R. D. Bertrand, F. B. Ogilvie, J. G. Verkade, J.A.C.S., 92, 1908, (1970).

19) R. F. Zahrobsky, J.A.C.S., 93, 3313, (1971).

20) R. Okawara, M. Wada, Advan. Organomet. Chem., 5, 137, (1967).

21) M. M. McGrady, R. S. Tobias, J.A.C.S., 87, 1909, (1963).

22) J. G. Verkade, L. D. Quin, "Phosphorus-31 N.M.R. Spectroscopy in Stereochemical Analysis", VCH, (1987).

23) R. A. Hoffman, S. Forsén, B. Gestblom, "N.M.R. Basic Principles and Progress", Vol. 5, Eds. P. Diehl, E. Fluck, R. Kosfeld, Springer-Verlag, (1971).

CHAPTER 4

COMPOUNDS CONTAINING A TRANSITION METAL-GROUP IV BOND

4.1 Introduction

There has been considerable interest in compounds containing a heavier group IV element (Si, Ge, Sn, Pb) directly bonded to a transition metal.[1] This arises from a number of different reasons including; metal-metal bond formation, synthesis of analogues of organic derivatives and the catalytic activity shown by some of these species. With the advent of modern multinuclear Fourier transform N.M.R. spectrometers, there has been recent interest in studying certain of these compounds by observing the spectra of the coordinated transition-metal nuclei and of the attached group IV element.[2,3] This has produced a considerable body of data concerning spin-spin coupling between the group IV element and the transition metal[2,4,5,6] and also between the group IV element and magnetic nuclei of other ligands in the complex,[2,5,7-10] which has proved a great aid in molecular structure determination and as an indicator of electronic distribution. In order properly to interpret the data (especially in the latter case), it is necessary not only to know the magnitudes of the coupling constants, but also their signs. To this end, multiple resonance experiments were carried out on a number of transition-metal complexes with tin and lead ligands. The majority of work in the literature (which gives the magnitudes, but not the signs of the coupling constants has concerned complexes with the M-$SnCl_3$,[3,4,6,7,8] moiety (M is most commonly Pt, or Rh) and more recently square-planar platinum complexes with $R_nX_{3-n}M'$,[5,11] (R = aryl, alkyl group, X = halogen, n = 0 to 3, M' =Sn, Pb) groups as ligands. These ligands often have formal electronic and stereochemical resemblances to corresponding complexes of tertiary phosphines and some trends in the pattern of reduced coupling constants

to ^{119}Sn ^{117}Sn and ^{207}Pb show qualitative agreement with the behaviour displayed by ^{31}P. 3,7

Also included in this section is an absolute sign determination upon the coupling constants involved in an organotin chalcogenide, where tin is coordinated to a B-metal, instead of a transition metal as with the other compounds in this Chapter.

In this chapter the spin systems upon which multiple resonance experiments were performed can generally be described as first order. Therefore a standard notation can be used to describe them, and the signs of the coupling constants can be deduced from the results. In the case of exceptions further details are given in the appropriate section.

The first order spin systems generally involved in the following multiple resonance experiments are adequately described by the AMX spin system given in Chapter 2. Each experiment is illustrated by giving schematic diagrams drawn to scale of the various spectra of the spin system involved and showing the associations between the lines of the different spectra as revealed by the multiple resonance experiments. From this are deduced the relative signs of the coupling constants involved.

4.2 KEY TO EXPERIMENTS

a) For each Compound are given:-

1) Structure

2) N.M.R. parameters:-

Chemical shifts are given in ppm relative to the appropriate standard, positive shifts being to higher frequency. Chemical shift standards are H_3PO_4 (^{31}P), Me_4Sn (^{119}Sn and ^{117}Sn), Me_4Si (^{1}H) Na_2PtCl_6 (^{195}Pt), Me_4Pb (^{207}Pb)

Coupling constants are in Hertz.

3) Samples were run as solutions in CH_2Cl_2.

4) Spectra were run at room temperature, unless otherwise stated.

b) For Each Sign Comparison Multiple Resonance Experiment:-

1) Diagram of molecular structure labelled to show specific isotopomer being considered in the following experiments. Each chemically different N.M.R. active nucleus or group of nuclei is alphabetically labelled.

2) Coupling constants to be compared.

3) Stick diagram of N.M.R. spectra of observed and irradiated nuclei for specific isotopomer being considered.

4) List of lines in the spectrum of the irradiated nucleus, at which irradiation was applied, cross referenced to the lines perturbed in the observed spectrum.

5) Statement of relative signs of the coupling constants.

c) A selection of spectra are given at the end of the Chapter to demonstrate the variety of multiple resonance experiments performed. For those experiments illustrated, the reference number is given with the coupling constants to be compared (item b) 2) above).

4.3 Trans - $[Pt(PEt_3)_2(SnCl_3)_2]^7$

$\delta(^{31}P)$	$\delta(^{119}Sn)$	$\delta(^{195}Pt)$	$^1J(^{195}Pt^{119}Sn)$	$^1J(^{195}Pt^{31}P)$	$^2J(^{119}Sn^{31}P)$
8.4	-41	-5062	23529	1671	236

$^2J(^{119}Sn^{117}Sn)$ (temp -80°C)

34674

A)

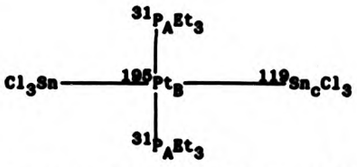

Comparison of signs $^1KSn_CPt_B$ / $^1KP_APt_B$

Observed nucleus ^{31}P

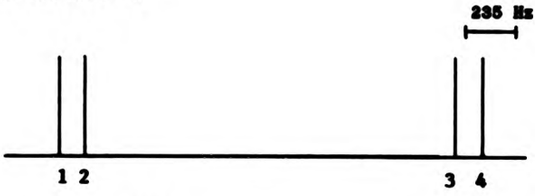

Irradiated nucleus ^{119}Sn

Line at which irradiation is applied	Line(s) perturbed
^{119}Sn 2	^{31}P 2, 4
^{119}Sn 5	^{31}P 1, 3

$^{1}KSn_{C}Pt_{B}$ and $^{1}KP_{A}Pt_{B}^{20}$ have the same sign

(+ ve) (+ ve)

Comparison of signs $^{2}KP_{A}Sn_{C}$ / $^{1}KPt_{B}Sn_{C}$

observed nucleus ^{31}P

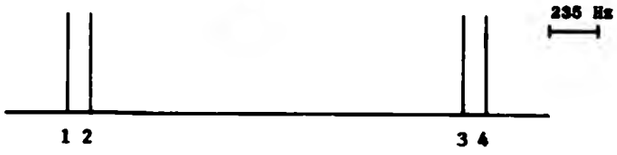

Irradiated nucleus ^{195}Pt

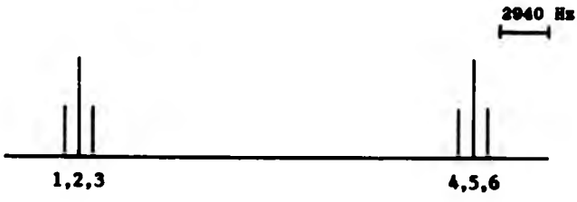

Line at which irradiation is applied	Line(s) perturbed
^{195}Pt 2	^{31}P 2, 4
^{195}Pt 5	^{31}P 1, 3

$^{2}KP_{A}Sn_{C}$ and $^{1}KPt_{B}Sn_{C}$ have opposite signs

(- ve) (+ ve)

B)

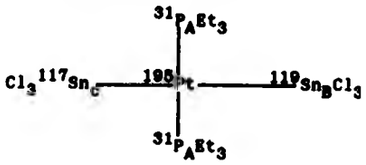

Comparison of signs $^{2}KSn_{B}Sn_{C}$ / $^{2}KSn_{C}P_{A}$

observed nucleus ^{31}P

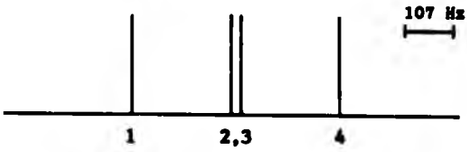

Irradiated nucleus ^{119}Sn

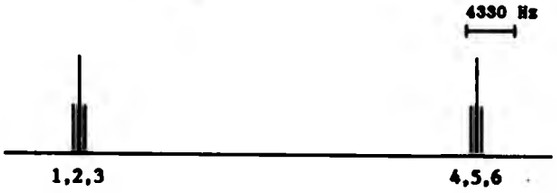

Line at which irradiation is applied	Line(s) perturbed
^{119}Sn 2	^{31}P 4
^{119}Sn 5	^{31}P 1

$^{2}KSn_{C}Sn_{B}$ and $^{2}KP_{A}Sn_{C}$ have opposite signs

(+ ve) (- ve)

4.4 Trans - $[Pt(PPh_3)_2(SnCl_3)H]$ [12]

$\delta(^{31}P)$	$\delta(^{1}H)$	$\delta(^{119}Sn)$	$\delta(^{195}Pt)$	$^{1}J(^{31}P^{195}Pt)$	$^{1}J(^{195}Pt^{119}Sn)$	$^{1}J(^{195}Pt^{1}H)$
28.2	-8.74	129	-5195	2648	11348	1300

$^{2}J(^{31}P^{119}Sn)$	$^{2}J(^{31}P^{1}H)$	$^{2}J(^{119}Sn^{1}H)$	(temp - 90°C)
215	8.8	1748	

A)

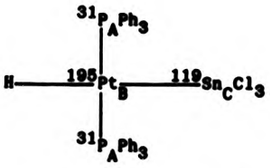

Comparison of signs $^{1}KPt_BP_A$ / $^{1}KPt_BSn_C$ (See FIG. 4.XVII)

Observed nucleus ^{31}P

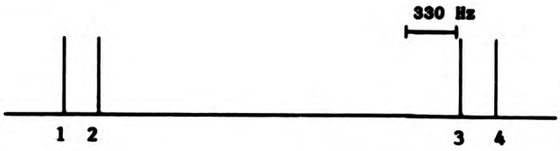

Irradiated nucleus ^{119}Sn

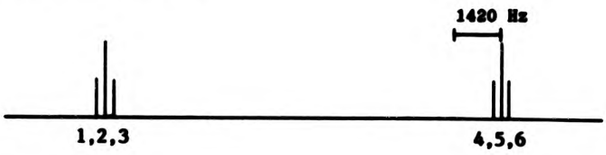

Line at which irradiation is applied	Line(s) perturbed
^{119}Sn 2	^{31}P 1, 2
^{119}Sn 5	^{31}P 3, 4

$^{1}KPt_BP_A$[20] and $^{1}KPt_BSn_C$ have the sign
(+ ve) (+ ve)

B)

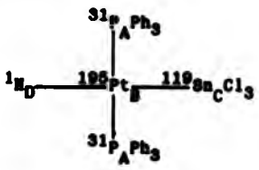

Comparison of signs $^{1}KPt_BSn_C$ / $^{1}KPt_BH_D$ (see FIG. 4.XVIII)

observed nucleus ^{119}Sn

Irradiated nucleus ^{1}H

Line at which irradiation is applied	Line(s) perturbed
^{1}H 2	^{119}Sn 1, 2, 3, 4, 5, 6
^{1}H 5	^{119}Sn 7, 8, 9, 10, 11, 12

$^{1}KPt_BSn_C$ and $^{1}KPt_BH_D$ have the same sign

(+ ve) (+ ve)

C)

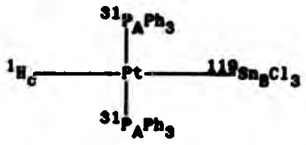

Comparison of signs $^{2}KP_{A}Sn_{B}$ / $^{2}KH_{C}Sn_{B}$

Observed nucleus ^{1}H

Irradiated nucleus ^{31}P

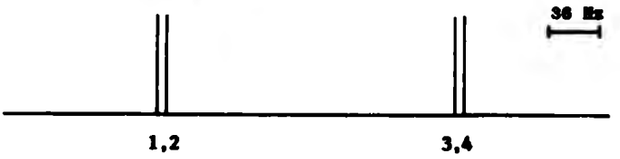

Lines at which irradiation is applied	Line(s) perturbed
^{31}P 1, 2	^{1}H 4, 6
^{31}P 3, 4	^{1}H 1, 3

$^{2}KP_{A}Sn_{B}$ and $^{2}KH_{C}Sn_{B}$ have opposite signs

(-ve) (+ve)

D)

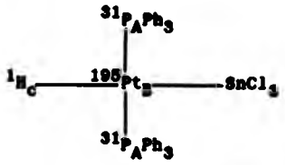

Comparison of signs $^{1}KP_{A}Pt_{B}$ / $^{1}KH_{C}Pt_{B}$ (See FIG. 4.XIX)

Observed nucleus ^{1}H

Irradiated nucleus ^{31}P

Lines at which irradiation is applied	Line(s) perturbed
^{31}P 1, 2	^{1}H 1, 3
^{31}P 3, 4	^{1}H 4, 6

$^{1}KP_{A}Pt_{B}^{20}$ and $^{1}KPt_{B}H_{C}$ have the same sign

(+ve) (+ve)

4.5 Cis-[PtCl($SnCl_3$)(P(p-$CH_3C_6H_4$)$_3$)$_2$][7]

	$\delta(^{31}P)$	$^1J(^{31}P^{195}Pt)$	$^2J(^{31}P^{119}Sn)$	$^2J(^{31}P^{31}P)$
P cis to Sn	7.5	36230	219.0	14.6
P trans to Sn	26.2	3139.6	4271.2	14.6

$\delta(^{119}Sn)$	$\delta(^{195}Pt)$	$^1J(^{119}Sn^{195}Pt)$	
-59	-4718	16321	(temp -50°C)

A)

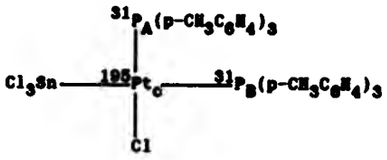

Comparison of signs $^1KP_APt_C$ / $^2KP_AP_B$ and $^1KP_BPt_C$ / $^2KP_AP_B$

Observed nucleus ^{31}P

Irradiated nucleus ^{195}Pt

Line at which irradiation is applied	Line(s) perturbed
^{195}Pt 1	$^{31}P_A$ 4, 8 $^{31}P_B$ 2, 6
^{195}Pt 4	$^{31}P_A$ 3, 7 $^{31}P_B$ 1, 5

$^{1}KP_APt_C^{20}$ and $^{2}KP_AP_B$ have opposite signs

(+ve) (-ve)

$^{1}KP_BPt_C^{20}$ and $^{2}KP_AP_B$ have opposite signs

(+ve) (-ve)

4.6 Cis-[PtCl($SnCl_3$)(P(p-$CH_3OC_6H_4$)$_3$)$_2$] [7]

	$\delta(^{31}P)$	$^1J(^{31}P^{195}Pt)$	$^2J(^{31}P^{119}Sn)$	$^2J(^{31}P^{31}P)$
P cis to Sn	11.1	36647.5	214.8	14.6
P trans to Sn	28.1	3095.7	4301.8	14.6

$\delta(^{119}Sn)$	$\delta(^{195}Pt)$	$^1J(^{195}Pt^{119}Sn)$	
-58	-4742	16650	(temp - 60°C)

A)

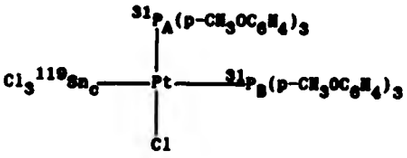

Comparison of signs $^2KP_AP_B$ / $^2KSn_CP_A$ and

$^2KP_AP_B$ / $^2KSn_CP_B$

Observed nucleus ^{31}P

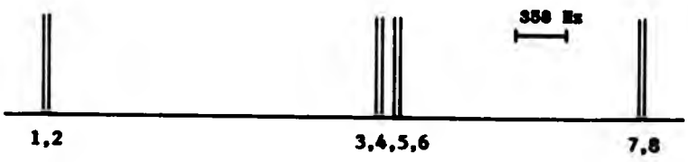

Irradiated nucleus ^{119}Sn

Line at which irradiation is applied	Line(s) perturbed
^{119}Sn 1	$^{31}P_A$ 4, 6 $^{31}P_B$ 1, 7
^{119}Sn 2	$^{31}P_A$ 4, 6 $^{31}P_B$ 2, 8
^{119}Sn 3	$^{31}P_A$ 3, 5 $^{31}P_B$ 1, 7

$^{2}KP_AP_B$ and $^{2}KSn_CP_A$ have the same sign

(-ve) (-ve)

$^{2}KP_AP_B$ and $^{2}KSn_CP_B$ have opposite signs

(-ve) (+ve)

4.7 Cis -[Pt(PPh_3)$_2$($SnPh_2Cl$)Ph] [5]

	$\delta(^{31}P)$	$^1J(^{31}P^{195}Pt)$	$^2J(^{31}P^{119}Sn)$	$^2J(^{31}P^{31}P)$
P trans to Sn	28.3	2681	2392	14.6
P trans to Ph	24.5	2139	149	14.6

$\delta(^{119}Sn)$	$\delta(^{195}Pt)$	$^1J(^{119}Sn^{195}Pt)$
32	-4780	14070

A)

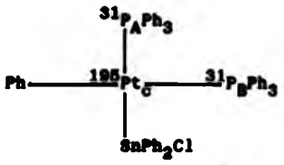

Comparison of signs $^1KP_APt_C$ / $^2KP_AP_B$ and $^1KP_BPt_C$ / $^2KP_BP_A$

Observed nucleus ^{31}P

Irradiated nucleus ^{195}Pt

Line at which irradiation is applied	Line(s) perturbed
^{195}Pt 1	$^{31}P_A$ 2, 8 $^{31}P_B$ 4, 6
^{195}Pt 2	$^{31}P_A$ 1, 7 $^{31}P_B$ 4, 6
^{195}Pt 3	$^{31}P_A$ 2, 8 $^{31}P_B$ 3, 5
^{195}Pt 4	$^{31}P_A$ 1, 7 $^{31}P_B$ 3, 5

$^{1}KP_APt_C^{20}$ and $^{2}KP_AP_B$ have opposite signs

(+ve) (-ve)

$^{1}KP_BPt_C^{20}$ and $^{2}KP_AP_B$ have opposite signs

(+ve) (-ve)

B)

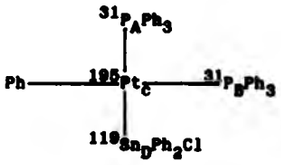

Comparison at signs $^1KSn_DPt_C$ / $^2KSn_DP_A$ and $^1KSn_DPt_C$ / $^2KSn_DP_B$

Observed nucleus ^{31}P

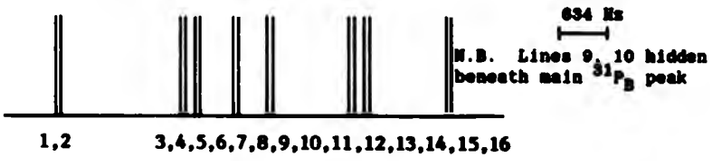

Irradiated nucleus ^{195}Pt

Line at which irradiation is applied	Line(s) perturbed
^{195}Pt 1	$^{31}P_A$ 2 $^{31}P_B$ 6, 14
^{195}Pt 8	$^{31}P_A$ 7, 15 $^{31}P_B$ 3, 11

$^1KSn_DPt_C$ and $^2KSn_DP_A$ have the same signs

(+ve) (+ve)

$^1KSn_DPt_C$ and $^2KSn_DP_B$ have opposite signs

(+ve) (-ve)

Comparison of signs $^{2}KSn_{D}P_{A}$ / $^{2}KP_{A}P_{B}$ and $^{2}KSn_{D}P_{B}$ / $^{2}KSn_{D}P_{A}$

Observed nucleus ^{31}P

Irradiated nucleus ^{119}Sn

Line at which irradiation is applied	Line(s) perturbed
^{119}Sn 1	$^{31}P_{A}$ 1 $^{31}P_{B}$ 4, 6
^{119}Sn 2	$^{31}P_{A}$ 2 $^{31}P_{B}$ 4, 6
^{119}Sn 3	$^{31}P_{A}$ 1 $^{31}P_{B}$ 3, 5

$^{2}KSn_{D}P_{A}$ and $^{2}KP_{A}P_{B}$ have opposite signs

(+ve) (-ve)

$^{2}KSn_{D}P_{B}$ and $^{2}KP_{A}P_{B}$ have the same sign

(-ve) (-ve)

4.8 $(Et_4N)_2$ $[Pt(SnCl_3)_4(PEt_3)]$ [13]

$\delta(^{31}P)$	$\delta(^{119}Sn)$	$\delta(^{195}Pt)$
6.0	-102	-5633

Average coupling constants seen at room temperature

$^1J(^{195}Pt^{31}P)$	$^1J(^{195}Pt^{119}Sn)$	$^2J(^{31}P^{119}Sn)$	$^2J(^{119}Sn^{117}Sn)$
2322	15444	449	6830

A) $[^{195}Pt_B(^{119}Sn_CCl_3)(SnCl_3)_3(^{31}P_AEt_3)]^{2-}$

Comparison of signs $^1KP_APt_B$ / $^1KPt_BSn_C$

Observed nucleus ^{31}P

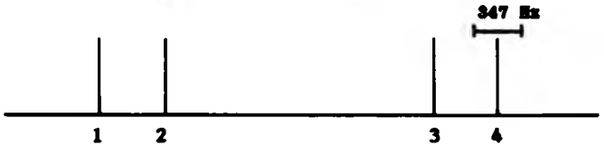

Irradiated nucleus ^{119}Sn

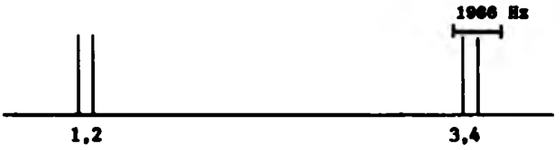

Line at which irradiation is applied	Line(s) perturbed
^{119}Sn 1	^{31}P 1, 2
^{119}Sn 2	^{31}P 1, 2
^{119}Sn 3	^{31}P 3, 4
^{119}Sn 4	^{31}P 3, 4

$^1K(Pt_BP_A)$[20] and $^1K(Sn_CPt_B)$ have the same sign
(+ve) (+ve)

Comparison of signs $^{1}KSn_{C}Pt_{B}$ / $^{2}KSn_{C}P_{A}$

Observed nucleus ^{31}P

Irradiated nucleus ^{195}Pt

Line at which irradiation is applied	Line(s) perturbed
^{195}Pt 1	^{31}P 1, 3
^{195}Pt 2	^{31}P 1, 3
^{195}Pt 3	^{31}P 2, 4
^{195}Pt 4	^{31}P 2, 4

$^{1}KSn_{C}Pt_{B}$ and $^{2}KSn_{C}P_{A}$ have the same sign

(+ve) (+ve)

B) $[Pt(^{119}Sn_BCl_3)(^{117}Sn_CCl_3)(SnCl_3)_2(^{31}P_AEt_3)]^{2-}$

Comparison of signs $^2KP_ASn_C$ / $^2KSn_CSn_B$ (see FIG. 4.XX)

Observed nucleus ^{31}P

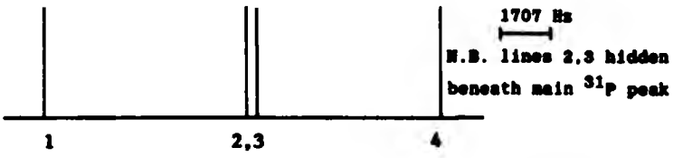

Irradiated nucleus ^{119}Sn

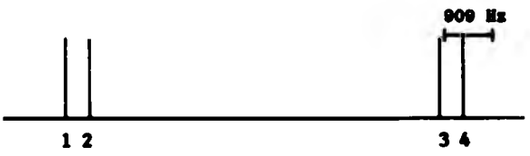

Line at which irradiation applied	Line(s) perturbed
^{119}Sn 1	^{31}P 1
^{119}Sn 2	^{31}P 1
^{119}Sn 3	^{31}P 4
^{119}Sn 4	^{31}P 4

$^2KP_ASn_C$ and $^2KSn_CSn_B$ have the same sign

(+ve) (+ve)

At a sufficiently low temperature the ^{119}Sn n.m.r. spectrum of the limiting solution structure can be obtained. This is consistent with the structure given below. The resolved couplings can be related to the average coupling constants seen at room temperature, thereby giving the signs of these couplings.

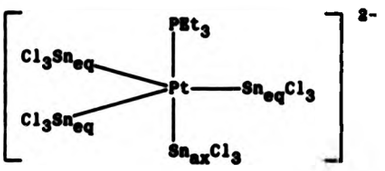

$(^{119}Sn_{eq})$	$(^{119}Sn_{ax})$	$^{2}J(^{31}P^{119}Sn_{eq})$	$^{2}J(^{31}P^{119}Sn_{ax})$
-83	-162	207	2392

$^{1}J(^{195}Pt^{119}Sn_{eq})$	$^{1}J(^{195}Pt^{119}Sn_{ax})$	$^{2}J(^{119}Sn_{eq}{}^{117}Sn_{eq})$	
19262	6470	15955	(temp -90°C)

$^{2}J(^{119}Sn^{31}P)$

$$^{2}J(^{119}Sn^{31}P)_{\text{average}} = \frac{[3X^{2}J(^{31}P^{119}Sn_{eq})]+{}^{2}J(^{31}P^{119}Sn_{ax})}{4} \quad (4.1)$$

If the couplings to Sn_{ax} and Sn_{eq} have the same sign the averaged coupling constant equals $\pm$763 Hz.

If couplings to Sn_{ax} and Sn_{eq} have opposite signs the averaged coupling constant equals $\pm$443 Hz, which may be compared with the experimental value of 449 Hz. Therefore the two couplings have opposite signs. Due to the magnitude of $^{2}J(^{31}P^{119}Sn_{ax})$ this coupling will determine the sign of the averaged coupling.

Therefore $^{2}K(PSn_{ax})$ is positive and

$^{2}K(PSn_{eq})$ is negative

$^{1}J(^{119}Sn^{195}Pt)$

$$^{1}J(^{119}Sn^{195}Pt)_{\text{average}} = \frac{[3X^{2}J(^{195}Pt^{119}Sn_{eq})]+{}^{2}J(^{195}Pt^{119}Sn_{ax})}{4} \quad (4.2)$$

If the couplings to Sn_{ax} and Sn_{eq} have the same sign the averaged coupling constant equals $\pm$16064 Hz.

If the coupling to Sn_{ax} and Sn_{eq} have opposite signs the averaged

coupling constant equals ± 12629 Hz.

The experimental average value of + 15444 Hz compares most favourably to the case where both coupling constants have the same sign and

therefore $^{1}K(PtSn_{ax})$ is positive and

$^{1}K(PtSn_{eq})$ is positive

$^{2}J(^{119}Sn^{117}Sn)$

The case of $^{2}J(^{119}Sn^{117}Sn)$ is more complicated than the other two, since not only are the couplings averaged, but also the two different tin sites become equivalent at room temperature.

There are three possible tin to tin coupling constants that involve at least one ^{119}Sn, $^{117}Sn_{eq}$ to $^{119}Sn_{eq}$, $^{117}Sn_{eq}$ to $^{119}Sn_{ax}$, and $^{119}Sn_{eq}$ to $^{119}Sn_{ax}$. Moreover in the averaged room temperature spectrum the axial and equatorial tin sites become equivalent, thereby removing the $^{119}Sn_{ax}$ to $^{119}Sn_{eq}$ coupling.

FIG. 4.I Tin Sites in $[Pt(PEt_3)(SnCl_3)_4]^{2-}$

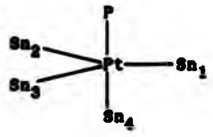

Given that the coupling from an axial ^{117}Sn to an equatorial ^{119}Sn is the same as that for an axial ^{119}Sn to an equatorial ^{117}Sn, the averaged room temperature coupling can be determined by considering the possible arrangements of two spin $^{1}/_{2}$ tin nuclei in the four possible tin sites (shown in the Fig. 4.I given in table 4.1).

Table 4.1 Possible Arrangements of two spin $^1/_2$ Tin Nuclei in FIG 4.I

Site occupied		Coupling arising	
1st Tin	2nd Tin	$^2J(Sn_{eq}-Sn_{eq})$	$^2J(Sn_{eq}-Sn_{ax})$
1	2	/	
1	3	/	
1	4		/
2	3	/	
2	4		/
3	4		/
	Total =	3	3

Therefore

$$^2J(^{119}Sn\text{-}^{117}Sn)_{\text{average}} = \frac{[(3X\,^2J(^{119}Sn_{eq}\text{-}^{117}Sn_{eq})]+[3X\,^2J(^{117}Sn_{eq}\text{-}^{117}Sn_{ax})]}{6}$$

$$= \frac{^2J(^{119}Sn_{eq}\text{-}^{117}Sn_{eq}) + ^2J(^{119}Sn_{eq}\text{-}^{117}Sn_{ax})}{2} \quad (4.3)$$

Given the magnitudes of the averaged coupling and of $^2J(^{119}Sn_{eq}\text{-}^{117}Sn_{eq})$, $^2J(^{117}Sn_{ax}\text{-}^{119}Sn_{eq})$ and $^2J(^{117}Sn_{eq}\text{-}^{119}Sn_{eq})$ must be of opposite sign, with the larger coupling being positive.

The satellites due to axial to equatorial tin-tin coupling on the equatorial tin resonance (the most intense peak in the tin spectrum) are less intense than those due to equatorial to equatorial coupling. This prevents their detection due to the signal to noise ratio obtained. It is expected that the equatorial-equatorial coupling will be larger than the equatorial-axial coupling: this would give

$$+6830 = \frac{15922 - ^2J(^{119}Sn_{eq}\text{-}^{117}Sn_{ax})}{2}$$

$$\therefore \; ^2J(^{119}Sn_{eq}\text{-}^{117}Sn_{ax}) = -2295 \text{ Hz}$$

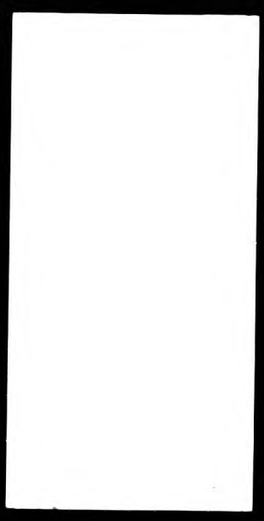

This would give satellites relatively close to the main equatorial tin signal possibly coincident with other satellites due to coupling to ^{195}Pt and equatorial ^{119}Sn.

4.9 $[Pt(SnCl_3)_3(P(OEt)_3)_2]^{-7}$

$\delta(^{31}P)$	$\delta(^{119}Sn)$	$\delta(^{195}Pt)$	$^1J(^{195}Pt^{119}Sn)$	$^1J(^{195}Pt^{31}P)$
77.0	-117	-5234	18962	2850

$^2J(^{119}Sn^{117}Sn)$	$^2J(^{119}Sn^{31}P)$	(temp -50°C)
16394	314	

A)

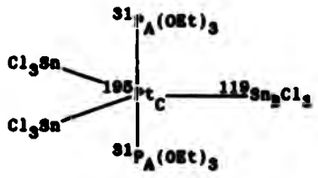

Comparison of signs $^1KSn_BPt_C$ / $^1KP_APt_C$

Obeserved nucleus ^{31}P

Irradiated nucleus ^{119}Sn

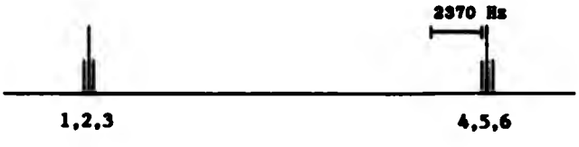

Line at which irradiation is applied	Line(s) perturbed
^{119}Sn 2	^{31}P 1, 3
^{119}Sn 5	^{31}P 2, 4

$^{1}KSn_{B}Pt_{C}$ has the same sign as $^{1}KP_{A}Pt_{C}$[20]

(+ve) (+ve)

Comparison of sign $^{2}KSn_{B}P_{A}$ / $^{1}KSn_{B}Pt_{C}$

Observed nucleus ^{31}P

Irradiated nucleus ^{195}Pt

Line at which irradiation is applied	Line(s) perturbed
^{195}Pt 2	^{31}P 3, 6
^{195}Pt 5	^{31}P 1, 4

$^{1}KSn_{B}Pt_{C}$ and $^{2}KSn_{B}P_{A}$ have opposite signs

(+ve) (-ve)

B)

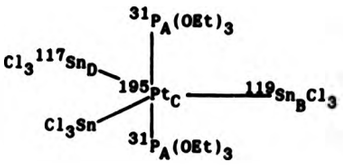

Comparison of signs $^1KSn_BSn_B$ / $^1KSn_DP_A$

Observed nucleus ^{31}P

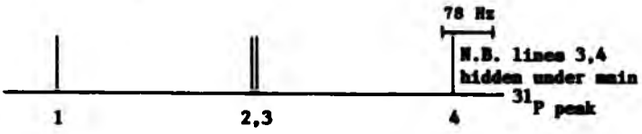

Irradiated nucleus ^{119}Sn

Line at which irradiation is applied	Line(s) perturbed
^{119}Sn 1	^{31}P 4
^{119}Sn 2	^{31}P 1

$^2KP_ASn_D$ and $^2KSn_BSn_D$ have opposite signs

(-ve) (+ve)

4.10 $[Rh(SnCl_3)_2(COD)(P(p\text{-}CH_3OC_6H_4)_3)]^-[PPh_3CH_2Ph]^+$ [14]

$\delta(^{31}P)$	$\delta(^{119}Sn)$	$\delta(^{103}Rh)$	$^1J(^{31}P^{103}Rh)$	$^1J(^{119}Sn^{103}Rh)$	$^2J(^{31}P^{119}Sn)$
41	34.8	-3800	115	679	366

$^2J(^{19}Sn^{117}Sn)$ (temp -60°C)

3218

A)

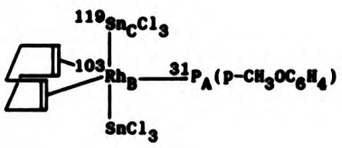

Comparison of signs $^1KP_ARh_B$ / $^1KRh_BSn_C$

Observed nucleus ^{31}P

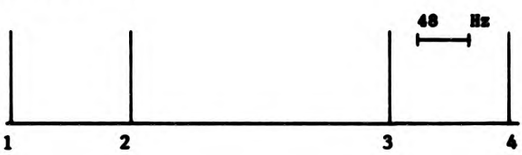

Irradiated nucleus ^{119}Sn

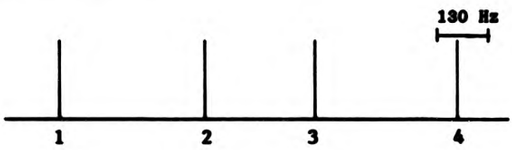

Line at which irradiation applied	Line(s) perturbed
^{119}Sn 1	^{31}P 1, 3
^{119}Sn 4	^{31}P 2, 4

$^{1}KP_{A}Rh_{B}^{26}$ and $^{1}KRh_{B}Sn_{C}$ have the same sign

(+ve) (+ve)

Comparison of signs $^{1}KSn_{C}Rh_{B}$ / $^{2}KP_{A}Sn_{C}$ (See FIG.4.XXI)

Observed nucleus ^{31}P

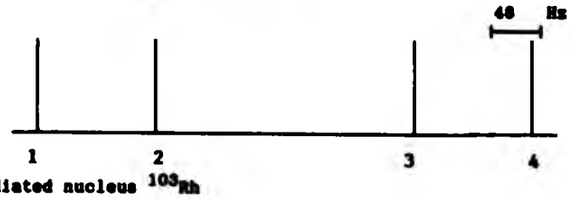

Irradiated nucleus ^{103}Rh

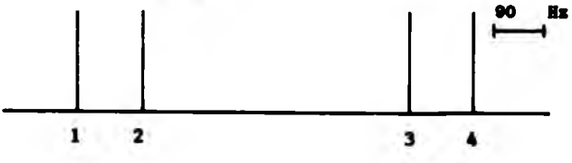

Line at which irradiation is applied	Line(s) perturbed
^{103}Rh 1	^{31}P 3, 4
^{103}Rh 4	^{31}P 1, 2

$^{K}Sn_{C}Rh_{3}$ and $^{2}KP_{A}Sn_{C}$ have opposite signs

(+ve) (-ve)

4.11 Cis-$[Pt(PPh_3)_2(PbPh_3)Ph]$[11]

	$\delta(^{31}P)$	$^1J(^{31}P^{195}Pt)$	$^2J(^{31}P^{207}Pb)$	$^2J(^{31}P^{31}P)$
P cis to Pb	20.3	1967.8	258.8	12.2
P trans to Pb	28.0	2934.6	3461.9	12.2

$\delta(^{195}Pt)$	$\delta(^{207}Pb)$	$^1J(^{195}Pt^{207}Pb)$
-102	-95.5	18374

A)

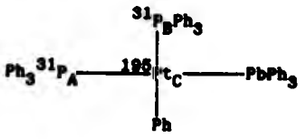

Comparison of signs $^1KP_APt_C$ / $^2KP_AP_B$ and $^1KP_BPt_C$ / $^2KP_AP_B$

(See FIG. 4.XXII)

Observed nucleus ^{31}P

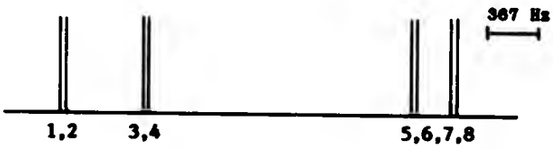

Irradiated nucleus ^{195}Pt

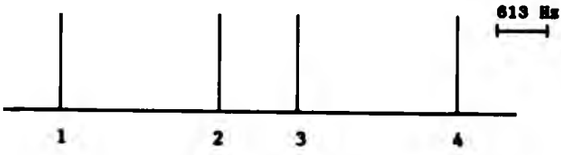

Line at which irradiation is applied	Line(s) perturbed
^{195}Pt 1	$^{31}P_A$ 2, 8 $^{31}P_B$ 4, 6
^{195}Pt 2	$^{31}P_A$ 1, 7 $^{31}P_B$ 4, 6
^{195}Pt 3	$^{31}P_A$ 2, 8 $^{31}P_B$ 3, 5
^{195}Pt 4	$^{31}P_A$ 1, 7 $^{31}P_B$ 3, 5

$^{1}KP_APt_C^{20}$ and $^{2}KP_AP_B$ have opposite signs

(+ve) (-ve)

$^{1}KP_BPt_C^{20}$ and $^{2}KP_AP_B$ have opposite signs

(+ve) (-ve)

B)

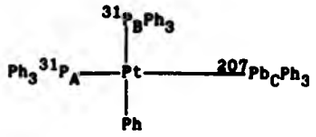

Comparison of signs $^{2}KP_{A}P_{B}$ / $^{2}KPb_{C}P_{A}$ and $^{2}KP_{A}P_{B}$ / $^{2}KPb_{C}P_{B}$

Observed nucleus ^{31}P

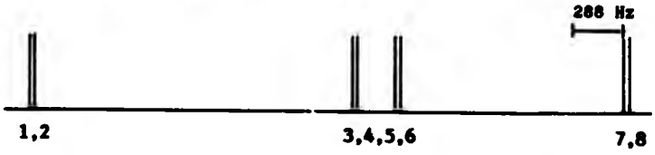

Irradiated nucleus ^{207}Pb

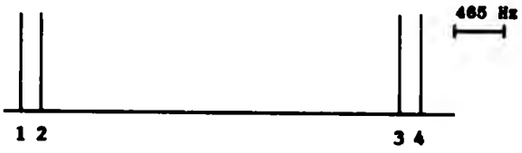

Line at which irradiation is applied	Line(s) perturbed
^{207}Pb 1	$^{31}P_{A}$ 1, 7 $^{31}P_{B}$ 4, 6
^{207}Pb 2	$^{31}P_{A}$ 2, 8 $^{31}P_{B}$ 4, 6
^{207}Pb 3	$^{31}P_{A}$ 1, 7 $^{31}P_{B}$ 3, 5
^{207}Pb 4	$^{31}P_{A}$ 2, 8 $^{31}P_{B}$ 3, 5

$^{2}KP_{A}P_{B}$ and $^{2}KP_{A}Pb_{C}$ have opposite signs

(-ve) (+ve)

$^{2}KP_{A}P_{B}$ and $^{2}KP_{B}Pb_{C}$ have the same signs

(-ve) (-ve)

C)

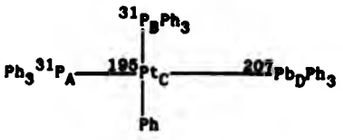

Comparison of signs $^{1}KP_{A}Pt_{C}$ / $^{1}KPt_{C}Pb_{D}$ and $^{1}KP_{B}Pt_{C}$ / $^{1}KPt_{C}Pb_{D}$

Observed nucleus ^{31}P

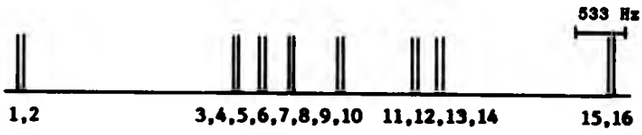

Irradiated nucleus ^{207}Pb

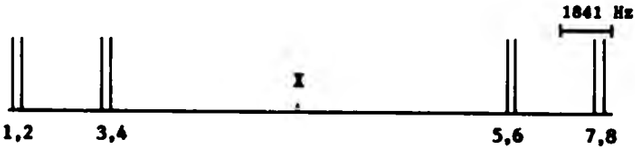

The above schematic diagram shows the ^{195}Pt satellites of the ^{207}Pb spectrum. These satellites are not symmetrically arranged about the main ^{207}Pb peaks (due only to coupling to ^{31}P); the position of which is marked 'X' in the diagram. The ^{207}Pb satellites of the ^{195}Pt spectrum show a similar distortion. This is caused by second order effects between ^{207}Pb and ^{195}Pt. [15] The large magnitude of $^{1}J(^{195}Pt^{207}Pb)$ means that, although the coupling is heteronuclear, when compared to the difference between the resonant frequencies of ^{207}Pb and ^{195}Pt, the coupled spectra must be interpreted as being due to an AB instead of a AX type of interaction. The extent of the second order distortion depends upon the size of the magnetic field of the N.M.R. spectrometer, since the larger the magnetic field, the larger the difference in resonant frequencies. The ^{207}Pb and ^{195}Pt spectra were recorded on a N.M.R. spectrometer with a different magnetic field strength to the

spectrometer upon which the multiple resonance experiments were performed. Therefore the positions of the ^{207}Pb lines to be irradiated had to be calculated, not only to allow for the change in resonant frequency due to the magnetic field strength, but also for the change in distortion due to second order effects. This acted as a test to prove that the distortion was indeed due to heteronuclear second order effects alone and not isotope effects as well, as has been considered previously.[15] The distortion was calculated using equation (4.4).

$$C = [(\nu^{195}Pt - \nu^{207}Pb)^2 + {}^1J(^{195}Pt^{207}Pb)^2]^{\frac{1}{2}} - {}^1J(^{195}Pt^{207}Pb) \quad (4.4)$$

Where $\nu^{195}Pt = 12,783,972$ Hz

$\nu^{207}Pb = 12,497,401$ Hz

${}^1J(^{195}Pt^{207}Pb) = 18,374$ Hz

and C is the separtion given in FIG. 4.II

FIG. 4.II

Diagram of an AB spectrum

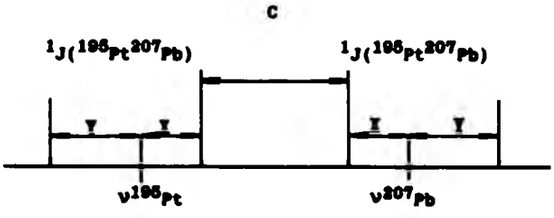

Using the above values in equation (4.4)

C = 268785 Hz

Therefore since

$^{195}Pt - {}^{207}Pb = 286571$ Hz

X = 8893 Hz

Y = 9481 Hz

Since both ^{195}Pt and ^{207}Pb are also coupled to ^{31}P, the distorted positions around $\nu^{207}Pb$, calculated in terms of X and Y, relate to the

positions of first order multiplets due to ^{31}P coupling. The successful use of the calculated line positions proved that only second order effects are responsible for the distortions observed.

Line at which irradiation is applied	Line(s) perturbed
^{207}Pb 1	$^{31}P_A$ 1, 9 $^{31}P_B$ 4, 6
^{207}Pb 8	$^{31}P_A$ 8, 16 $^{31}P_B$ 11, 13

$^{1}KP_APt_C{}^{20}$ and $^{1}KPt_CPb_D$ have the same sign
(+ve) (+ve)

$^{K}P_BPt_C{}^{20}$ and $^{1}KPt_CPb_D$ have the same sign
(+ve) (+ve)

4.12 Cis - $[Pt(PPh_3)_2(SnPh_2SnPh_3)Ph]$[16]

	$\delta(^{31}P)$	$^1J(^{31}P^{195}Pt)$	$^2J(^{31}P^{119}Sn)$	$^2J(^{31}P^{31}P)$	$^3J(^{31}P^{119}Sn)$
P cis to Sn	20.8	2009.3	146.5	14.6	0.0
P trans to Sn	26.6	2468.3	1965.3	14.6	161.1

	$\delta(^{119}Sn)$	$^1J(^{119}Sn^{195}Pt)$	$^2J(^{119}Sn^{195}Pt)$
$SnPh_3$	-157.1		1724
$SnPh_2$	-90.5	11934	

$\delta(^{195}Pt)$

-265.6

A)

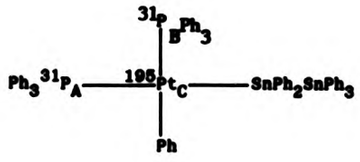

Comparison of signs $^1KP_APt_C$ / $^2KP_AP_B$ and $^1KP_BPt_C$ / $^2KP_AP_B$

Observed nucleus ^{31}P

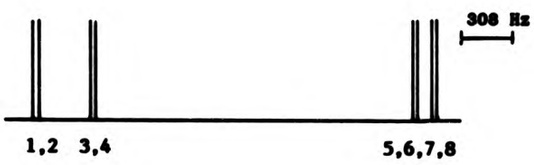

Irradiated nucleus ^{195}Pt

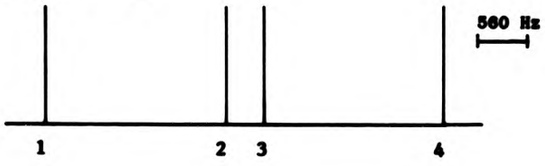

Line at which irradiation is applied	Line(s) perturbed
^{195}Pt 1	$^{31}P_A$ 2.8 $^{31}P_B$ 4.6
^{195}Pt 2	$^{31}P_A$ 1.7 $^{31}P_B$ 4.6
^{195}Pt 3	$^{31}P_A$ 2.8 $^{31}P_B$ 3.5
^{195}Pt 4	$^{31}P_A$ 1.7 $^{31}P_B$ 3.5

$^{1}KP_APt_C^{20}$ and $^{2}KP_AP_B$ have opposite signs

(+ve) (-ve)

$^{1}KP_BPt_C^{20}$ and $^{2}KP_AP_B$ have opposite signs

(+ve) (-ve)

B)

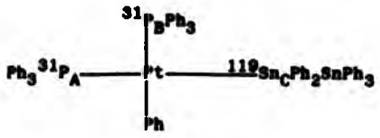

Comparison of signs $^2KP_ASn_C$ / $^2KP_AP_B$ and $^2KP_BSn_C$ / $^2KP_AP_B$

Observed nucleus ^{31}P

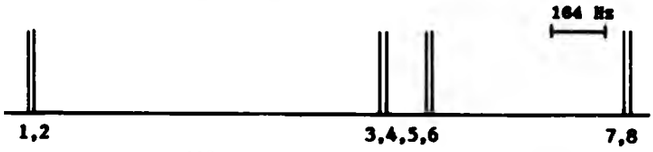

Irradiated nucleus ^{119}Sn

Line at which irradiation is applied	Line(s) perturbed
^{119}Sn 1	$^{31}P_A$ 1, 7 $^{31}P_B$ 4, 6
^{119}Sn 2	$^{31}P_A$ 2, 8 $^{31}P_B$ 4, 6
^{119}Sn 3	$^{31}P_A$ 1, 7 $^{31}P_B$ 3, 5
^{119}Sn 4	$^{31}P_A$ 2, 8 $^{31}P_B$ 3, 5

$^2KP_AP_B$ and $^2KP_ASn_C$ have opposite signs

(-ve) (+ve)

$^2KP_AP_B$ and $^2KP_BSn_C$ have the same signs

(-ve) (-ve)

c)

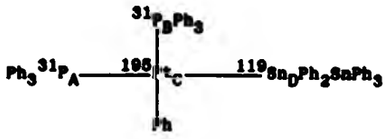

Comparison of signs $^{2}KSn_{D}P_{A}$ / $^{1}KSn_{D}Pt_{C}$

Observed nucleus ^{31}P

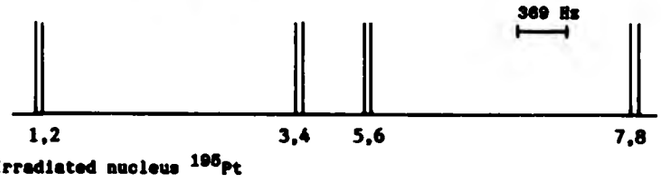

Irradiated nucleus ^{195}Pt

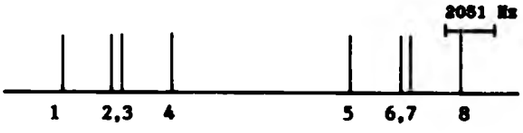

Line at which irradiation is applied	Line(s) perturbed
^{195}Pt 1	$^{31}P_{A}$ 2, 6
^{195}Pt 8	$^{31}P_{A}$ 3, 7

$^{2}KSn_{D}P_{A}$ and $^{1}KSn_{D}Pt_{C}$ have the same sign

(+ve) (+ve)

D)

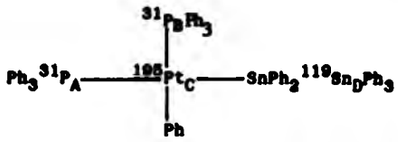

1) Comparison of signs $^{1}KP_{A}Pt_{C}$ / $^{2}KPt_{C}Sn_{D}$ (See FIG4,XXIII)

Observed nucleus ^{31}P

Irradiated nucleus ^{119}Sn

Line at which irradiation is applied	Line(s) perturbed
^{119}Sn 1	$^{31}P_{A}$ 1, 2, 3, 4
^{119}Sn 4	$^{31}P_{A}$ 5, 6, 7, 8

$^{1}KP_{A}Pt_{C}$ 20 and $^{2}KPt_{C}Sn_{D}$ have the same sign

(+ve) (+ve)

2) Comparison of signs $^{2}KPt_{C}Sn_{D}$ / $^{3}KP_{A}Sn_{D}$

Observed nucleus ^{31}P

Irradiated nucleus ^{195}Pt

Line at which irradiation is applied	Line(s) perturbed
^{195}Pt 1	$^{31}P_A$ 2, 6
^{195}Pt 8	$^{31}P_A$ 3, 7

$^{2}KPt_{C}Sn_{D}$ and $^{3}KP_{A}Sn_{D}$ have the same sign
(+ve) (+ve)

4.13 $[Pt(SnPh_3)_2(Ph_2PC_2H_4PPh_2)]$[17]

$\delta(^{31}P)$	$\delta(^{119}Sn)$	$\delta(^{195}Pt)$	$^1J(^{31}P^{195}Pt)$	$^1J(^{119}Sn^{195}Pt)$
-8.7	-58.6	-917.1	2293	9649

$^1J(^{31}P^{31}P)$	$^2J_{cis}(^{31}P^{119}Sn)$	$^2J_{trans}(^{31}P^{119}Sn)$
11	142	1611

A)

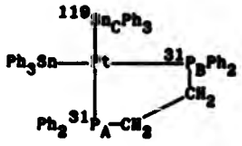

Comparison of signs $^2KP_AP_B$ / $^2KP_ASn_C$ and $^2KP_AP_B$ / $^2KP_BSn_C$

Observed nucleus ^{31}P

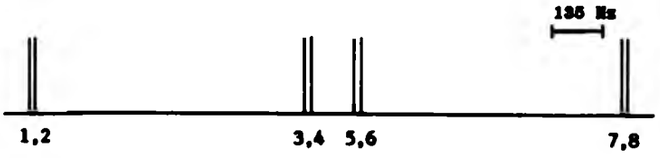

Irradiated nucleus ^{119}Sn

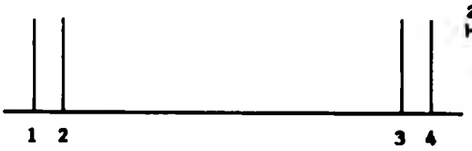

The labelled nuclei in the above diagram form an AA'X spin system (see Chapter 3) (A,A' = ^{31}P; X = ^{119}Sn). However the X spectrum resembles that of an AMX spin system. This is because the intensity of the two degenerate lines, positioned centrally between the two M lines, are negligible, and only the M and S lines, which have similar intensities, are resolved in the ^{119}Sn spectrum. This leads to some

confusion as to which pair of lines (inner or outer) are the N and which are the S lines. Hence the relative signs of J(AX) and J(A'X) cannot be determined merely from analysing the spectrum, as is normal with an AA'X spin system. The AA' part of the spectrum is easily detected yielding directly a value of J(AA'). The unusual nature of the spectrum is explained by the fact that the magnitude of J(AA') is very small when compared to N and L (see equations 3.1 and 3.2) and therefore equations (3.4) and (3.5) can be effectively replaced by equations (4.5) and (4.6) respectively.

$$S = L \quad (4.5)$$

$$D_{\pm} = \tfrac{1}{2}L \quad (4.6)$$

Therefore the magnitudes of the three coupling constants can be read off the ^{31}P and ^{119}Sn spectra directly, as if the system were AMX (and similarly the sign determinating multiple resonance experiments can be effectively interpreted in the same way). By successively irradiating all four lines in the X spectrum and observing the AA' spectrum, not only are the relative signs of the coupling constants determined, but also the N and S lines can be assigned. The results can be interpreted with the aid of the energy level diagrams given in FIG. 3.X and FIG. 3.XI. However the labelled schematic diagrams of the X and AA' spectra cannot be applied to this case. If the inner pair of lines in the X spectrum are the N lines, then FIG. 4.IIIa gives the appropriate schematic diagram of the spectra. In the other case, where the outer lines are the N lines FIG.4.IIIb is appropriate.

FIG. 4.III - Schematic diagram of an AA'X spectrum

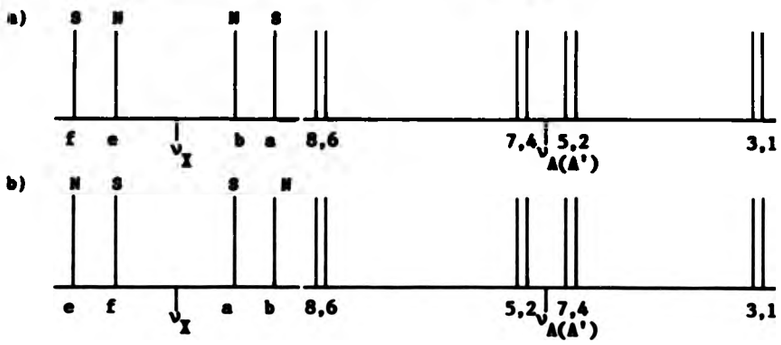

By examining the energy level diagrams in FIG. 3.X and FIG. 3.XI, it can be seen that irradiation at the frequency of any X transition will perturb four AA' lines and because the numbering of the lines is different in FIG.4.IIIa) and b), the assignment of the N and S lines can be deduced from which four lines are perturbed in the AA' spectrum when any one X transition is irradiated. From the results it can be seen that FIG. 4.IIIa) shows the correct assignment and that the larger $^2J(^{119}Sn^{31}P)$ is of opposite sign to the smaller $^2J(^{119}Sn^{31}P)$.

Although the relative signs of J(AX), J(A'X) and J(AA') can also be extracted by using the AA'X energy level diagrams to interpret the results, as stated earlier the results can also be considered as deriving from a pseudo AMX spin system (A,M = ^{31}P; X = ^{119}Sn) with the inner four ^{31}P lines being due to A transitions J(AX) is taken as the smaller $^2J(^{119}Sn^{31}P)$) and the outer four lines due to M transitions J(MX) is the larger $^2J(^{119}Sn^{31}P)$). This leads to the same conclusions, but makes interpretation easier.

Line at which irradiation is applied	Line(s) perturbed
^{119}Sn 1	$^{31}P_A$ 1, 7 $^{31}P_B$ 4, 6
^{119}Sn 2	$^{31}P_A$ 2, 8 $^{31}P_B$ 4, 6
^{119}Sn 3	$^{31}P_A$ 1, 7 $^{31}P_B$ 3, 5
^{119}Sn 4	$^{31}P_A$ 2, 8 $^{31}P_B$ 3, 5

$^2KP_AP_B$ and $^2KP_ASn_C$ have opposite signs

(-ve) (+ve)

$^2KP_AP_B$ and $^2KP_BSn_C$ have the same signs

(-ve) (-ve)

B)

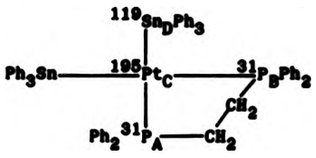

1) Comparison of signs $^1KPt_CSn_D$ / $^2KP_ASn_D$ and $^1KPt_CSn_D$ / $^2KP_BSn_D$

Observed nucleus ^{31}P

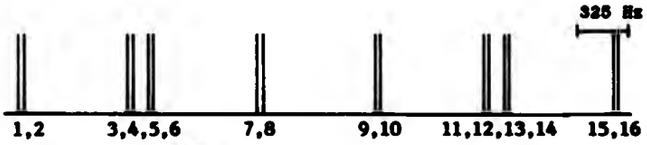

Irradiated nucleus ^{195}Pt

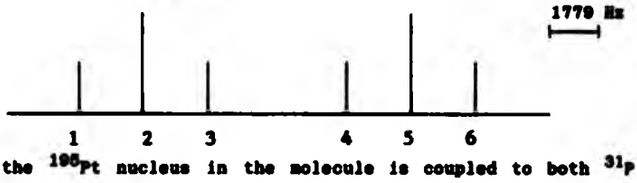

Since the ^{195}Pt nucleus in the molecule is coupled to both ^{31}P equally, no further second order effects are introduced into the ^{31}P spectrum. However, the presence of one ^{119}Sn is required so that the two ^{31}P are magnetically inequivalent and the required sign comparisons can be carried out.

Line at which irradiation is applied	Line(s) perturbed
^{195}Pt 1	$^{31}P_A$ 2, 10 $^{31}P_B$ 6, 14
^{195}Pt 6	$^{31}P_A$ 7, 15 $^{31}P_B$ 3, 11

$^{K}Pt_CSn_D$ and $^{2}KP_ASn_D$ have the same signs
(+ve) (+ve)

$^{1}KPt_CSn_D$ and $^{2}KP_BSn_D$ have opposite signs
(+ve) (-ve)

2) Comparison of signs $^{1}KP_APt_C$ / $^{1}KPt_CSn_D$ and $^{1}KP_BPt_C$ / $^{1}KPt_CSn_D$

Observed nucleus ^{31}P

Irradiated nucleus ^{119}Sn

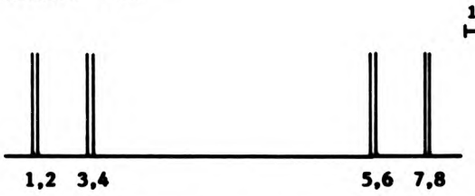

Line at which irradiation is applied	Line(s) perturbed
^{119}Sn 1	$^{31}P_A$ 1, 7 $^{31}P_B$ 4, 8
^{119}Sn 8	$^{31}P_A$ 10, 16 $^{31}P_B$ 11, 13

$^{1}KP_APt_C^{20}$ and $^{1}KPt_CSn_D$ have the same signs
(+ve) (+ve)

$^{1}KP_BPt_C^{20}$ and $^{1}KPt_CSn_D$ have the same signs
(+ve) (+ve)

4.14 $[Pt_2(\mu\text{-dppm})_2(SnCl_3)_2]$[18]

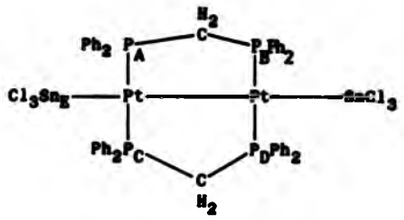

(^{31}P)	(^{119}Sn)	(^{195}Pt)	$^1J(^{31}P^{195}Pt)$	$^2J(^{31}P^{195}Pt)$
-3.6	43.0	-633.4	2644	105

$^2J(^{31}P_A{}^{31}P_B)$	$^2J(^{31}P_A{}^{31}P_D)$	$^2J(^{31}P_A{}^{119}Sn_B)$	$^3J(^{31}P_A{}^{119}Sn_B)$
48.9	26.3	268.6	26.3

$^1J(^{119}Sn^{195}Pt)$	$^2J(^{119}Sn^{195}Pt)$	$^1J(^{195}Pt^{195}Pt)$
11892	9370	7805

This compound gives complex spectra for all the nuclei mentioned above. The natural abundance of these nuclei (^{31}P:100%, ^{195}Pt:33.8%, ^{119}Sn:8.58%) lead to a number of different isotopomers exhibiting a variety of spin systems, and the observed spectra are the sum of the individual spectra from each isotopomer. By analysing these spectra the magnitude, and in some cases the relative signs, of the coupling constants can be derived. However, in certain cases it was necessary to perform multiple resonance experiments to determine the signs of certain coupling constants and to assign others.

Firstly we consider molecules without any spin ½ tin nuclei and with either zero, one or two ^{195}Pt nuclei [19] as shown in FIG. 4.IV.

FIG. 4.IV Isotopomers of $[Pt(\mu\text{-dppm})(SnCl_3)]_2$ containing 0-2 ^{195}Pt nuclei

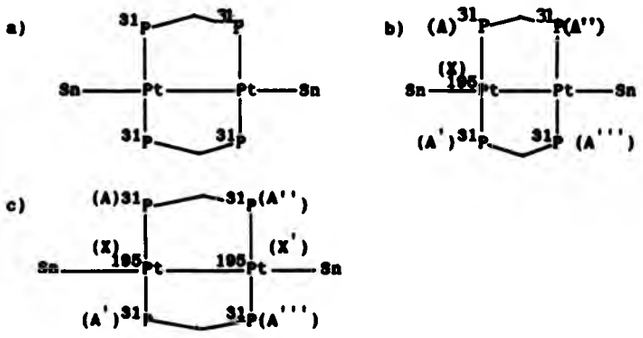

The ^{31}P spectrum of species a) is a singlet, since all four phosphorus are equivalent, but species b) and c) give more complex spectra owing to the magnetic inequivalence introduced by the presence of ^{195}Pt. The labelled nuclei in species b) form an $AA'A''A'''X$ spin system and with the exception of $J(AA')$, the coupling constants can be easily calculated from the ^{31}P spectrum in terms of a number of parameters (N, L, J(AX), $J(A''X)$, which are labelled on the ^{31}P spectrum shown in FIG. 4.V, and these are given by equations (4.7) and (4.8)

$$N = J(AA'') + J(AA''') \qquad (4.7)$$

$$L = J(AA'') - J(AA''') \qquad (4.8)$$

J(AX) and $J(A'X)$ can also be obtained directly from the ^{195}Pt spectrum of this isotopomer which appears as a simple triplet of triplets. Species c) forms an $AA'A''A'''XX'$ spin system and its ^{31}P spectrum contains two relatively intense lines labelled by the separation N' in FIG. 4.V which is given by equation (4.9).

$$N' = J(AX) + J(A'X) \qquad (4.9)$$

FIG.4.V ^{31}P Spectrum Of $[Pt_2(\mu\text{-dppm})_2(SnCl_3)_2]$

Since the magnitudes of J(AX) and J(A''X) are already known from the analysis of the ^{31}P spectrum of species b) and since $|N'|$ is equal to $|J(AX) - J(A''X)|$, the two coupling constants $^{1}J(^{31}P^{195}Pt)$ and $^{2}J(^{31}P^{195}Pt)$ are of opposite signs. Since $^{1}J(^{31}P^{195}Pt)$ is always positive[20], it follows that $^{2}J(^{31}P^{195}Pt)$ is negative. $^{1}J(^{195}Pt^{195}Pt)$ cannot be directly observed, but can be calculated from second-order features in the ^{31}P spectrum of species c). Besides the two intense N' lines, a number of weaker lines due to species c) were detected in the ^{31}P spectrum and are marked on the ^{31}P spectrum in FIG. 4.VI. Using the values of the other coupling constants already determined, from analysis of the spectra of species b) and c), the ^{31}P and ^{195}Pt spectra were calculated using the previously reported value of $^{1}J(^{195}Pt^{195}Pt)$ (7628 Hz)[18]. The lines in the calculated spectra did not coincide with the lines in the observed spectra. Therefore in order to obtain a more accurate value for the magnitude of $^{1}J(^{195}Pt^{195}Pt)$, an interactive calculation using a computer program based on LAOCOON was performed using the positions of the lines marked on the ^{31}P spectrum in FIG. 4.VI and allowing only $^{1}J(^{195}Pt^{195}Pt)$ to vary[21] from an initial value of 7300 Hz after five interactions, a value of 7605 Hz for $^{1}J(^{195}Pt^{195}Pt)$ was obtained. The ^{31}P spectrum was then recalculated a number of times using values of $^{1}J(^{195}Pt^{195}Pt)$ which varied by differing amounts. It was found that a change of $\pm$20 Hz in $^{1}J(^{195}Pt^{195}Pt)$ resulted in a change of about 1 Hz in the calculated positions of the ^{31}P lines used for the original interactive calculation. Since the positions of the observed lines could only be determined to this accuracy, $\pm$20 Hz reflects the error in the magnitude of $^{1}J(^{195}Pt^{195}Pt)$. This may seem large, but in a coupling constant in the region of 7800 Hz, this is not significant and since the compound is fluctional, the magnitude of the coupling constant is probably temperature sensitive as well. FIG. 4.VI shows the observed

FIG.4.VIa ^{31}P Spectrum Of Species c)

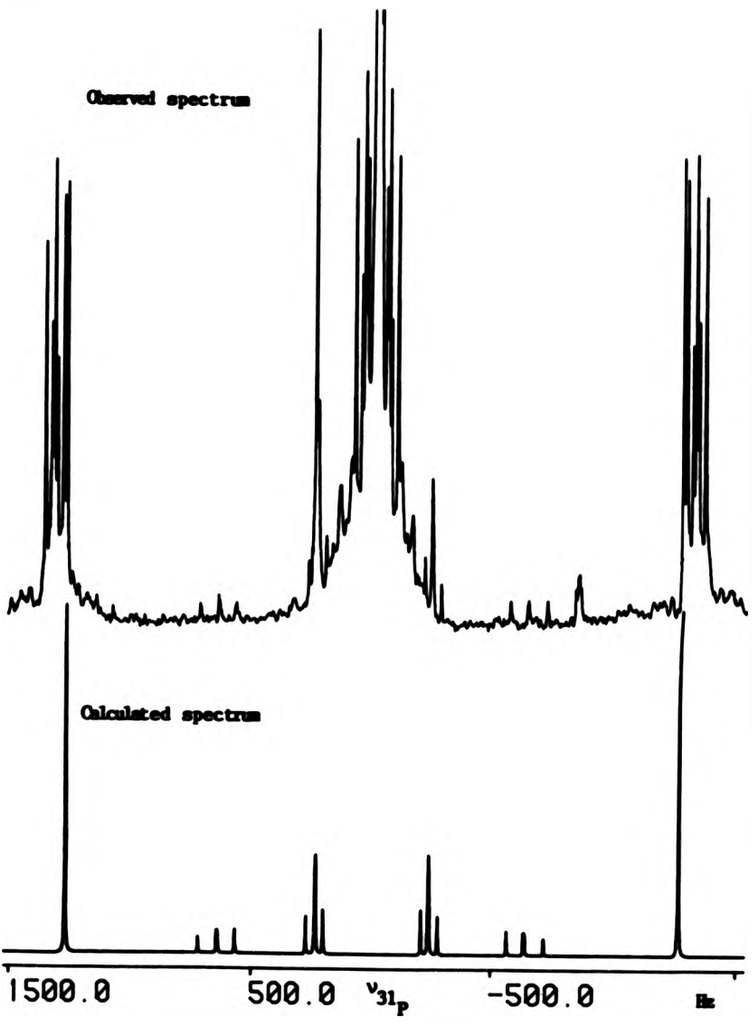

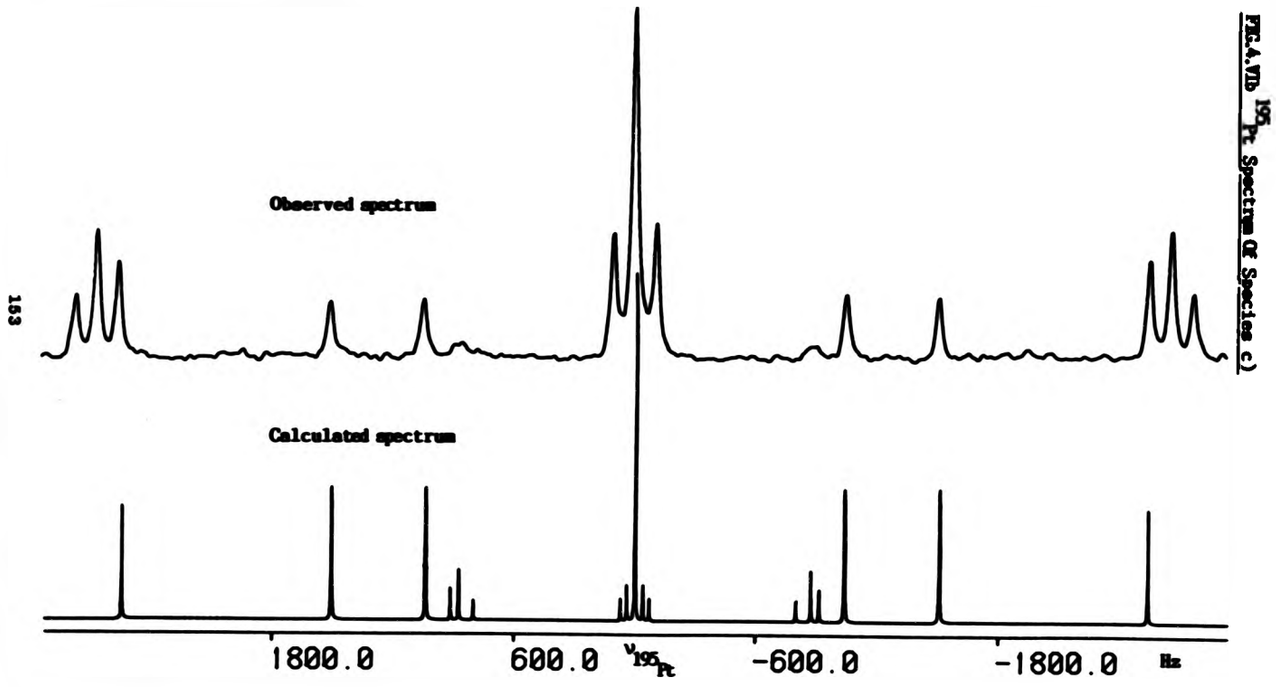

FIG.4.VIb ^{195}Pt Spectrum Of Species c)

^{31}P and ^{195}Pt spectra compared to the spectra calculated from the value of $^{1}J(^{195}Pt^{195}Pt)$ determined. Table (4.2) gives the energy levels derived from the calculations; table (4.3) the calculated ^{31}P line positions, and table (4.4) the calculated ^{195}Pt line positions. Each line is cross-referenced to its associated energy levels and is also cross-referenced to any progressively or regressively connected transitions.

The sign of $^{1}J(^{195}Pt^{195}Pt)$ cannot be derived or calculated from the analysis of the spectra and requires a multiple resonance experiment for its determination. As mentioned above the N' lines are the most intense in the ^{31}P spectrum of species c) and the sign of N' is known to be positive. From the calculated spectra in tables (4.3) and (4.4) and the energy levels in table (4.2), it can be seen that these lines are due to a number of degenerate transitions. Of these transitions a number share energy levels with very weak unobserved ^{195}Pt transitions, which appear at the extremes of the ^{195}Pt spectrum of species c) and have their positions determined by a number of coupling parameters including $^{1}J(^{195}Pt^{195}Pt)$. By irradiating at the frequency of ^{195}Pt transitions and observing the effect on the N' lines in the ^{31}P spectrum the relative signs of $^{1}J(^{195}Pt^{195}Pt)$ and N' can be determined. The most suitable ^{195}Pt transitions are numbers 75 ($\nu^{195}Pt$ - 8751 Hz) and 126 ($\nu^{195}Pt$ + 8751 Hz) in table (4.4). Each is connected to ^{31}P transitions which are components of one N' line only. Line 75 is connected to the ^{31}P transitions 16 and 22 ($\nu^{31}P$ - 1269.5 Hz) and line 126 is connected to 49 and 56 ($\nu^{31}P$ + 1269.5 Hz). These connectivities are based on calculated spectra with $^{1}J(^{195}Pt^{195}Pt)$ being positive. If the calculations are repeated with $^{1}J(^{195}Pt^{195}Pt)$ being negative the connectivities are reversed. Therefore by irradiating at the frequency of the calculated position of one of these unobserved

TABLE.4.2 Energy Levels Calculated For Species c)

CALCULATED ENERGY LEVELS

1	4727.8318	37449	33	5850.7699	4168
2	3458.3317	37385	34	-6042.3952	4161
3	3383.1317	36937	35	-6044.9954	4105
4	3032.0317	37448	36	-6451.6241	33281
5	3009.4317	37441	37	-6562.3563	32840
6	2188.8318	36929	38	-6567.3521	33344
7	2113.6318	36873	39	2421.6989	32776
8	2076.5598	37440	40	2350.7701	33280
9	1762.5318	37377	41	1996.8757	4104
10	1739.9318	37384	42	1975.5592	4097
11	1350.7036	36936	43	-5853.2339	4608
12	919.3317	36872	44	-5924.1625	32769
13	844.1318	36928	45	-6278.0227	32832
14	493.0317	36845	46	-6299.3393	4160
15	470.4317	37376	47	2188.8318	4096
16	-350.1682	36844	48	-5616.0953	32768
17	2188.8318	33353	49	-350.1682	585
18	-5616.0953	4681	50	919.3318	584
19	2421.6991	33352	51	844.1318	577
20	2350.7704	33345	52	493.0317	521
21	1996.8757	33289	53	470.4317	73
22	1975.5591	32841	54	2188.8317	576
23	-5853.2338	4680	55	2113.6317	520
24	-5924.1624	4673	56	2076.5598	513
25	-6278.0226	4617	57	1762.5318	72
26	-6299.3391	4169	58	1739.9318	65
27	2987.8408	32833	59	1350.7037	9
28	2984.6924	32777	60	3458.3317	64
29	2148.3760	33288	61	3383.1317	512
30	1762.5317	4672	62	3032.0318	8
31	1739.9318	4616	63	3009.4318	1
32	1350.9194	4609	64	4727.8318	0

TABLE.4.3 Calculated ^{31}P Line Positions For Species c)

ORDERED SPECTRUM OF ANGLES WITH 180 VALUE 1

NUMBER	FREQUENCY	INTENSITY	LABEL	ENERGY LEVELS	CONNECTED TRANSITIONS PROGRESSIVE	REGRESSIVE
1	-8984.688	0.027	249	37 - 39	37 47 70 89 124 126	24 28 44 75 77 80
2	-8918.122	0.044	208	38 - 40	40 59 69 92 125	11 23 46 76 88
3	-8912.023	0.031	133	24 - 27	44 46 68 106 108 130	6 27 47 79 93 95
4	-8837.926	0.030	122	23 - 28	42 46 67 107 127	25 28 45 48 82 94
5	-8112.994	0.112	275	44 - 47	24 48 68 83 122	37 71 84
6	-8072.530	0.121	135	24 - 29	28 48 66 97 105 130	3 43 47 79 96 104
7	-8061.071	0.026	235	75 - 41	33 64 90	32 38 87
8	-8061.071	0.026	160	26 - 30	32 63 99 129	33 39 80 102
9	-8017.954	0.057	149	25 - 31	30 62 100 120	31 40 51 101
10	-8017.954	0.057	220	34 - 42	31 61 91	30 41 86
11	-8001.540	0.106	218	33 - 40	35 59 60 92	2 36 46 85
12	-7966.866	0.116	66	18 - 20	29 60 69 116	42 107
13	-1269.500	2.000	300	52 - 57	21 90 114	99
14	-1269.500	4.000	133	60 - 64	14 71 79	83
15	-1269.500	2.000	307	53 - 58	19 81 115	100
16	-1269.500	4.000	309	54 - 60	16 22 75 97 106	71 89
17	-1269.500	4.000	301	49 - 56	22 117	79 113
18	-1269.500	2.000	292	51 - 55	20 82 116	76 78 107
19	-1269.500	2.000	328	58 - 63	15 100	73 91
20	-1269.500	2.000	314	55 - 61	18 76 78 107	74 92
21	-1269.500	2.000	323	57 - 62	13 99	72 98
22	-1269.500	4.000	288	50 - 54	16 17 79 113	75 97 106
23	-716.118	1.623	261	38 - 43	29 48 69 74 125	2 26 36 67 76 119
24	-638.194	1.960	284	37 - 44	5 47 70 71 124 126	1 45 48 75 77 122
25	-633.922	1.968	86	30 - 38	12 46 67 107 109	4 40 69 94 116
26	-598.398	0.042	248	36 - 43	29 48 74 123	23 36 67 78 119
27	-566.162	3.201	73	19 - 27	24 44 68 106 108 112	3 43 70 93 95 113
28	-273.323	3.200	108	29 - 39	6 27 43 89 96 104	1 44 45 80 97 108
29	-237.139	3.884	274	43 - 48	23 26 36 67 119	99 74
30	-238.627	1.942	204	31 - 42	9 40 91 101	10 42 86 100
31	-238.627	1.943	152	28 - 34	10 41 120	9 41 81
32	-234.344	1.944	198	30 - 41	8 39 90 102	7 43 87 99
33	-234.344	1.944	148	26 - 33	7 38 129	8 44 88
34	-232.867	3.888	97	17 - 19	27 45 70 113 118	66 112 117
35	-200.464	4.101	127	23 - 32	11 36 42 127	4 45 48 68 82
36	200.464	4.101	221	33 - 43	29 35 68 74	11 23 36 67 119
37	232.867	3.888	268	39 - 47	1 28 44 83 88	5 84 89
38	234.344	1.944	240	35 - 46	33 64 72	7 63 121
39	234.344	1.944	100	21 - 30	32 63 99 111	8 64 102 114
40	238.627	1.943	113	22 - 31	30 62 100 110	9 61 101 115
41	238.628	1.943	231	34 - 45	31 61 73	10 62 120
42	237.139	3.884	69	18 - 23	4 35 45 48 82	12 127
43	273.323	3.888	78	19 - 29	28 34 65 97 105 112	6 27 70 96 104 113
44	566.162	3.201	169	27 - 39	3 27 37 89 93 95	1 28 45 80 106 108
45	598.398	0.042	130	28 - 36	26 42 78 127	4 35 45 82 123
46	633.922	1.968	178	28 - 40	4 25 89 92 94	2 11 67 88 107
47	638.194	1.960	143	24 - 37	1 24 66 75 77 130	3 6 70 79 124 126
48	716.118	1.623	132	29 - 38	2 23 42 76 127	4 35 45 69 82 128
49	1269.500	6.000	5	2 - 6	57 58 95 104 126	

continued

TABLE.4.3 Continued

50	1269.000	2.000	12	3 - 7	28	94	123	126				
51	1269.000	2.000	20	4 - 9	26	102						
52	1269.000	2.000	27	9 - 10	24	101						
53	1269.000	4.000	53	12 - 16	20	84						
54	1269.000	2.000	40	10 - 15	32	86	120					
55	1269.000	2.000	34	7 - 13	30	88	119					
56	1269.000	2.000	43	9 - 14	31	87	121					
57	1269.000	4.000	1	1 - 2	49	112	130					
58	1269.000	6.000	39	6 - 12	49	93	88	122				
59	7966.068	0.116	268	40 - 48	2	11	46	88				
60	8061.540	0.106	91	20 - 33	11	12	36	109				
61	8017.956	0.027	116	22 - 34	10	41	110					
62	8017.956	0.027	307	31 - 45	9	40	75	101				
63	8061.671	0.056	200	30 - 46	8	29	72	102				
64	8061.671	0.056	108	21 - 38	7	38	111					
65	8072.539	0.121	190	29 - 44	5	6	43	71	96	104		
66	8112.996	0.112	62	17 - 24	3	6	47	79	110			
67	8037.926	0.028	181	38 - 43	4	28	29	74	94			
68	8012.023	0.031	174	27 - 44	3	5	27	71	93	98		
69	8018.122	0.044	96	30 - 38	2	12	23	76	109			
70	8084.088	0.027	83	19 - 37	1	24	34	75	77	112		

112	130					
107	127					
111	129					
110	128					
88	122					
101						
94	123	126				
102						
110						
98	104	126				
29	92					
28	38	69	116			
31	40	115				
30	41	100	120			
32	38	99	121			
33	39	114				
24	28	68	97	108	122	
34	117	130				
23	26	36	46	107	119	
24	44	65	106	108	122	
25	48	60	116	129		
27	43	47	113	124	126	

TABLE.4.4 Calculated ^{195}Pt Line Positions For Species c)

ORDERED SPECTRUM OF NUCLEI WITH ISO VALUE 3

NUMBER	FREQUENCY	INTENSITY	LABEL	ENERGY LEVELS	PROGRESSIVE CONNECTED TRANSITIONS	REGRESSIVE
71	-9302.494	0.056	10265	66 - 69	14 74 68 68 122	5 16 39
72	-9231.371	0.056	10278	56 - 62	38 63 121	21 90
73	-9207.454	0.057	10272	65 - 63	41 62 120	19 91
74	-9236.366	0.058	10262	63 - 61	23 36 36 67 119	20 39 92
75	-8791.188	0.060	10291	37 - 54	16 67 70 126 126	1 22 24 77 97 106
76	-8600.984	0.178	10298	30 - 55	20 68 69 125	2 18 23 78 107
77	-8638.916	0.123	10293	17 - 56	17 70 124 126	1 24 78 105 108
78	-8569.256	0.084	10196	56 - 95	70 95 123	18 25 76 107
79	-6841.494	0.056	10087	24 - 50	22 66 130	3 6 17 67 113
80	-6792.371	0.056	10067	26 - 52	13 129	8 33 116
81	-6748.454	0.057	10064	29 - 53	15 128	9 31 115
82	-6697.366	0.058	10054	23 - 51	18 42 127	4 35 65 68 116
83	-2539.000	2.000	10279	67 - 64	3 37 64	14
84	-2539.000	2.000	10277	16 - 67	93 63	5 37
85	-1906.638	1.942	10222	13 - 48	98 99 92	2 11 46 119
86	-1909.127	1.943	10240	15 - 42	94 91	10 30 120
87	-1903.044	1.944	10231	14 - 41	96 90	7 32 121
88	-1902.367	1.944	10213	12 - 39	37 98 89	1 20 44 93 122
89	-1036.633	1.944	10245	39 - 60	1 14 20 44 88	16 37 71
90	-1035.156	1.944	10238	41 - 62	7 32 87	21 72
91	-1033.073	1.943	10260	62 - 63	10 30 86	19 73
92	-1032.362	1.942	10250	40 - 61	2 11 46 88	20 59 74
93	-911.301	1.101	10093	8 - 27	44 68 106 108	3 27 95 96 120
94	-871.061	1.018	10082	7 - 28	46 90 67 107	4 25 98 123 128
95	-799.029	0.717	10069	6 - 27	44 69 68 106 108	3 27 98 93 104 126
96	-71.016	0.776	10095	8 - 29	28 65 97 105	6 43 93 104 124
97	-40.456	1.223	10193	29 - 54	6 16 43 96 104	22 28 68 75 105 106
98	-0.216	2.000	10130	11 - 32	103	13 32 63
99	-0.000	2.000	10162	30 - 57	8 21 39 102	15 30 62
100	-0.000	2.000	10149	31 - 58	9 19 40 101	9 40 94
101	0.000	2.000	10121	10 - 31	30 52 62 100	8 29 96
102	0.000	2.000	10100	9 - 30	32 51 63 99	6 43 98 95 96 126
103	0.216	2.000	10170	32 - 59	99	20 68 77 97 108
104	40.456	1.223	10071	6 - 29	28 69 65 97 105	22 64 68 75 97 108
105	71.016	0.776	10158	29 - 56	6 43 96 104	18 66 67 76 78
106	799.029	0.717	10141	27 - 54	3 16 27 92 95	64 68 77 105 106
107	871.061	1.018	10140	28 - 55	4 20 25 94	12 98 127
108	911.301	1.101	10143	27 - 56	3 27 93 99	92 120
109	1032.361	1.942	10014	3 - 29	28 40 69 116	91 129
110	1033.073	1.943	10032	5 - 32	40 61 115	24 49 130
111	1035.156	1.944	10023	4 - 31	39 60 114	17 27 43 70 79
112	1036.633	1.944	10005	2 - 19	27 42 57 70 113	39 64 88
113	1902.367	1.944	10037	19 - 50	22 54 112	40 61 81
114	1903.044	1.944	10047	21 - 52	13 111	28 60 69 82
115	1906.127	1.943	10052	22 - 53	15 110	36 66
116	1906.639	1.942	10042	20 - 51	12 10 109	97
117	2539.000	2.000	10063	17 - 49	17 108	23 26 36 67 85
118	2539.000	2.000	10081	1 - 17	34 66 117	41 62 86
119	6697.366	0.058	10225	13 - 43	29 88 76	78 63 87
120	6748.454	0.057	10243	15 - 45	94 93	24 53 65 68 88
121	6792.371	0.056	10236	14 - 44	96 72	95 55 94 125
122	6841.494	0.056	10218	12 - 44	5 58 71	17 70 93 96 126
123	8569.256	0.084	10090	7 - 36	26 59 78	48 55 69 94 123
124	8638.916	0.123	10103	3 - 37	1 24 75 77	47 58 70 95 104 124
125	8609.984	0.178	10092	7 - 38	2 23 58 76	42 58 109
126	1791.188	0.060	10079	6 - 37	1 24 49 78 77	52 110
127	9236.365	0.058	10017	3 - 25	4 35 15 48 82	91 111
128	9207.454	0.057	10035	5 - 28	9 31 81	49 66 112
129	9231.371	0.056	10028	4 - 26	8 33 80	
130	9302.494	0.056	10010	2 - 24	3 6 47 97 79	

^{195}Pt transitions either ^{31}P transitions 16 and 22 or 49 and 58 will be perturbed, depending on the sign of $^{1}J(^{195}Pt^{195}Pt)$. By examining the intensities of the degenerate ^{31}P transitions which make up each N' line, it can be seen that potentially perturbed transitions (16, 22, 49, 58) make up $^{3}/_{8}$th of each N' lines total intensity. Therefore the intended multiple resonance experiment will perturb only $^{3}/_{8}$th of the affected N' line at most. In order to maximise the perturbation caused, and since the positions of the relevant ^{195}Pt lines are more sensitive to variations in the magnitude of $^{1}J(^{195}Pt^{195}Pt)$ than the observed ^{31}P lines due to species c), the maximum available ^{195}Pt irradiation power was used without causing undue interference. This experiment is shown in FIG. 4.VII . Irradiation of the high frequency ^{195}Pt line perturb the high frequency N' line in the ^{31}P spectrum (and similarly irradiation the low frequency ^{195}Pt line, perturbs the high frequency N' line). $^{1}J(^{195}Pt^{195}Pt)$ is therefore positive since N' is positive.

There are four isotopomers containing ^{119}Sn nuclei, as shown in FIG. 4.VIII which contribute to the observed spectra.

FIG. 4.VIII Isotopomers of $[Pt(\mu\text{-dppm})(SnCl_3)]_2$ containing one ^{119}Sn and 0-2 ^{195}Pt nuclei

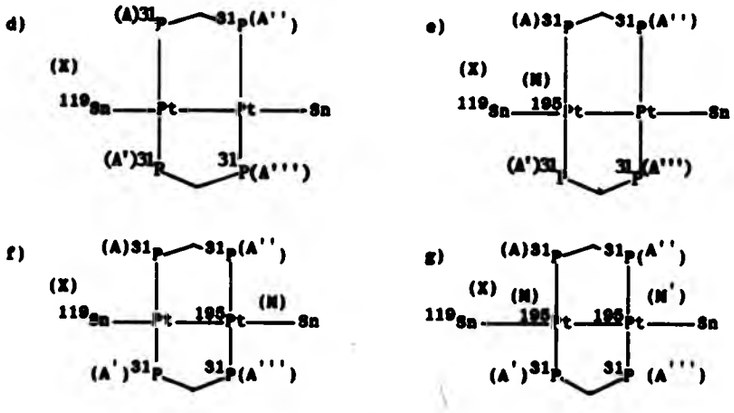

FIG.4.VII Comparison Of The Signs Of $^{1}K(PtPt)$ And N'

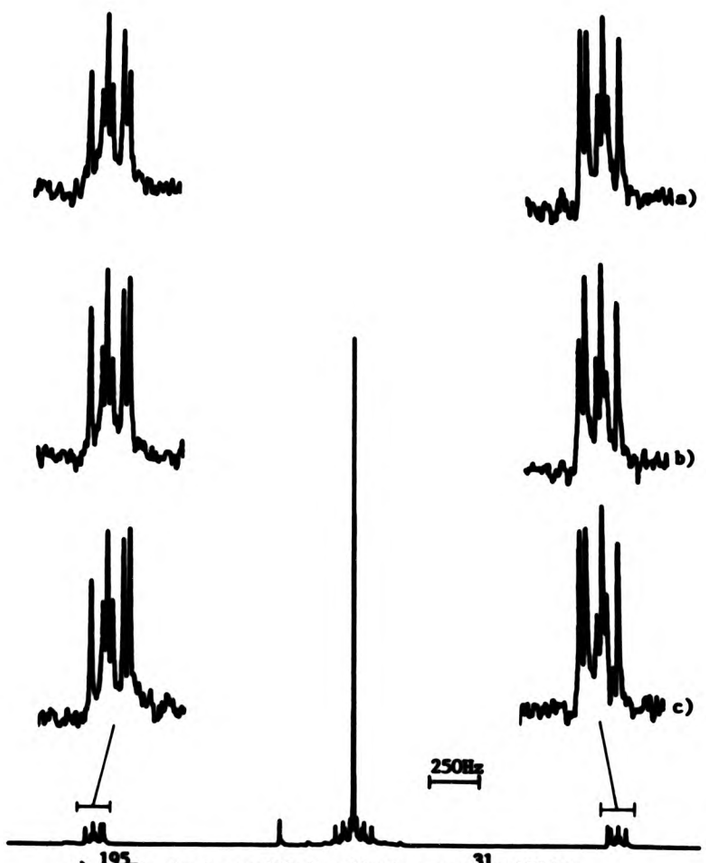

a) ^{195}Pt spectrum with irradiation at $\nu^{31}_{31}P+8751Hz$
b) ^{195}Pt spectrum with irradiation at $\nu^{31}P-8751Hz$
c) ^{195}Pt spectrum without irradiation

The labelled nucleus in species d) form an $AA'A''A'''X$ spin system and in principle can be analysed in a similar fashion to species b).[19] However due to overlapping of lines in the ^{31}P and ^{119}Sn spectra it is easier to obtain $^{2}J(^{31}P^{119}Sn)$ and $^{3}J(^{31}P^{119}Sn)$ from analysis of the ^{119}Sn spectra of species e) and f). Both species e) and f) are $AA'A''A'''MX$ spin systems. Their ^{119}Sn spectra consist of doublets of triplets of triplets. The triplets of triplets are identical for both species and yield values of $^{2}J(^{31}P^{119}Sn)$ and $^{3}J(^{31}P^{119}Sn)$ directly. The doublet splittings are given by $^{1}J(^{119}Sn^{195}Pt)$ and $^{2}J(^{119}Sn^{195}Pt)$ respectively for species e) and f). However it is not possible to tell from the ^{119}Sn spectrum which of these two platinum-to-tin coupling values is the one-bond and which the two-bond coupling constant. Species g) is an $A'A''A'''MM'X$ spin system and the only lines detected, which are due to this species, are in the ^{119}Sn spectrum shown in FIG. 4.IX . The couplings $^{2}J(^{119}Sn^{31}P)$ and $^{3}J(^{119}Sn^{31}P)$ give rise to the same triplet of triplets structure as for species e) and f), for the tin to phosphorus coupling interaction. However this multiplet structure is further split by the tin-to-platinum interaction. This feature can be described with reference to the $AA'X$ spin system[22] described in chapter 3 (except here $A,A' = ^{195}Pt$, $X = ^{119}Sn$). The two multiplets seen in the ^{119}Sn spectrum can be treated as the M lines in the X spectrum of an $AA'X$ spin system. The separation between these two multiplets is therefore given by $|^{1}J(^{119}Sn^{195}Pt) + {}^{2}J(^{119}Sn^{195}Pt)|$, and since, from the ^{119}Sn spectrum, this equals $|^{1}J(^{119}Sn^{195}Pt)| + |^{2}J(^{119}Sn^{195}Pt)|$, the signs of $^{1}J(^{119}Sn^{195}Pt)$ and $^{2}J(^{119}Sn^{195}Pt)$ are the same.

In order to establish the absolute signs of the above two coupling constants, it is necessary to relate the sign of either of them to the sign of one of the couplings [$^{1}J(^{31}P^{195}Pt)$, $^{2}J(^{31}P^{195}Pt)$, or $^{1}J(^{195}Pt^{195}Pt)$] whose signs have already been determined. This requires

FIG.4.IX ^{119}Sn Spectrum Of $[Pt_2(\mu\text{-dppm})_2(SnCl_3)_2]$ At Room Temperature

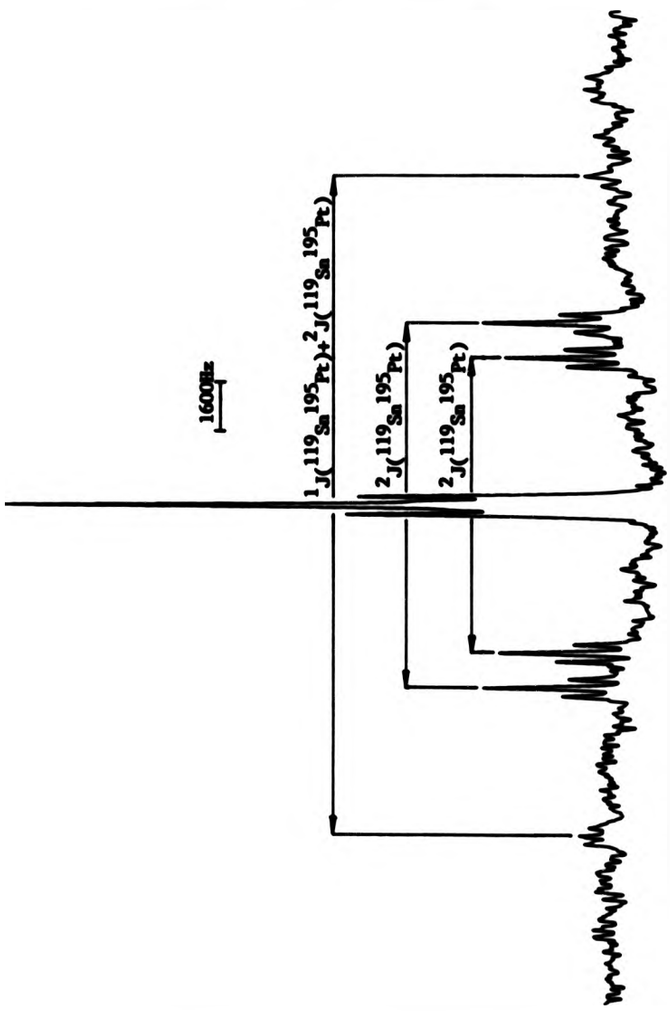

a multiple resonance experiment and two such possible experiments will also give the absolute assignment of $^{1}J(^{119}Sn^{195}Pt)$ and $^{2}J(^{119}Sn^{195}Pt)$. Both involve species e) and f), and use $^{1}J(^{31}P^{195}Pt)$ and $^{2}J(^{31}P^{195}Pt)$ as the couplings of known sign. The ^{31}P spectra of species e) and f) are different, although they derive from similar spin systems and involve the same coupling constants. In the two possible multiple resonance experiments the aim is, for each isotopomer, to associate together its ^{31}P and ^{119}Sn spectra, thereby assigning $^{1}J(^{119}Sn^{195}Pt)$ and $^{2}J(^{119}Sn^{195}Pt)$. The ^{31}P spectra of species e) and f) can be considered as ^{119}Sn satellites of species b). In species b) the two phosphorus nuclei labelled (A) and (A') are magnetically inequivalent to those labelled (A'') and (A'''). All ^{31}P transitions are centered around $\nu^{31}P$, but transitions due to ^{31}P (A) and (A') appear as the outer multiplets separated by $^{1}J(^{31}P^{195}Pt)$ (see FIG.4.V) and those due to ^{31}P (A'') and (A') appear as the inner multiplets separated by $^{2}J(^{31}P^{195}Pt)$ (see FIG. 4.V).

Each set of ^{31}P transitions has associated tin satellites due to both species e) and f). In species e), $^{2}J(^{31}P^{119}Sn)$ is associated with the outer ($^{1}J(^{31}P^{195}Pt)$) multiplets and $^{3}J(^{31}P^{119}Sn)$ with the inner ($^{2}J(^{31}P^{119}Sn)$) multiplets, and in species f), $^{2}J(^{31}P^{119}Sn)$ is associated with the inner ($^{2}J(^{31}P^{195}Pt)$) multiplets and $^{3}J(^{31}P^{119}Sn)$ with the outer ($^{1}J(^{31}P^{195}Pt)$) multiplets.

One of the possible multiple resonance experiments on this system is to irradiate at the frequencies of the triplets of triplets in the ^{119}Sn spectrum due to species e) and f) in turn and observe the effects on the ^{31}P spectrum. There are however certain drawbacks to this experiment. Also present in the observed ^{31}P spectrum are lines due to species similar to species e) and f) except they contain ^{117}Sn (spin ½, natural abundance 7.6%) instead of ^{119}Sn. These lines overlap with

those due to species e) and f) and can obscure any perturbation effects caused by the ^{119}Sn irradiation. The other possibility is to irradiate ^{31}P lines due to species e) and f) and observe the ^{119}Sn spectrum. In the event of interference problems caused by the proximity of the ^{31}P and ^{119}Sn frequencies, ^{117}Sn can be observed instead since its frequency is further away from the ^{31}P frequency (Any result obtained for ^{117}Sn is analogous to the ^{119}Sn result). There are four possible sets of $^{119/117}Sn$ satellites in the ^{31}P spectrum which can be irradiated and these, shown in FIG. 4.X can be described in terms of the nuclei involved and the coupling constants which determine the frequency to be irradiated.

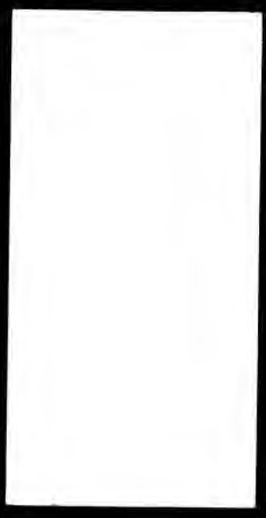

FIG. 4.X Arrangements of coupled nuclei which give rise to lines due to ^{119}Sn and ^{195}Pt coupling in the ^{31}P spectrum

1) ^{31}P | ^{119}Sn—^{195}Pt——

$\nu^{31}P \pm \frac{1}{2}({}^{1}J(^{31}P^{195}Pt) + {}^{2}J(^{31}P^{119}Sn))$

2) ^{31}P | ^{119}Sn—^{195}Pt——

$\nu^{31}P \pm \frac{1}{2}({}^{2}J(^{31}P^{195}Pt) + {}^{3}J(^{31}P^{119}Sn))$

3) ^{31}P | ^{119}Sn—— ——^{195}Pt

$\nu^{31}P \pm \frac{1}{2}({}^{1}J(^{31}P^{195}Pt) + {}^{3}J(^{31}P^{119}Sn))$

4) ^{31}P | ^{119}Sn— —^{195}Pt

$\nu^{31}P \pm \frac{1}{2}({}^{2}J(^{31}P^{195}Pt) + {}^{2}J(^{31}P^{119}Sn))$

FIG. 4.X 1) and 2) involve species e) and FIG. 4.X 3) and 4) involve species f). The two irradiation experiments described by FIG. 4.X 2) and 3) will cause the collapse (or perturbation) of the triplet splitting caused by $^{3}J(^{31}P^{119}Sn)$ in the affected tin multiplet. Since this splitting is relatively small compared to the splitting caused by $^{2}J(^{31}P^{119}Sn)$, better resolution is required in order to distinguish any effect on the tin spectrum, compared to the experiments described by FIG.4.X 1) and 4), which perturb the $^{2}J(^{31}P^{119}Sn)$ triplet splitting. Also in experiments 2) and 3) other $^{119/117}Sn$ satellites due to the same species are relatively close, being separated by $^{2}J(^{31}P^{119}Sn)$, which limits the ^{31}P irradiation power that can be used without affecting the other satellites. FIG. 4.XI a) shows the result of irradiating at $\nu^{31}P - \frac{1}{2}(|^{2}J(^{31}P^{195}Pt)| + |^{2}J(^{31}P^{119}Sn)|)$, as described by FIG.4.X 4), and observing ^{119}Sn. The high frequency inner ^{119}Sn multiplet is perturbed, proving that the smaller tin-to-platinum coupling (9370 Hz) is $^{2}J(^{119}Sn^{195}Pt)$ and that $^{2}K(SnPt)$ is of opposite sign to $^{2}K(PPt)$ (i.e.

FIG.4.XI Assignment And Sign determination Of $^{1}J(^{119}Sn^{195}Pt)$ And $^{2}J(^{119}Sn^{195}Pt)$

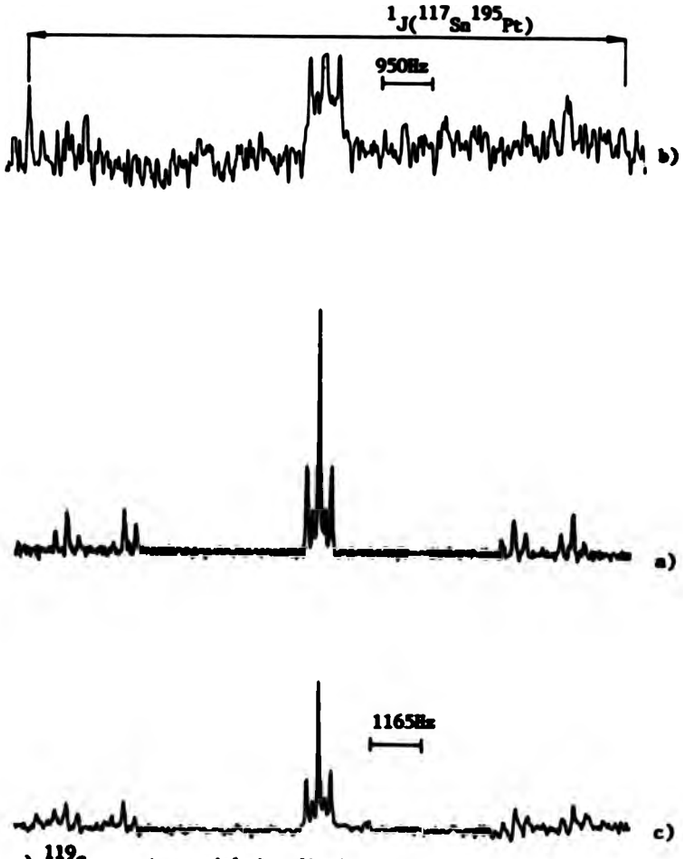

a) ^{119}Sn spectrum with irradiation at $\nu^{31}P-\frac{1}{2}(|^{2}J(^{31}P^{195}Pt)| + |^{2}J(^{31}P^{119}Sn)|)$

b) ^{117}Sn spectrum with irradiation at $\nu^{31}P-\frac{1}{2}(|^{1}J(^{31}P^{195}Pt)| + |^{2}J(^{31}P^{117}Sn)|)$

c) ^{119}Sn spectrum without irradiation

$^{2}K(SnPt)$ is (+ve); [$^{2}J(^{119}Sn^{195}Pt)$ is (-ve) since $\gamma(^{119}Sn)$ is (-ve)]). The perturbation effect observed is a change in intensities of the outer components of the triplet splitting caused by $^{2}J(^{31}P^{119}Sn)$. Higher ^{31}P irradiation power could not be used without causing undue electronic interference in the ^{119}Sn spectrum. Therefore for the experiment described by FIG.4.X 1) the ^{117}Sn spectrum was observed whilst irradiating at $\nu^{31}P - \frac{1}{2}(|^{1}J(^{31}P^{195}Pt)| + |^{2}J(^{31}P^{117}Sn)|)$. This allowed higher ^{31}P irradiation power to be used and caused the low frequency outer ^{117}Sn multiplet to be split to such an extent that it could not be detected against the base-line noise as shown in FIG. 4.XI b). Therefore $^{1}J(^{119}Sn^{195}Pt)$ is the large tin to platinum coupling (11892 Hz) and $^{1}K(SnPt)$ is the same sign as $^{1}K(PPt)$ (i.e. $^{1}K(SnPt)$ is (+ve); [$^{1}J(^{119}Sn^{195}Pt)$ is (-ve) since $\gamma(^{119}Sn)$ is (-ve)]). This agrees with the result determined from spectral analysis, that $^{1}J(^{119}Sn^{195}Pt)$ and $^{2}J(^{119}Sn^{195}Pt)$ have the same sign.

4.15 $[Te(SnPh_3)_2]^{23}$

$\delta(^{119}Sn)$	$\delta(^{125}Te)$	$^1J(^{119}Sn^{125}Te)$	$^2J(^{119}Sn^{117}Sn)$
-143	-132	3225	233

A)

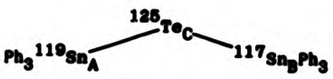

Comparison of signs $^1KSn_BTe_C$ / $^2KSn_BSn_A$ (See FIG. 4.XXIV)

Observed nucleus ^{119}Sn

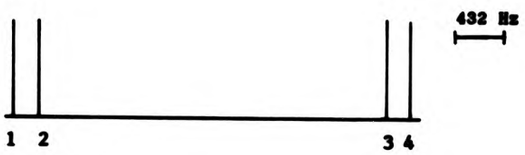

Irradiated nucleus ^{125}Te

Line at which irradiation is applied	Line(s) perturbed
^{125}Te 1	^{119}Sn 1, 3
^{125}Te 4	^{119}Sn 2, 4

$^{1}KSn_{B}Te_{C}^{24}$ and $^{2}KSn_{B}Sn_{A}$ have the same sign.

(-ve) (-ve)

For reasons of sensitivity an INEPT sequence was used to acquire the ^{119}Sn spectrum, polarisation transfer being effected from the ortho protons of the phenyl groups using timings corresponding to an assumed $^{3}J(^{119}Sn^{1}H)$ of 40 Hz.

4.16 Discussion

To facilitate the rationalization of the results obtained for the transition metal complexes in this chapter, they will be discussed further under four headings, $^{1}J(M'-M)$, $^{2}J(M'-X)$, $^{2}J(M'-M)$ and $^{3}J(M'-X)$ (where M' = ^{119}Sn, ^{207}Pb; M = ^{195}Pt, ^{103}Rh; X = ^{119}Sn, ^{31}P, ^{1}H). The coupling constants involved in $(Ph_3Sn)_2Te$ will then be discussed following this section.

4.17 $^{1}J(M'-M)$

The absolute signs of ten $^{1}J(^{119}Sn-^{195}Pt)$, one $^{1}J(^{119}Sn-^{103}Rh)$ and one $^{1}J(^{207}Pb-^{195}Pt)$ have been determined and are given in table (4.5). In all cases the reduced coupling constant is large and positive. Given that the coupling is dominated by the Fermi-contact contribution, this indicates large s-orbital contributions from both M' and M to the M'-M bonding molecular orbital[26].

At first glance the values of $^{1}K(Pb-Pt)$ and $^{1}K(Sn-Rh)$ appear anomalous, when compared to the range of values for $^{1}K(Sn-Pt)$ in table (4.5), $^{1}K(Pb-Pt)$ being appreciably larger and $^{1}K(Sn-Rh)$ appreciably smaller than $^{1}K(Sn-Pt)$. To a large extent this is due to differences in the valence s-electron densities at the nucleus $|\Psi_X(0)|^2$. However when adjusted by using calculated values of $|\Psi_X(0)|^2$ obtained from the literature[27], there is still a discrepancy between these three couplings, which is demonstrated in table (4.6).

Table 4.5 $^1J(M'-M)$ and $^1K(M'-M)$

	$^1J(^{195}Pt^{119}Sn)$(a)	$^1K(PtSn)$ (b)
trans-$[Pt(PEt_3)_2(SnCl_3)_2]$	-23529	+2447.016
trans-$[Pt(PPh_3)_2(SnCl_3)H]$	-11348	+1180.192
cis-$[PtCl(SnCl_3)(P(CH_2C_6H_4)_3)_2]$	-16321	+1697.384
cis-$[Pt(PPh_3)_2(SnPh_2Cl)Ph]$	-14070	+1463.28
$[Pt(SnCl_3)_4(PEt_3)]^{2-}$ Sn_{ax}	-6470	+672.88
Sn_{eq}	-19262	+2003.248
$[Pt(SnCl_3)_3(P(OEt_3))_2]^-$	-18962	+1974.128
cis-$[Pt(PPh_2)_2(Sn_2Ph_5)Ph]$	-11934	+1241.136
$[Pt(SnPh_3)_2dppm]$	-9649	+1003.496
$[Pt_2dppm_2(SnCl_3)_2]$	-11892	+1236.768
cis-$[Pt(PPh_3)_2(PbPh_3)Ph]$	+16374(c)	+3389.19(d)
$[Rh(SnCl_3)_2(COD)(P(CH_3OC_6H_4)_3)]^-$	+679(e)	+962.09(f)

(a) /Hz

(b) $/10^{20}Hz^{-2}N^{-3}$

(c) $^1J(^{195}Pt^{207}Pb)$

(d) $^1K(PtPb)$

(e) $^1J(^{103}Rh^{119}Sn)$

(f) $^1K(RhSn)$

Table 4.8 Comparison of Coupling Constants Involving Different Nuclei

Compound	N	N'	$^1J(N-N')$ (a)	$^1K(N-N')$ (b)	X	$\frac{^1K(N-N')}{\lvert\Psi_X(0)\rvert^2}$ [27] (c)
cis-[Pt(PPh_3)$_2$Ph($PbPh_3$)]	Pt	Pb	18374	3309	Pb	122
cis-[Pt(PPh_3)$_2$Ph($SnPh_3$)]	Pt	Sn	-12686	1319	Sn	75
[Rh($SnCl_3$)$_2$(COD)($P(p\text{-}C\overset{\ddagger}{H}_3C_6H_4)_3$)]$^-$	Rh	Sn	679	482	Rh	75
[Pt($SnCl_3$)$_3$($P(OEt)_3$)$_2$]	Pt	Sn	-18962	1974	Pt	158

(a) /Hz

(b) $/10^{20}N_A{}^2\gamma_N{}^2\gamma_{N'}{}^2$

(c) $10^{-10}N_A{}^2$

This may be due to the large polarisability of the atom in the case of lead and to a lesser extent for tin as well. Also it has been shown from calculations of coupling constants using relativistically parameterized extended Huckel (REX) wave functions[28], that in the case of heavy nuclei, the use of nonrelativistic atomic valence s electron densities is not always reliable.

Out of the N'-N couplings being considered, $^1J(^{119}Sn\text{-}^{195}Pt)$ has had the largest number of values measured [2-8,13,18]. These cover a wide range (5,780-30,5376 Hz) giving a change in the size of the coupling constant of approximately a factor of five. This plethora of values allows various trends to be established in the way $^1J(^{119}Sn\text{-}^{195}Pt)$ varies.

As expected the size of the coupling constant increases upon substitution of more electronegative groups on tin[5] as shown in table (4.7). This is due to a change in the hybridisation of the tin. In accordance with Bent's rule[29] the hybrid orbitals used to bond to the electronegative substituents will contain more tin p-character and therefore the hybrid orbital used to bond to the more electropositive

transition metal will contain less p- and more s-character. This is supported by crystallographic data. It has been observed as a general feature of tin-transition metal complexes that the bond angle

Table 4.7

Compound	$^2J(^{119}Sn-^{195}Pt)$ /Hz[5]		
	n		
	0	1	2
cis-[Pt(Ph)(PPh$_3$)$_2$(SnPh$_{3-n}$Cl$_n$)]	12,686	14,066	16,889
cis-[Pt(Ph)(PPh$_3$)$_2$(SnPh$_{3-n}$Br$_n$)]	12,686	13,940	16,241
cis-[Pt(Ph)(PPh$_3$)$_2$(SnPh$_{3-n}$I$_n$)]	12,686	13,735	-

N-Sn-R is greater than, and the bond angle R-Sn-R' is less than, the tetrahedral angle[30] (where N = transition metal; R', R = organic groups, halides). Also the R-Sn-R' angles become more acute, and the R-Sn-N angles correspondingly more obtuse, upon changing R from an organic group to a halide[30]. Only one X-ray structure is available for a complex containing a Pt-Pb bond[31]. This also exhibits the same geometrical arrangement of bonds around lead. Another feature of tin-transition metal complexes is that the tin-transition metal distances are generally found to be shorter than the sum of the covalent single bond radii of the two atoms[30]. Also the bond length decreases as organic substituents on the tin are replaced by halides[30]. This behaviour is consistent with an increase in the tin s-character of the tin-metal σ-bonding molecular orbital. A relationship between bond length and s-character of the bond is supported by the rough correlation between the magnitude of $^1J(^{119}Sn^{195}Pt)$ and Pt-Sn bond length reported by Pregosin et al[32]. Table (4.8) gives the pertinent bond lengths and angles for the Pt-Pb complex and a number of transition metal -SnCl$_3$ complexes for which the structures have been published since the last review [1,30] covering this topic.

Table 4.8

Bond Lengths And Angles For Selected Group IV-Transition Metal Complexes

Complex	BOND DISTANCES (b)		BOND ANGLES (b)	
	M-Sn(a)	Sn-Cl(a)	M-Sn-Cl	Cl-Sn-Cl
$[(\eta^6\text{-}C_6H_6)Ru(SnCl_3)(prophos)]$[33]	2.581	2.365		
$[Pd_2(\mu\text{-}dppm)_2(SnCl_3)Cl]$[34]	2.586	2.374 -2.418 (2.344)	114.3-124.0 (120.1)	91.4-101.1 (96.7)
$[Ru(SnCl_3)_5Cl]^{4-}$ [35]	2.553-2.599 (2.574)	2.361-2.404 (2.388)	116.6-130.7 (121.7)	92.1-97.7 (94.8)
trans-$[Pt(SnCl_3)_2(AsMe_3)_2]$ [36]	2.574-2.614 (2.602)	(2.380)		
cis-$[PtCl_2(SnCl_3)_2]^{2-}$ [37]	2.343-2.367 (2.355)	2.340-2.406 (2.369)	119.5-124.4 (121.3)	96.5 (96.5)
$[Pt(SnCl_3)(\mu\text{-}Cl)(PEt_3)]_2$[32]	2.487	(2.32)		
$[Pt(SnCl_3)_5]^{3-}$ [38]	2.551-2.572 (2.559)	2.34-2.374 (2.363)	117.7-122.3 (119.8)	96.3-100.1 (97.4)
$[IrH_2(SnCl_3)(PPh_3)_2]$[10]	2.623	2.382-2.397 (2.391)	118.1-124.5 (121.01)	94.9-96.7 (95.8)
$[Pt(Cl)(NH_2C_6H_4\text{-}p\text{-}Cl)(SnCl_3)(PEt_3)]$[4]	2.514			
trans-$[Pt(SnCl_3)_2(P(OPh)_3)_2]$[15]	2.580	2.332-2.347 (2.342)	118.1-121.8 (118.2)	97.8-102.6 (99.5)
cis-$[PtPh(PPh_3)_2(PbPh_3)]$[31]	2.686(c)	2.248-2.286 (2.270) (d)	112.1-178.8 (116.7) (e)	96.9-101.5 (98.4) (f)

a) Å. b) where more than one value is reported the range of values is given and the average value in parenthesis. c) Pt-Pb. d) Pb-C. e) M-Pb-C. f) C-Pb-C

The magnitude of $^{1}J(^{119}Sn\text{-}^{195}Pt)$ also depends upon the nature of the other ligands attached to platinum. The ligand *trans* to the Sn-Pt bond has the greatest effect on the coupling constant and a *trans*-influence series has been established where the magnitude of $^{1}J(^{119}Sn\text{-}^{195}Pt)$ increases, as the *trans* ligand changes, in the order Cl > $SnCl_3$ > As > P > H[7] The change in magnitude of the coupling constant in this instance can be due to changes in either $|\Psi_{Pt}S(0)|^2$ or Π_{PtSn}.

It is unlikely that changes in $|\Psi_{Pt}S(0)|^2$ are significant since, complexes containing two or more tin ligands with different ligands trans to them, can have widely varying values of $^{1}J(^{119}Sn\text{-}^{195}Pt)$ even though $|\Psi_{Pt}S(0)|^2$ must be the same for all platinum to tin coupling interactions. $[Pt(SnCl_3)_4(PEt_3)]^{2-}$ is an extreme example of this, with $^{1}J(^{119}Sn_{eq}\text{-}^{195}Pt)$ equal to 19262 Hz. and $^{1}J(^{119}Sn_{ax}\text{-}^{195}Pt)$ equal to 6470 Hz ($^{1}J(^{119}Sn\text{-}^{195}Pt)$ changes by a factor of three). Also if variations in $^{1}J(^{119}Sn\text{-}^{195}Pt)$ were due mainly to changes in $|\Psi_{Pt}S(0)|^2$, all ligands on the platinum would be expected to exert an equal influence on the coupling constant.

However since the *trans*-ligand has by far the greatest effect on the magnitude of $^{1}J(^{119}Sn\text{-}^{195}Pt)$, changes in the hybridization of platinum are the predominant effect, causing the observed variations in $^{1}J(^{119}Sn\text{-}^{195}Pt)$. The *trans*-influence[39] has been explained using two models of bonding; one which evokes Π-bonding between the transition metal and the ligands, and another where only changes in the σ-bonding upon rehybridization are used to account for the observed trends.

In the first model the normal σ-interaction between the transition metal and tin is reinforced by $\underline{d}\Pi\text{-}\underline{d}\Pi$ bonding involving overlap of filled platinum *d*-orbitals with vacant *d*-orbitals on the tin. The main evidence for this model is the short Pt-Sn distances[1], which are assumed to be a consequence of theΠ-bonding. Increases in $^{1}J(^{195}Pt\text{-}^{119}Sn)$

caused by increases in the electronegativity of the substituents on tin reflects a lowering in the energy of the tin *d*-orbitals, resulting in a better overlap with the platinum *d*-orbitals. This leads to a shorter Pt-Sn bond and better *s*-orbital overlap. Similarly, *trans* ligands which are weaker Π-acceptors reduce the competition with tin for $d\Pi$-electrons allowing a greater $d\Pi$-$d\Pi$ overlap, and this again leads to shorter Pt-Sn bonds and larger values of $^{1}J(^{119}Sn\text{-}^{195}Pt)$.

In the model which only considers σ-interactions the hybrid transition-metal orbital used in the Pt-Sn bonding molecular orbital, is a mixture of *s*-, *p*-, and *d*- character. The hybrid orbital used in bonding to the *trans*-ligand will also be a mixture of the same *s*-, *p*-, and *d*-orbitals (Different *p*- and possibly different *d*-orbitals will be used for bonding to *cis*-ligands). The specific mix of orbital-character required by the orbital overlap with the *trans*-ligand will determine what remaining orbital-character is available to form the hybrid orbital used in bonding to tin. For instance a highly electronegative chlorine ligand will form a more ionic bond with platinum, which requires a transition-metal hybrid orbital of a high *p*- and *d*-character which concentrates electron density near the chlorine. This allows more *s*-orbital and less *p*- and *d*-orbital character to be used in forming the hybrid orbital used in bonding to tin. Therefore the Pt-Sn bond will be shorter and $^{1}J(^{119}Sn\text{-}^{195}Pt)$ larger. Alternatively, if the *trans* ligand is a hydride, it will require a hybrid orbital which has more transition-metal *s*-character. Therefore the hybrid orbital used in bonding with tin will contain less *s*-character, and proportionally more *p*- and *d*-character, resulting in a longer Sn-Pt bond and a smaller value of $^{1}J(^{119}Sn\text{-}^{195}Pt)$.

This second bonding model would appear more likely in the light of the observed geometry of the bonds around tin and the effect on the bond

angles, of changes in the electronegativity of the substituents upon tin[30]. Also, hydride ligands are considered to be poor π - acceptors, yet result in relatively small $^{1}J(^{119}Sn-^{195}Pt)$ values, as trans ligands[3]. Therefore $d\pi - d\pi$ bonding does not predominate[40] and σ-bonding interactions generally determine the properties of tin-platinum bonds[1] (and probably of Group IV - transition metal bonds in general).

$^{1}J(^{119}Sn-^{195}Pt)$ is generally somewhat smaller in five, than in four co-ordinate complexes[7,37]. This is probably due to the different hybridization states of platinum. In the trigonal-bipyramidal five co-ordinate species, platinum must divide its available s-character among five hybrid orbitals forming σ-bonds to the ligands. Whereas in the square planar four co-ordinate species only four hybrid orbitals are required, among which the available platinum s-character is divided, allowing a greater concentration of s-character in any single hybrid orbital.

4.18 $^{2}J(M'-X)$

The absolute signs of seventeen $^{2}J(^{119}Sn-^{31}P)$ (thirteen via square-planar platinum, three via trigonal-bipyramidal platinum and one via trigonal-bipyramidal rhodium), four $^{2}J(^{119}Sn-^{117}Sn)$ (one via square-planar platinum and two $^{2}J(^{207}Pb-^{31}P)$ (via square-planar platinum) coupling have been determined and are given in table (4.9). For the square-planar complexes, where the coupled nuclei are arranged trans to each other, the reduced coupling constants are positive, in all cases. When the coupled nuclei are arranged cis to each other the reduced coupling constants are negative in all cases. For the trigonal-bipyramidal complexes, all the axial-axial and equatorial-equatorial reduced coupling constants are positive, and all the axial-equatorial reduced coupling constants are negative.

Table 4.9 $^2J(M'-X)$ and $^2K(M'-X)$

Complex	X	trans-$^2J(^{119}SnX)$(a)	trans-$^2K(SnX)$(b)	cis-$^2J(^{119}SnX)$(a)	cis-$^2K(SnX)$(b)
trans-$[Pt(SnCl_3)_2(PEt_3)_2]$	^{117}Sn	+34674	+1965.2		
	^{31}P			+236	-13.0
trans-$[PtH(SnCl_3)(PPh_3)_2]$	^1H	-1748	+39.0		
	^{31}P			+215	-11.9
cis-$[PtCl(SnCl_3)(P(p\text{-}CH_3C_6H_5)_3)_2]$	^{31}P	-4271	+235.8		
	^{31}P			+219	-12.1
cis-$[PtCl(SnCl_3)(P(p\text{-}CH_3OC_6H_5)_3)_2]$	^{31}P	-4301	+237.4		
	^{31}P			+214	-11.8
cis-$[Pt(PPh_3)_2(SnPh_2Cl)Ph]$	^{31}P	-2392	+132.0		
	^{31}P			+149	-8.2
cis-$[Pt(PPh_3)_2(Sn_2Ph_5)Ph]$	^{31}P	-1965	+108.5		
	^{31}P			+146	-8.1
cis-$[Pt(SnPh_3)_2(dppe)]$	^{31}P	-1611	+88.9		
	^{31}P			+142	-7.8
$[Pt_2(\mu\text{-}dppm)_2(SnCl_3)]_2$	^{31}P			+287	-15.6
	^{31}P				
cis-$[Pt(PPh_3)_2(PbPh_3)Ph]$	^{31}P	+3461 (c)	+340.2 (d)		
	^{31}P			-258 (c)	-25.4 (d)
$[Pt(SnCl_3)_4(PEt_3)]^{2-}$	^{31}P	-2392 (e)	+132.0 (e)		
	^{31}P			+207 (f)	-11.4 (f)
	^{117}Sn	+15955 (g)	+913.5 (g)		
	^{117}Sn			-2295 (h)	-131.4 (h)
$[Pt(SnCl_3)_3(P(OEt)_3)_2]^-$	^{117}Sn	+16394 (g)	+938.6 (g)		
	^{31}P			+314 (f)	-17.3 (f)
$[Rh(SnCl_3)_2(COD)(P(p\text{-}CH_3OC_6H_4))]^-$	^{31}P			+366 (i)	-20.2 (i)

a) $/H_z$. b) $/10^{20}NA^{-2}\pi^{-3}$. c) $^2J(^{207}PbX)$. d) $^2K(PbX)$. e) $P_{ax}Sn_{ax}$. f) $P_{ax}Sn_{eq}$. g) $Sn_{eq}Sn_{eq}$. h) $Sn_{eq}Sn_{ax}$. i) $P_{eq}Sn_{ax}$

These results are in agreement with those predicted by Jameson's approach to geminal coupling interactions[41], based upon the signs of the one-bond couplings $^1K(M-Y)$ and $^1K(M-X)$, and the X-M-Y bond angle, which is discussed in chapter I (Y = Sn, Pb, M = Pt, Rh and X = N, P, Sn in this instance). As can be seen from the description of the multiple resonance experiments in this chapter, in all cases $^1K(M-Y)$ and $^1K(M-X)$ are found to be positive, therefore making both the terms Sx, and Sy, in equation (1.9), positive. The sign of the third term, P_{XMY} depends on a number of factors, including the X-M-Y bond angle. P_{XMY} is frequently negative when the bond angle is between 90° and 110° and positive when greater than 110°. The product of these three terms ($Sx.P_{XMY}Sy$) determines $^2K(X-Y)$ in equation (1.9).

The signs predicted for $^2K(X-Y)$ by this approach, based upon idealised geometrical arrangements for square-planar and trigonal-bipyramidal complexes, are in agreement with the experimentally determined signs for $^2K(X-Y)$.

As with $^1K(Pb-Pt)$ and $^1K(Sn-Pt)$ the differences in the values of $^2K(Pb-P)$ and $^2K(Sn-P)$, for the respective trans and cis couplings, are only partially explained by the valence s-electron density at the nucleus, $|\Psi_X(0)|^2$, being larger for lead than tin as shown in table (4.10). The large polarisability of the nucleus in tin and lead probably accounts for the discrepancy in this case as well. However the situation is further complicated by the presence of an intervening atom, which introduces another variable factor to the coupling mechanism. This is more evident when attempting to apply the same argument to the variations in magnitude of trans-$^2K(Sn-X)$, where X = N, P, Sn, shown in table 4.10. The difficulties in producing similar chemical environments for the intervening platinum atom in each case, results in variations in the platinum hybridization. This will affect the orbital overlap in the

Table 4.10 Comparison of Coupling Constants Involving Different Nuclei

	N'	X	$^2J(N'-X)$ (b)	$^2K(N'-X)$ (c)	Y	$\frac{^2K(N'-X)}{\|\Psi_Y(0)\|^2}$ Z? (d)
cis-[Pt(Ph)(PPh_3)$_2$($PbPh_3$)]	^{207}Pb	^{31}P	3461(e)	340.2	Pb	12.2
	^{207}Pb	^{31}P	-288(f)	-28.4	Pb	-0.9
cis-[Pt(Ph)(PPh_3)$_2$($SnPh_3$)]	^{119}Sn	^{31}P	-1934(e)	106.8	Sn	0.1
	^{119}Sn	^{31}P	161(f)	-8.9	Sn	-0.5
trans-[PtH($SnCl_3$)(PPh_3)$_2$]	^{119}Sn	^1H	1748(e)	30.0	H	16.1[a]
cis-[PtCl($SnCl_3$)($P(p\text{-}ClC_6H_4)_3$)$_2$]	^{119}Sn	^{31}P	4271(e)	235.7	P	32.5
trans-[Pt($SnCl_3$)$_2$(PEt_3)$_2$]	^{119}Sn	^{117}Sn	34674(e)	2173.1	Sn	123.2

a) $|\Psi_H(0)|^2$ taken from ref 43

b) /Hz

c) $/10^{20}N_A{}^2\gamma_n{}^2$

d) $10^{-10}N_A{}^2$

e) trans

f) cis

molecular orbitals, by which the Fermi-contact mechanism transmits the coupling interaction. This affects the mutual polarisability term, $\Pi_{M'X}$, and makes it extremely difficult to separate out the effect due to changes in $|\Psi X(0)|^2$.

Ignoring the signs and only considering the magnitudes of the different M'-X coupling constants measured, where the intervening atom is a transition metal, $^2J(^{119}Sn-^{117}Sn)$ has the largest range[2] going from 648-37,164 Hz $^2J(^{119}Sn-^{31}P)$, for which the greatest number of values are known[2], ranges from 21-4298 Hz; $^2J(^{207}Pb-^{31}P)$ from 188-4015 Hz[11,17] and $^2J(^{119}Sn-^{1}H)$ from 102-1831 Hz[3,43].

It would appear that there is no relationship between $^2J(M'-X)$ and $^1J(M'-M)$[2]. This is not unexpected since the molecular orbitals which contribute to each coupling constant will be different. Those which contribute to $^1J(M'-M)$ must include M as well as the M', s-orbital density, whereas for $^2J(M'-X)$ any type of M-orbital can participate in a contributing molecular orbital, since it is the M' and X s-orbital coefficients for that molecular orbital which are important.

When considering the effect upon $^2J(M'-X)$, of changes in the substituents on M', only $^2J(^{119}Sn-^{31}P)$[5] and $^2J(^{207}Pb-^{31}P)$[11] in square-planar platinum complexes have had an adequate range of values measured with a variety of different substituents on M'. The magnitude of the trans coupling increases with increasing electronegativity of the substituents as is normally expected, which is shown in table (4.11). However the cis couplings in the same complexes exhibit no apparent dependence upon the electronegativity of the substituents upon M'. There are insufficient data available to draw any definite conclusions about the effect of changing the electronegativity of the substituents upon X. However, the same trend as observed above would appear to hold for $^2J(^{119}Sn-^{31}P)$ based upon the effect of going from a phosphine to a

phosphite complex (the -OR group being more electronegative than the -R group). Trans-$^{2}J(^{119}Sn-^{31}P)$ is 4271 Hz[44] in cis-[PtCl($SnCl_3$)($P(p-C_6H_4CH_3)_3$)$_2$] and 6750 Hz[13] in cis-[PtCl($SnCl_3$)($P(OPh)_3$)$_2$], whereas cis-$^{2}J(^{119}Sn-^{31}P)$ is 219 Hz[44] in the $P(p-C_6H_4CH_3)_3$ complex and 195 Hz[13] in the $P(OPh)_3$ complex. Any relationship between $^{2}J(M'-X)$ and the electronegativity of the substituents of the coupled nuclei would appear to be dependent upon the geometry at the transition metal and may be connected to the observed geometrically related magnitude change and sign reversal for $^{2}J(M'-X)$.

As noted earlier the group IV ligands discussed in this section are iso-electronic and iso-structural with tertiary phosphines in analogous complexes. As when comparing $^{2}K(Sn-P)$ and $^{2}K(Sn-Sn)$, the difference in $|\Psi_{X}(0)|^{2}$ between phosphorus and tin does not completely explain the smaller magnitude of $^{2}K(PP)$ compared to $^{2}K(SnP)$ and $^{2}K(SnSn)$. This probably explained by differences in Π_{AB}[7]. The hybridization state of tin, being a more polarisable atom than phosphorus, is probably affected more by variations in the electronegativity of the groups attached to it. This will result in a greater s-orbital contribution to the tin hybrid orbital used in forming the bonding molecular orbital to the electropositive transition metal, as discussed under $^{1}J(M'-M)$. Therefore in Π_{AB} the coefficients for the ligand s-orbital for the contributing molecular orbitals will be greater for tin (and also lead) than for phosphorus. In analogous complexes, if similar molecular orbital diagrams can be applied in both cases, the excitations between appropriate molecular orbital energy levels will result in larger contributions (both positive and negative) to Π_{AB} for the tin complex.

Table 4.11 The Effect of Changes In The M' Substituents Upon $^2J(M'-^{31}P)$

Complex	R_3	M'	$^2J(M'-^{31}P)$/Hz	
			Trans	Cis
cis-[$(R_3Sn)PtPh(PPh_2)_2$] [5]	Cl_3	^{119}Sn	3881	240
	$PhCl_2$	^{119}Sn	2959	195
	$PhBr_2$	^{119}Sn	2954	184
	Ph_2Cl	^{119}Sn	2398	151
	Ph_2Br	^{119}Sn	2398	152
	Ph_2I	^{119}Sn	2380	153
	Ph_3	^{119}Sn	1934	161
cis-[$(R_3Pb)PtPh(PPh_3)_2$] [11]	Ph_2Br	^{207}Pb	4015	245
	Ph_2I	^{207}Pb	3970	240
	Ph_3	^{207}Pb	3460	260

providing the energy difference between energy levels does not vary greatly. This will result in coupling constants of greater magnitude, irrespective of sign, where tin (or lead) replaces phosphorus as one of the coupled nuclei.

The main evidence for the similarity between these group IV ligands and tertiary phosphines derives from the analogous behaviour of $^{2}J(^{31}P^{31}P)$ and $^{2}J(M'-X)$ as far as geometrical dependence and the effect of changing the transition metal is concerned[7]. In square-planar and octahedral complexes of 2nd and 3rd row transition metals, trans $^{2}J(^{31}P^{31}P)$ is positive and much greater in magnitude than cis $^{2}J(^{31}P^{31}P)$ which is generally negative[45]. The ratio of magnitudes, trans $^{2}J(^{31}P^{31}P)$:cis $^{2}J(^{31}P^{31}P)$ can vary from 5:1 up to 20:1.[46] For example, in $[PtCl_2(PMe_3)_2]$, $^{2}J(^{31}P^{31}P)$ is +510 Hz in the trans complex and -18.9 Hz in the cis complex.[47] Similar variations in magnitude and sign are observed for $^{2}J(^{119}Sn^{31}P)$, $^{2}J(^{207}Pb^{-31}P)$ and $^{2}J(^{119}Sn^{-117}Sn)$ (although no sign has been determined for cis-$^{2}J(^{119}Sn^{-117}Sn)$, in cis-$[PtCl_2(SnCl_3)_2]$ $^{2}J(^{119}Sn^{-117}Sn)$ is 2485 Hz[37] and agrees with the trend, if a negative sign is assumed) for square-planar complexes as can be seen in table (4.9). It may therefore be justifiable to use the Pople and Santry[48] style molecular orbital approach proposed by Verkade[46] to explain the signs of trans-and cis- $^{2}J(^{31}P^{31}P)$. This is the same basic approach which is described in more detail in Chapter III for octahedral complexes, where the signs of the various contributions to the mutual polarisability, Π_{AB}, from the different energy-level transitions depend on the symmetry of the molecular orbitals involved. This is applied here to the molecular orbital diagram for a square-planar complex shown in FIG. 4.XII. Only ligand-transition metal sigma bonding molecular orbital energy levels are shown. Table (4.12) gives the energy level

FIG. 4.XII

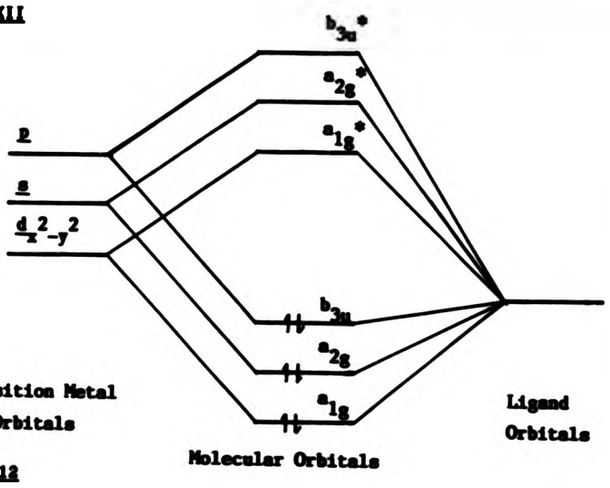

Table 4.12

The signs of Contributions to $^2J(N'-X)$ from Energy Level Transitions in FIG.4.XIII

Transition	Trans	Cis
$b_{3u} \rightarrow a_{1g}^*$	+ve	-
$b_{3u} \rightarrow a_{2g}^*$	+ve	-
$b_{3u} \rightarrow b_{3u}^*$	-ve	-
$a_{2g} \rightarrow a_{1g}^*$	-ve	+ve
$a_{2g} \rightarrow a_{2g}^*$	-ve	-ve
$a_{2g} \rightarrow b_{3u}^*$	+ve	-
$a_{1g} \rightarrow a_{1g}^*$	-ve	-ve
$a_{1g} \rightarrow a_{2g}^*$	-ve	+ve
$a_{1g} \rightarrow b_{3u}^*$	+ve	-

transitions and the signs of their contributions to Π_{AB} for a trans and a cis-$^2J(M'-X)$. The trans coupling is dominated by the HOMO-LUMO transition b_{3u} -> a_{1g}^*, which gives a positive contribution, resulting in a positive sign for all trans-$^2K(M'-X)$. The b_{3u} level consists of a (n-1) d- and the a_{1g}^* an np-transition metal orbital. Therefore it is expected that trans-$^2J(M'-X)$ should be inversely proportional to the (n-1)d to np energy separation, as is observed for trans-$^2J(^{31}P^{31}P)$ in $[MX_2P_2]$ complexes (M= Ni,Pt,Pd)[49]. This is observed for trans-$^2J(^{119}Sn-^{117}Sn)$ and trans-$^2J(^{119}Sn-^{31}P)$ in analogous Pt and Pd complexes measured under identical conditions. In trans-$[M(AsEt_3)_2(SnCl_3)_2]$ ^{7} $^2J(^{119}Sn-^{117}Sn)$ = 37164 Hz (M = Pd) and 35090 Hz (M = Pt). In cis - $[MCl(SnCl_3)(P(p\text{-}C_6H_5CH_3))_2]^-$ ^{7} $^2J(^{119}Sn-^{31}P)$ = 4848 Hz (M = Pd) and 9298 Hz (M = Pt).

This correlation is not observed for the cis coupling[7] since this is determined by different electronic excitations. Due to symmetry considerations, only four transitions contribute to cis-$^2J(M'-X)$ of which a_{2g}-> a_{1g}^* has the lowest energy difference. This transition gives a positive contribution to Π_{AB} for cis-$^2J(M'-X)$, which is counteracted by the next two transitions of lowest energy separation; a_{2g}-> a_{2g}^* and a_{1g} -> a_{1g}^*, which give negative contributions. The balance between these three contributions is dominated by the latter two transitions, resulting in a negative sign for $^2K(M'-X)$. This combination for cis-$^2J(M'-X)$ as opposed to only one dominant contribution for trans-$^2J(M'-X)$ may account for the lack of a relationship between, $^2J(M'-X)$ and the electronegativity of the M' and X substituents.

For trigonal-bipyramidal complexes there are several splitting parameters whose ratios vary with the ligand-metal distances. Hence no unique molecular-orbital diagram exists for this geometry[50] to which

this rationale for the observed signs of $^2K(M'-X)$ can be applied. It may be possible to draw an analogy between the axial-axial and axial-equatorial $^2J(M'-X)$ which can be considered in terms of geometrical arrangement of the coupled nuclei to relate to the trans and cis couplings respectively in square-planar and octahedral complexes. In both cases on the grounds of symmetry, molecular-orbitals based on transition metal p-orbitals only contribute to the trans coupling. This leads to different energy transitions being dominant in each case and resulting in a positive sign for trans-$^2K(M'-X)$ and a negative sign for cis-$^2K(M'-X)$.

This may be justifiable since axial-axial and axial-equatorial $^2J(M'-X)$ show the same experimental magnitudes and signs as trans- and cis-$^2J(M'-X)$ in square-planar complexes as can be seen in table (4.9). This leaves equatorial-equatorial $^2J(^{119}Sn-^{117}Sn)$ which is positive and large, though generally somewhat smaller than trans-$^2J(^{119}Sn-^{117}Sn)$ in a square-planar complex. If inclusion of transition-metal p-orbital based molecular orbitals is the key factor in determining that the dominant transition gives a positive reduced coupling constant, then for equatorial-equatorial coupled nuclei, one would expect the σ-overlap between ligand s-orbitals and a transition metal p-orbital to be less than for trans arranged nuclei, due to the decrease in the M'-M-X bond angle from 180^o to 120^o.

This would result in smaller ligand s-orbital coefficients for the contributing molecular orbitals giving a smaller value for π_{AB} and $^2J(^{119}Sn-^{117}Sn)$ though it would still have a positive sign. To support this we note that equatorial-equatorial $^2J(^{119}Sn-^{117}Sn)$ also shows the same dependence upon the (n-1)d to np energy difference as trans-$^2J(^{119}Sn-^{117}Sn)$ in a square planar complex. In $[M(SnCl_3)_3(PEt_3)_2]^-$ equatorial-equatorial $^2J(^{119}Sn-^{117}Sn)$ equals 20990 Hz (M = Pd) and 18182

Hz (M = Pt)[7].

The observed magnitude and sign of $^2J(^{119}Sn-^{31}P)$ (+ 366 Hz : i.e. $^2K(SnP)$ -ve) in the five co-ordinate rhodium complex $[Rh(COD)(SnCl_3)_2(P(p\text{-}CH_3OC_6H_4)_3)]^-$, although slightly larger, does not seem anomalous when compared to axial-equatorial $^2J(^{119}Sn-^{31}P)$ in trigonal-bipyramidal platinum complexes[2]. The ^{119}Sn spectrum shows that the two $-SnCl_3$ ligands are equivalent and can therefore both be assigned to either axial or equatorial positions if a rigid trigonal-bipyramidal structure is assumed. However the observed magnitude of $^2J(^{119}Sn-^{117}Sn)$ ($\pm$ 3218 Hz, no sign could be determined for this coupling constant) is somewhat small when compared to those same trigonal-bipyramidal platinum complexes[2]. One possibility is that the complex is fluxional[51] and some fast intramolecular process occurs, whereby the axial-equatorial positions exchange and average coupling constants are observed which are derived from a number of conformers. Such processes are known to occur in some five co-ordinated rhodium d 8 complexes[52]. Another possibility is that the chelating diolefin distorts the structure of the complex[6], which is somewhere between a trigonal-bipyramid and a square-pyramidal geometry. This is supported by the magnitude of $^2J(^{119}Sn-^{117}Sn)$ (13,513 Hz) in $(PPN)_2[Rh(SnCl_3)_3(CN(cy))_2]$[6], which does not contain a chelating diolefin, and is similar to the observed magnitude equatorial-equatorial $^2J(^{119}Sn-^{117}Sn)$ in trigonal-bipyramidal platinum complexes[2]. Also in the complex $[Pt(C_4Me_4)(SnCl_3)_3]^-$ [7], for which a pseudo "piano stool" (see FIG. 4.XIII) structure is proposed, $^2J(^{119}Sn-^{117}Sn)$ is 2392 Hz.

FIG. 4.XIII Structure of $[Pt(C_4Me_4)(SnCl_3)_3]^-$

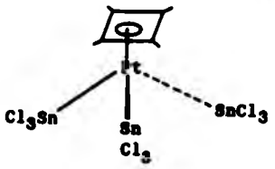

It is quite possible that fluxional behaviour and structural distortion both occur in this type of trichloro tin-rhodium complex, which makes the problem of separating out the different factors which determine the magnitudes and signs of the coupling constants overly complicated.

4.19 $^2J(M'-M)$

The magnitudes and absolute signs of two $^2J(^{119}Sn-^{195}Pt)$ (one via square-planar platinum and one via tetrahedral tin) have been determined and are given in table (4.13).

Table 4.13 Magnitude and signs of $^2J(M'-M)$ and $^2K(M'-M)$

Compound	$^2J(^{119}Sn-^{195}Pt)$(a)	$^2K(SnPt)$(b)
$[Pt_2(\mu\text{-dppm})_2(SnCl_3)_2]$	-9370	+974
cis-$[Pt(PPh_3)_2(Ph)(SnPh_2SnPh_3)]$	-1724	+179

a) /Hz

b) $/10^{20}N_A^{-2}\pi^{-3}$

In both cases the reduced coupling constant is positive. However there is a marked difference in the magnitudes and given the nature of the intervening atom in each case, the two coupling constants will be considered separately.

FIG. 4.IV shows the structure of $[Pt_2(\mu\text{-dppm})_2(SnCl_3)_2]$[18], where the intervening atom in $^2J(^{119}Sn\text{-}^{195}Pt)$ is a square-planar platinum.

FIG. 4.IV Structure of $[Pt(\mu\text{-dppm})(SnCl_3)]_2$

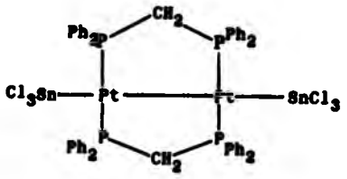

It may be appropriate to group $^2J(^{195}Pt\text{-}^{119}Sn)$ in this compound with $^2J(N'\text{-}X)$ via square-planar platinum which is discussed in the previous section. As with $^2K(N'\text{-}X)$ in these compounds, the sign of $^2K(SnPt)$ is in agreement with that predicted by Jameson's approach[41] to two bond couplings. The positive sign of $^2K(SnPt)$ is as expected, given the magnitude of the Pt-Pt-Sn bond angle consistent with the trans orientation of the coupled nuclei. (In $[Pd_2(\mu\text{-dppm})_2Cl(SnCl_3)]$ the Pd-Pd-Sn bond angle is 165.8°[34]). Also the two one-bond reduced coupling constants to the intervening atom, $^1K(SnPt)$ and $^1K(PtPt)$ are positive.

The noted similarity between $^2J(N'\text{-}X)$ and $^2J(^{31}P^{31}P)$ in analogous phosphine complexes[7] extends to this complex as well. In the isostructural complex $[Pt_2(\mu\text{-dppm})_2(P_eMe_2Ph)_2]$[53], $^2K(P_ePt)$ is also positive. However in $[Pt_2(\mu\text{-dppm})_2(SnCl_3)_2]$, the magnitude of $^2J(^{119}Sn\text{-}^{195}Pt)$ (-9370 Hz) is very similar to that of $^1J(^{119}Sn\text{-}^{195}Pt)$ (-11892 Hz), whereas in the PMe_2Ph complex[53] $^1J(^{31}P_e\text{-}^{196}Pt)$ (+1938 Hz) is over twice the size of $^2J(^{31}P_e\text{-}^{195}Pt)$ (+ 650 Hz).

The range of known complexes containing the Sn-Pt-Pt fragment is quite small. However the expected increase in the magnitude of $^2J(^{119}Sn\text{-}^{195}Pt)$ and $^1J(^{195}Pt\text{-}^{195}Pt$ is observed in $[Pt_2(\mu\text{-dppm})_2(SnCl_3)Cl]$[18] ($^2J(^{119}Sn^{195}Pt)$ = 9670 Hz, $^1J(^{195}Pt^{195}Pt)$ = 8200 Hz), where one terminal $-SnCl_3$ group trans to the Pt-Pt bond is replaced by a more

electronegative chloride.

FIG. 4.XV shows the structure of cis-$[Pt(PPh_3)_2(Ph)(Sn_2Ph_5)]$[16] where the intervening atom in $^2J(^{119}Sn\text{-}^{195}Pt)$ is tetrahedral tin.

FIG. 4.XV Structure of cis-$[Pt(PPh_3)_2Ph(Sn_2Ph_5)]$

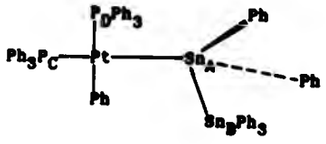

Comparison with the previous compound is inappropriate, not only since the intervening atom in $^2J(^{119}Sn\text{-}^{195}Pt)$ is different, but also the coupling pathway was essentially linear in $[Pt_2(\mu\text{-dppm})_2(SnCl_3)_2]$, whereas in the above complex it is bent, due to the tetrahedral geometry of the bonds around Sn_A.

Jameson's approach[41] to geminal coupling interactions cannot be tested in this molecule since $^1J(^{119}Sn_A\text{-}^{119}Sn_B)$ could not be observed, let alone have its sign determined. Also the exact geometry of the bonds around Sn_A, which will have a distorted tetrahedral geometry, is uncertain.

$^2J(^{119}Sn\text{-}^{195}Pt)$ has been reported for a series of compounds, $[Pt(PPh_3)_2(Ph_3SnC(S)R)]$[54] (R = SMe, SC_3H_5, SCH_2Ph, NMeH, pyrr) where the intervening atom is tetrahedral carbon, their structure being as shown in FIG. 4.XVI.

FIG. 4.XVI Structure of $[Pt(PPh_3)_2(Ph_3SnC(S)R)]$

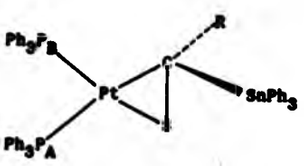

The reported $^2J(^{119}Sn-^{195}Pt)$ cover the range 237-250 Hz. This large difference in magnitude is due to a number of factors; the most significant of which is probably that two coupling pathways, $^2J(^{119}Sn^C{}^{195}Pt)$ and $^3J(^{119}Sn^C{}^S{}^{195}Pt)$ exist, which contribute to the observed coupling. These may have opposite signs, explaining the much smaller magnitude when compared to cis-$[Pt(PPh_3)_2Ph(Sn_2Ph_5)]$.

If the analogy to phosphine complexes is extended to this complex, Sn_A can be compared to the phosphorus atom co-ordinated to platinum and Sn_B to a carbon atom bonded to the phosphorus in the phosphine ligand. In the square planar complexes cis and trans-$[Pt(PR_3)Cl_2]$ (R = Et, n-Pr, n-Bu) $^2J(^{195}Pt^{13}C)$ varies from 20 to 41 Hz[55]. Although no sign is known for this coupling, a simple comparison of the magnitudes of the reduced coupling constants, allowing for the difference in $|\Psi_{ns}X(0)|^2$ between tin and carbon, shows that $^2K(PC)$ is still at least five times smaller than $^2K(SnPt)$. If phosphorus is replaced by arsenic in the same complex, $^2J(^{13}C^{195}Pt)$ increases to between 31.5 and 54.2 Hz[56], which indicates that this type of coupling may be extremely sensitive to the nature, as well as the geometry, of the bonds around the intervening atom.

4.20 $^3J(M'-X)$

The magnitude and absolute sign of one $^3J(^{119}Sn-^{31}P)$ (via tetrahedral tin and square planar platinum) was determined and is: cis-$[Pt(PPh_3)_2Ph(Sn_2Ph_5)]$, $^3J(^{119}Sn-^{31}P)$,- 161.1 Hz ($^3K(Sn-P)$ + $8.9 \times 10^{20} N_A^{-2} \pi^{-3}$).

The reduced coupling constant was found to be positive. The structure of the compound is given in FIG. 4.XV and the coupled nuclei are marked Sn_B and P_C. No coupling between Sn_B and P_D was detected.

However this coupling is expected to be very small, based upon the $^3J(^{207}Pb-^{31}P)$ couplings reported for the analogous lead compound cis-$[Pt(PPh_3)_2Ph(Pb_2Ph_5)]$[11] (This compound was not included in this

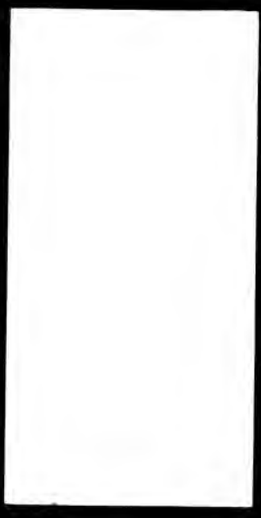

study since it is only stable in solution for an extremely short period). $^{3}J(^{207}Pb-^{31}P)$, where the phosphorus is trans to the $-Pb_2Ph_5$ ligand is 465 Hz, whereas where the phosphorus is cis to the $-Pb_2Ph_5$ ligand $^{3}J(^{207}Pb-^{31}P)$ is only 13 Hz. The magnitudes of ^{119}Sn couplings are generally smaller than of the analogous ^{207}Pb couplings due to the difference in $|\Psi_X(0)|^2$, and therefore any lines due to coupling between Sn_B and P_D will be hidden under the main peaks of the ^{31}P spectrum and will be unresolved in the ^{119}Sn spectrum. This large difference in the size of $^{3}J(^{207}Pb-^{31}P)$, when the geometry of the bonds at platinum, which form part of the coupling pathway, changes from trans to cis is reminiscent of the geometric dependence of $^{2}J(M'-X)$ in square-planar platinum complexes discussed earlier. The change in magnitude in this case is actually larger (The ratio $^{3}J(^{31}P^{207}Pb)P_{cis\ to\ Ph}$: $^{3}J(^{31}P^{207}Pb)$ $P_{trans\ to\ Ph}$ = 38:1. $^{2}J(^{31}P^{207}Pb)$ $P_{cis\ to\ Ph}$: $^{2}J(^{31}P^{207}Pb)$ $P_{trans\ to\ Ph}$ = 16:1) for the three bond coupling compared to the two bond. This undoubtably reflects the different platinum orbitals which participate in the contributing molecular orbitals for the cis- and trans- coupling pathways. Whereas for $^{2}J(^{31}P-^{119}Sn_A)$ the overlap of platinum orbitals with only Sn_A s-orbitals needed to be considered. for $^{3}J(^{31}P-^{119}Sn_B)$ the platinum orbitals which overlap with Sn_A s- and p-orbitals are also important, since both these types of orbital may contribute to relevant moleculr orbitals, depending upon their overlap with Sn_B s-orbital density.

A simpler approach is to extend Jameson's treatment [41] since the signs of $^{1}K(PPt)$ and $^{2}K(PtSn)$ have been determined as positive and the P_C-Pt-Sn_A bond angle can be assumed to be 180°. If the three bond coupling is considered as derived from three components; K_{PPt} whose sign is the same as $^{1}K(PPt)$ (+ve), K_{PtSn_B} whose sign is the same as $^{2}K(PtSn_B)$ (+ve), and F_{PPtSn_B} whose sign is determined by the bond geometry at

platinum (i.e.$\sim$180°) and is therefore positive. The sum of these three terms predicts a positive sign which agrees with the observed result.

$^3J(^{119}Sn-^{31}P)$ has been reported for the series of compounds $[Pt(PPh_3)_2(Ph_3SnC(S)R)]$[54] (R = SMe, SC_3H_5, SCH_2Ph, NMeH, pyrr), which have the structure shown in FIG. 4.XVI. The intervening atoms between the coupled nuclei are tetrahedral carbon and distorted square-planar platinum. Although the bonds around platinum are approximately planar, the inter bond angles at platinum are highly distorted. (The bond angles are C - Pt - S: 48.5°, S - Pt - P_A : 103.0°, C - Pt - P_B : 108.2°, P_A -Pt - P_B : 100.3°). Even though the geometry of platinum is distorted, $^3J(^{119}Sn-^{31}P)$ still exhibits a rough cis/trans dependence when it comes to the coupling pathway via platinum, which can be seen in table (4.14). However the relative magnitudes of the coupling constants are less than where platinum is truly square-planar.

Table 4.14

$^3J(^{119}Sn-^{31}P)$ in $[Pt(PPh_3)_2(Ph_3SnC(S)R)]$[54] (See FIG. 4.XVI)

R	$^3J(^{119}Sn-^{31}P_A)$/Hz	$^3J(^{119}Sn-^{31}P_B)$/Hz
SMe	21	13
SCh_3H_5	22	12
SCh_2Ph	21	13
NMeH	42	6
pyrr	44	5

It should be noted that for all the above couplings, two coupling pathways are available, $^3J(^{119}SnCPt^{31}P)$ and $^4J(^{119}SnCSPt^{31}P)$, although one would expect the three bond coupling to be the dominant contribution to the coupling constant. Another interesting feature is that the

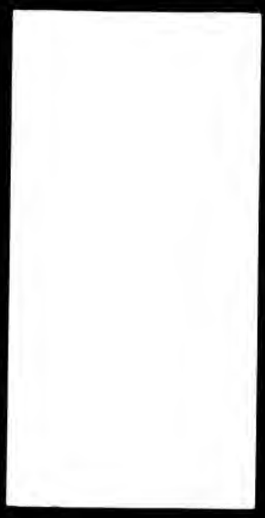

magnitudes of $^3J(^{119}Sn-^{31}P_A)$ and $^3J(^{119}Sn-^{31}P_B)$ are roughly doubled and halved respectively when the atom bonded to carbon in the substituent, labelled R in FIG. 4.XVI is changed from sulphur to nitrogen, indicating that the nature of the substituents upon the intervening atoms is also an important factor determining $^3J(^{119}Sn-^{31}P)$.

4.21 $(Ph_3Sn)_2Te$

The absolute sign of $^2K(SnSn)$ in $(Ph_3Sn)_2Te$ was found to be negative, given that the sign of $^1K(SnTe)$, previously determined by Kennedy & McFarlane[24], is also negative. Both coupling constants are given in table (4.15).

Table 4.15 Magnitudes and signs of coupling Constant in $(Ph_3Sn)_2Te$

$^1J(^{119}Sn-^{125}Te)$(a)	$^1K(SnTe)$(b)
-3225	-228.0
$^2J(^{119}Sn-^{117}Sn)$ (a)	$^2K(SnSn)$ (b)
-233	-14.6

a) /Hz

b) $/10^{20}NA^{-2}\pi^{-3}$

Unlike any of the other geminal coupling constants discussed in this thesis, the one-bond coupling $^1K(SnTe)$, which makes up the coupling pathway for $^2K(SnSn)$ is negative. Therefore when applying Jameson's approach[41] to this geminal coupling, the two terms which derive their signs from the one-bond couplings, K_{SnTe} and $K_{TeSn'}$ will have negative signs. Also given that the Sn-Te-Sn bond angle, from the crystal structure, is 103.68°[23], one would expect F_{SnTeSn} to be negative. The product of these three terms predicts a negative sign for $^2K(SnSn)$ which agrees with the result determined. This is possibly surprising since

exceptions to Jameson's approach are generally found when the intervening atom carries an electron lone-pair or pairs, as in this compound.

The magnitude of $^{2}J(^{119}Sn-^{117}Sn)$ is similar in all the tin chalcogenides $(Ph_3Sn)_2E$ (where E = S,Se,Te) as shown in table (4.16).

Table 4.16

$^{2}J(^{119}Sn-^{117}Sn)$ in $(Ph_3Sn)_2E$

E	$^{2}J(^{119}Sn^{117}Sn)$/Hz
O	412
S	210
Se	234
Te	233

However in $(Ph_3Sn)_2O$, $^{2}J(^{119}Sn^{117}Sn)$ is roughly twice the size compared to the other compounds. In the oxide the Sn-O-Sn fragment is essentially linear[2], whereas in the other compounds the Sn-E-Sn fragment is bent.[23] This can be explained by citing H-bonding for the oxide, but not the others where the bent structure of the molecules is due to the two electron lone-pairs on the chalcogen atom. In this situation it is probable that in each of the sulphur, selenium and tellurium compounds, $^{2}K(SnSn)$ has the same sign (i.e. negative). This agrees with the negative sign proposed for $^{2}K(SnSn)$ in the sulphide on the basis of the relationship between $^{2}K(SnSn)$ and $^{2}K(SnC)$[57].

FIG.4.XVIII Comparison Of The Signs Of $^{1}K(PtSn)$ And $^{1}K(PtH)$

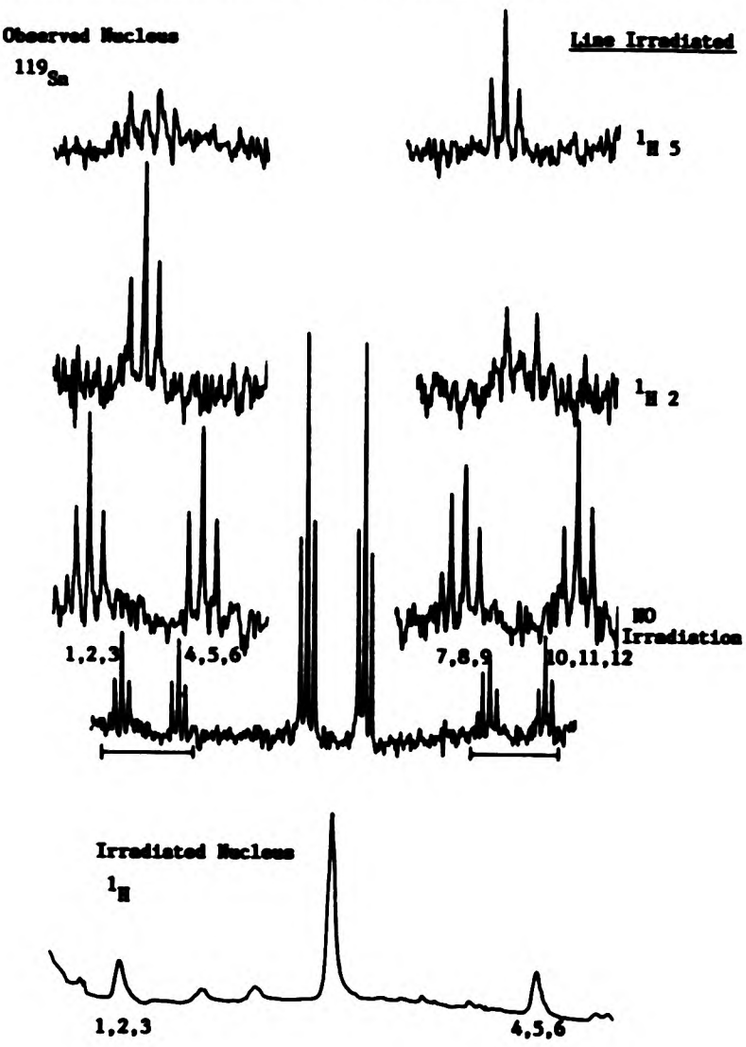

See Section 4.4 for details

FIG.4.XVIII Comparison Of The Signs Of $^{1}K(PtSn)$ And $^{1}K(PtH)$

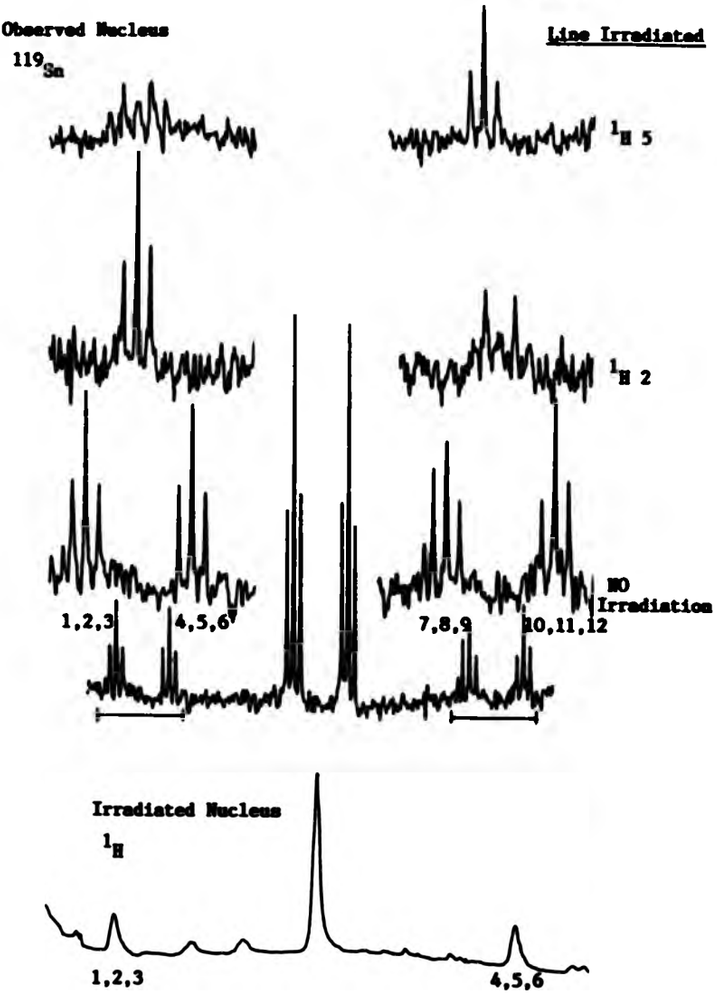

See Section 4.4 for details

FIG.4.XIX Comparison Of The Signs $^{1}K(PPt)$ And $^{1}K(HPt)$

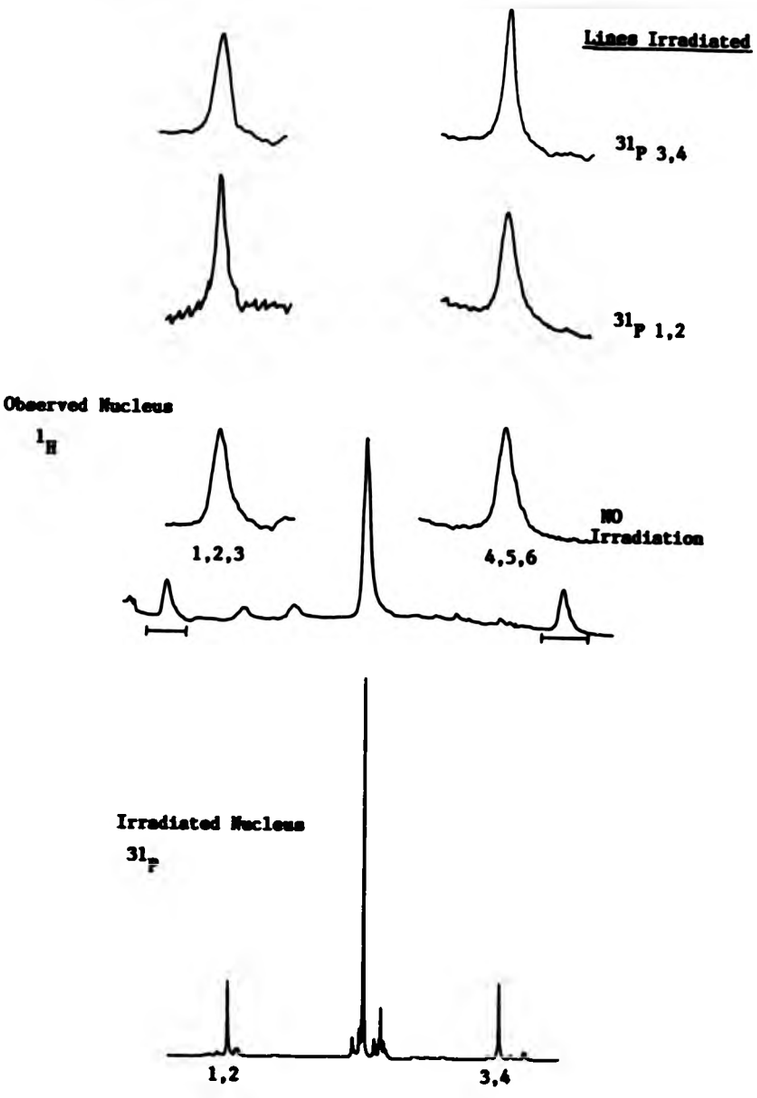

See Section 4.4 for details

FIG.4.XX Comparison Of The Signs Of $^2K_{(PSn)}$ And $^2K_{(SnSn)}$

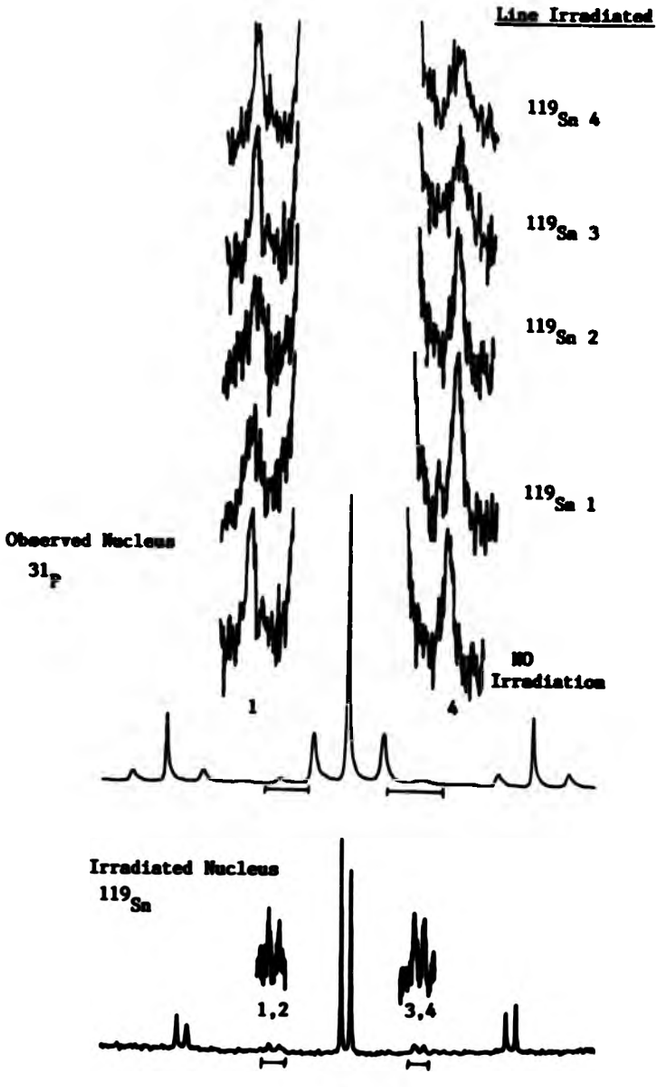

See Section 4.8 for details

FIG.4.XXI Comparison Of The Signs Of $^{2}K(PSn)$ And $^{1}K(RhSn)$

No spectrum is shown for the irradiated nucleus (^{103}Rh) in this particular example,since ^{103}Rh could not be directly obeserved and had to be determined by a $^{31}P-\{^{103}Rh\}$ multiple resonance experiment.For details of the ^{103}Rh positions irradiated refer to the section 4.10

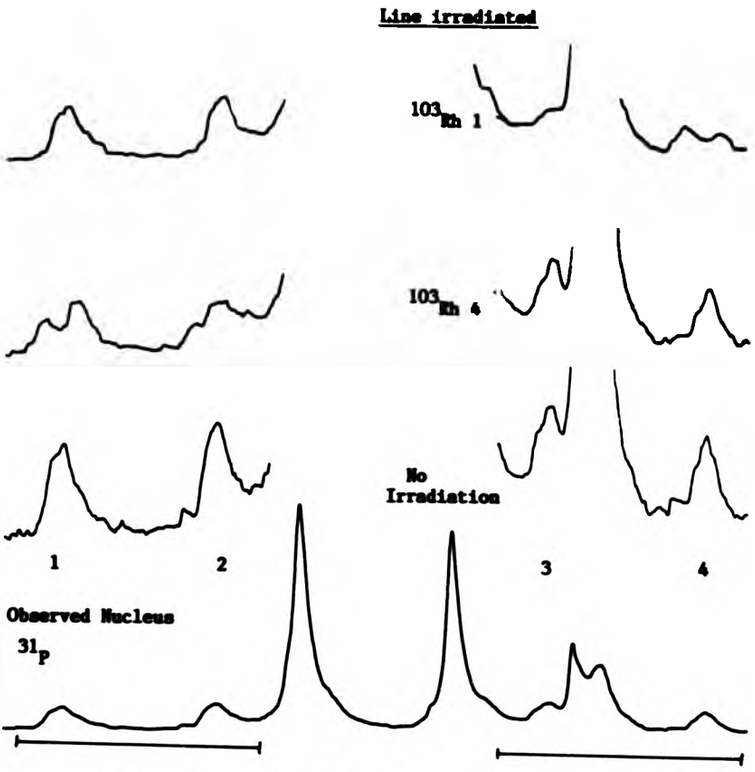

See Section 4.10 for details

FIG.4.XXII Comparison Of The Signs Of $^{1}K(PPt)$ And $^{2}K(PP)$

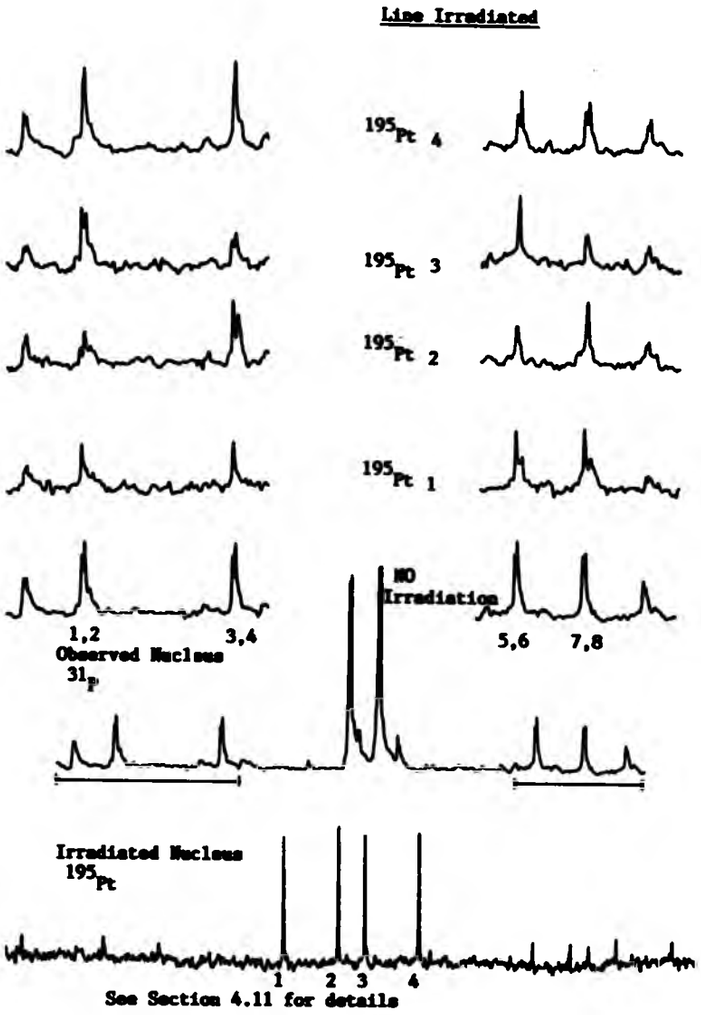

FIG.4.XXIII Comparison Of The Signs Of $^{1}K(PPt)$ And $^{2}K(PtSn)$

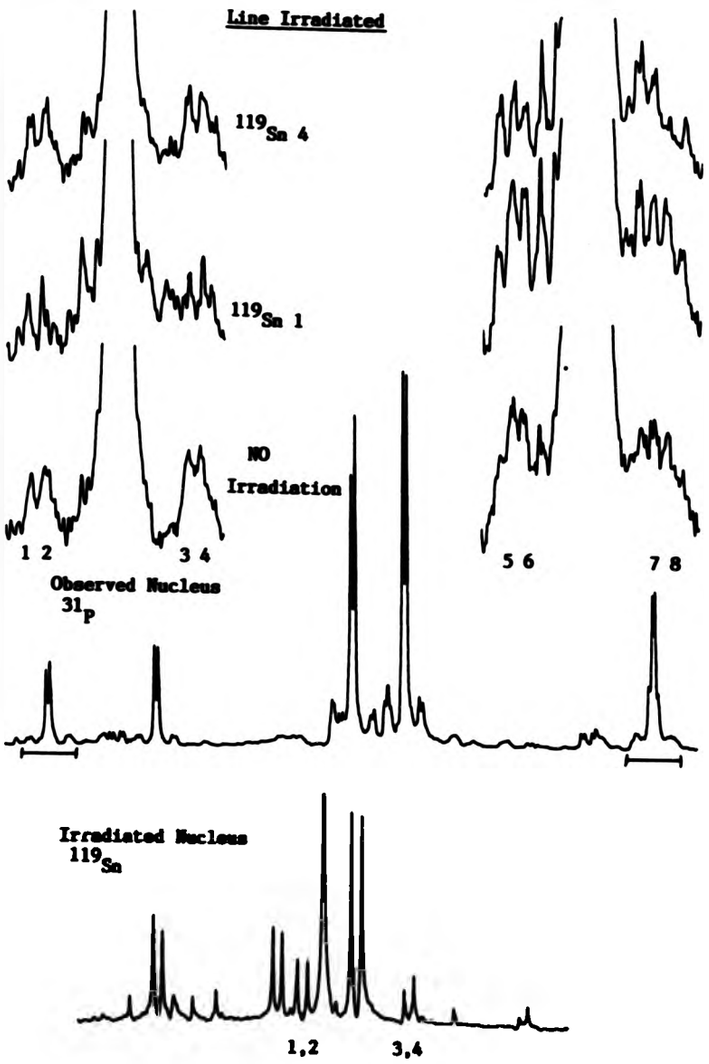

See Section 4.12

FIG.4.XXIV Comparison Of The Signs Of $^{1}K(SnTe)$ And $^{2}K(SnSn)$

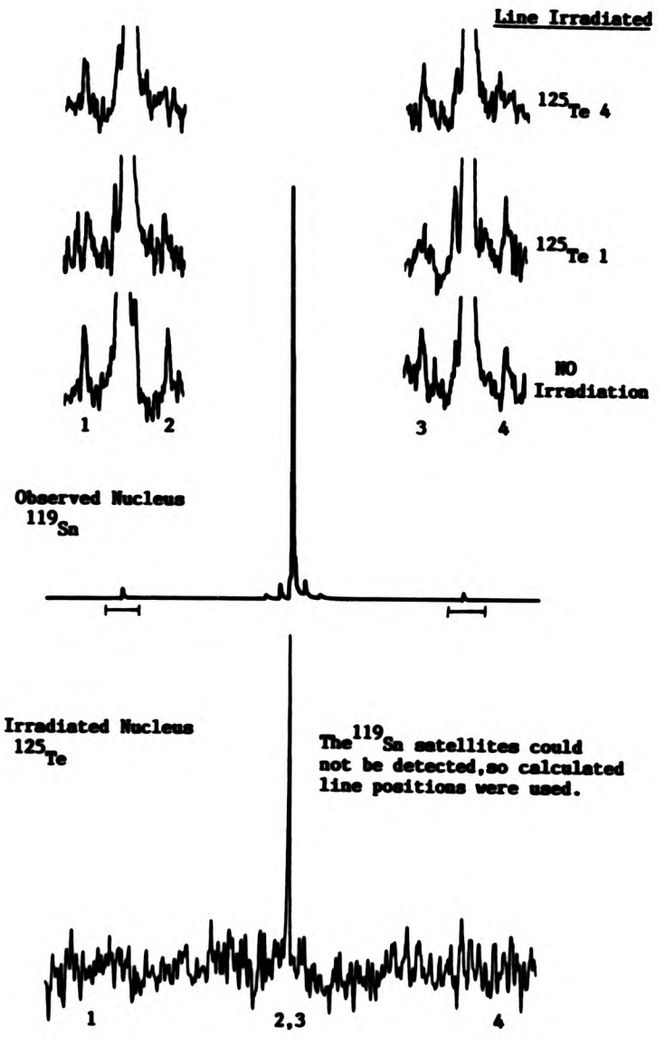

See Section 4.15 for details

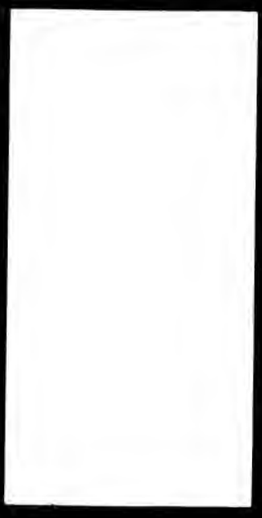

4.22 References

1) K.M. Mackay, B.K. Nicholson, "Comprehensive Organometallic Chemistry", Eds. G. Wilkinson, F.G.A. Stone, E.W. Abel, Pergamon, New York, (1982), vol. 6, 1043.

2) B. Wrackmeyer, Annu. Rep. N.M.R. Spectrosc., 16, (1985), 73.

3) K.H.A.O. Starzewski, P.S. Pregosin, Adv. Chem. Ser., 196, (1982), 23.

4) K.H.A.O. Starzewski, P.S.Pregosin, Angew. Chem. Int. Ed. Engl. (1980), 19, 316.

5) S. Carr, R. Colton, D. Dakternieks, J. Organomet. Chem., 249, (1983), 327.

6) M. Kretschmer, P.S. Pregosin, H. Ruegger, J. Organomet. Chem., 241, (1983), 87.

7) K.H.A.O. Starzewski, P.S. Pregosin, H. Ruegger, Helv. Chim. Acta., 65, (1982), 785.

8) A. Albinati, H. Moriyama, H. Ruegger, P.S. Pregosin, A. Togni, Inorg. Chem., (1985), 24, 4430.

9) H. Moriyama, T. Aoki, S. Shinoda, Y. Saita, J.C.S. Chem. Comm., 500, (1982).

10) M. Krethschmer, P.S. Pregosin, A. Albinati, A. Togni, J. Organomet. Chem., 281, (1985), 365.

11) S. Carr, R. Colton, D. Dakternieks, J. Organomet. Chem., 290, (1982), 143.

12) K.H.A.O. Starzewski, P.S. Pregosin, Inorg. Chim. Acta., 36, (1979), L445.

13) A. Albinati, P.S. Pregosin, H. Ruegger, Inorg. Chem. (1984), 23, 3223.

14) M. Kretschmer, P.S. Pregosin, M. Garralda, J. Organomet. Chem.,244, (1983), 175.

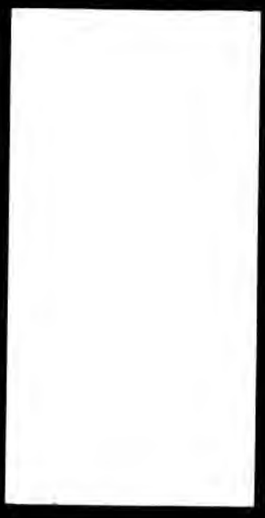

15) S. Carr, R. Colton, D. Dakternieks, J. Magn. Reson., 47, (1982), 156.

16) G. Butler, C. Eaborn, A. Pidcock, J. Organomet. Chem., 185, (1980), 367.

17) T.A.K. Al-Allaf, G. Butler, C. Eaborn, A. Pidcock, J. Organomet. Chem., 188, (1980), 335.

18) M.C. Grossel, R.P. Moulding, K.R. Seddon, Inorg. Chim. Acta. Lett., 64, (1982), L275.

19) M.P. Brown, R.J. Puddephatt, M. Rashidi, K.R. Seddon, J.C.S. Dalton, 951, (1977).

20) W. McFarlane, J.C.S.(A), 1922, (1967).

21) N.M. Boag, J. Browning, C. Crocker, P.L. Goggin, R.J. Goodfellow, M. Murray, J.L. Spencer, J. Chem. Research(M), 2955, (1978).

22) R.A. Hoffman, S. Forsen, B. Gestblom, "N.M.R. Basic Principles and Progress", Vol. 5, Eds. P. Diehl, E. Fluck, R. Kosfeld, Springer-Verlag, (1971).

23) F.W.B. Einstein, C.H.W. Jones, R.D. Sharma, Can. J. Chem., 61, 2611, (1983).

24) J.D. Kennedy, W. McFarlane, J. Organomet. Chem., 94, (1975), 7.

25) E.M. Hyde, J.D. Kennedy, B.L. Shaw, W. McFarlane, J.C.S. Dalton, 1571 (1972).

26) W. McFarlane, Quart. Rev. Chem. Soc. 23, 187, (1969).

27) J.R. Morton, K.F. Preston, J. Magn. Reson., 30, (1978), 577.

28) P. Pyykko, J. Organomet. Chem., 232,(1982), 21.

29) H.A. Bent, Chem. Rev., 61, 275, (1961).

30) J.A. Zubieta, J.J. Zuckerman, Prog. Inorg. Chem., 24, 251, (1978).

31) B. Crociani, M. Nicolini, D.A. Clemente, G. Bandoli, J. Organomet. Chem., 49, (1973), 249.

32) A. Albinati, R. Naegeli, K.H.A.O. Starzewski, P.S. Pregosin, H. Ruegger, Inorg. Chim. Acta., 76, (1983), L231.

33) G. Consiglio, F. Morandini, G. Ciani, A. Sironi, M. Kretschmer, J.A.C.S., 105, 1391, (1983).

34) M.M. Olmstead, L.S. Benner, H. Hope, A.L.Balch, Inorg. Chim. Acta., 32, (1979), 193.

35) L.J. Farrugia, B.R. James, C.L. Lassigme, E.J. Wells, Can. J. Chem., 60, 1304, (1982).

36) A. Albinati, R. Naegeli, H. Ruegger, P.S. Pregosin, Angew. Chem. Int. Ed. Engl., (1982), 21, 284.

37) N.W. Alcock, J.M. Nelson, J.C.S. Dalton., 2415, (1982).

38) J.M. Nelson, N.W. Alcock, Inorg. Chem., (1982), 21, 1196.

39) T.G. Appleton, H.C. Clark, L.E. Manzer, Coord. Chem. Rev., (1973), 335.

40) B.Y. Ho, J.J. Zuckerman, J.Organomet. Chem., 49, (1973), 1.

41) C.J. Jameson, J.A.C.S., 91, 6232, (1969).

42) G.W. Smith, Research Publication GMR-444 General Motor Corporation, Warren, Michigan, USA.

43) H.C. Clark, A.B. Goel, C. Billard, J. Organomet. Chem., 182, (1979), 431.

44) See Table (4.5).

45) Y. Koei, S. Shinoda, Y. Saito, Inorg. Nucl. Chem. Lett., 17, 147, (1981).

46) J.G. Verkade, Coord. Chem. Rev., (1972), 9.

47) R.J. Goodfellow, B.F. Taylor, J.C.S. Dalton, 1676, (1974).

48) J.A. Pople, D.P. Santry, Mol. Phys., (1964), 8, 1.

49) A. Bright, B.E. Mann, C. Masters, B.L. Shaw, R.M. Slade, R.E. Stainbank, J.C.S.(A), 1826 (1971).

50) F.A. Cotton, G. Wilkinson, "Advanced Inorganic Chemistry", 4th Ed., Wiley, (1980).

51) R. Uson, L.A. Oro, M.T. Pinillos, A. Arruebo, K.H.A.O. Starzewski, P.S. Pregosin, J.Organomet. Chem., 192, (1980), 227.

52) P. Meakin, J.P. Jesson, J.A.C.S., 95, 7272, (1973).

53) M.P. Brown, S.J. Franklin, R.J. Puddephatt, M.A. Thomson, K.R. Seddon, J.Organomet. Chem., 178, (1979), 281.

54) S.W. Carr, R. Colton, D. Dakternieks, B.F. Hoskins, R.J. Steen, Inorg. Chem., (1983), 22, 3700.

55) P.S. Pregosin., R. Kunz, Helv. Chim. Acta., 58, (1975), 1913.

56) G. Balimann, P.S. Pregosin, Helv. Chim. Acta., 58, (1975), 1913.

57) B. Wrackmeyer, J. Magn. Reson., 59, (1985), 141.

CHAPTER 5

EXPERIMENTAL

5.1 Preparations

General

All reactions were carried out under an atmosphere of dry nitrogen unless otherwise stated. Solvents were de-aerated prior to use having been dried by standard methods where required. Many reagents were synthesised by standard literature methods as indicated in the text.

5.2 Chapter 3

trans - $SnCl_4(PEt_3)_2$

PEt_3 (0.52 cm^3, 3.5 x 10^{-3} mol) was added dropwise to a solution of $SnCl_4$ (0.20 cm^3, 1.7 x 10^{-3} mol) in dry CH_2Cl_2 (5 cm^3) in an N.M.R. tube cooled in an ice bath. The reaction was then allowed to stand for 10 mins. at room temperature. Next the volume of solvent was reduced to 2 cm^3 by evaporation in a stream of dry nitrogen and the N.M.R. tube was sealed.

Analogous methods were used to prepare the other bis-phosphine tin (IV) tetrahalides. The quantities of reagents are specified below.

trans - $SnBr_4(PEt_3)_2$ PEt_3 (0.52 cm^3, 3.5 x 10^{-3} mol) added to $SnBr_4$ (0.75g, 1.7 x 10^{-3} mol).

trans - $SnCl_4(PBu^n_3)_2$ PBu^n_3 (0.87 cm^3, 3.5 x 10^{-3} mol) added to $SnCl_4$ (0.20 cm^3, 1.7 x 10^{-3} mol)

trans - $SnCl_4(PEt_3)_n(PBu^n_3)_{n-2}$ (n = 0-2)

A mixture of PEt_3 (0.26 cm^3, 1.7 x 10^{-3} mol) and PBu^n_3 (0.44 cm^3, 1.7 x 10^{-3} mol) in dry CH_2Cl_2 (2 cm^3) was added to the $SnCl_4$ (0.20 cm^3,

1.7×10^{-3} mol).

trans - $SnCl_nBr_{4-n}(PEt_3)_2$ (n = 0-4)

Two solutions were prepared with different ratios of the two halides.

a) Cl : Br = 1:1 PEt_3 (0.52, 3.5×10^{-3} mol) added to a mixture of $SnCl_4$ (0.10 cm^3, 0.9×10^{-3} mol) and $SnBr_4$ (0.37g, 0.9×10^{-3} mol).

b) Cl : Br = 1:2 PEt_3 (0.52 cm^3, 3.5×10^{-3} mol) added to a mixture of $SnCl_4$ (0.07 cm^3, 0.6×10^{-3} mol) and $SnBr_4$ (0.49g, 1.1×10^{-3} mol).

5.3 Chapter 4

cis - $[PtCl_2(PEt_3)_2]$

To a stirred suspension of $[PtCl_2(COD)]$ [1] (0.82g, 2.19×10^{-3} mol) (COD = 1,5-cyclooctadiene) in CH_2Cl_2 (5 cm^3) was added PEt_3 (0.37 cm^3, 4.4×10^{-3} mol) dropwise. The mixture was stirred for 1 hr. to give a clear colourless solution. Upon addition of MeOH, a white precipitate formed which was filtered off, washed with MeOH and dried under vacuum (yield 0.68g, 82%).

Analogous methods were used to prepared other compounds of the type $[PtCl_2(PR_3)_2]$ (PR_3 = phosphine, phosphite), i.e. direct reaction of $[PtCl_2(COD)]$ and two molar equivalents of the appropriate phosphine or phosphite.

trans - $[Pt(PEt_3)_2(SnCl_3)_2]$

A mixture of cis-$[PtCl_2(PEt_3)_2]$ (0.17g, 3.4×10^{-4} mol) and $SnCl_2$ (0.13g, 6.9×10^{-4} mol) in an N.M.R. tube was dissolved in dry CH_2Cl_2 (2.5 cm^3). The red-orange solution was allowed to stand for 3 days.

The NMR spectrum was then recorded, showing a mixture of trans-$[Pt(SnCl_3)_2(PEt_3)_2]$ and trans-$[PtCl(SnCl_3)(PEt_3)_2]$ to be present.

trans - $[PtHCl(PPh_3)_2]$

cis-$[PtCl_2(PPh_3)_2]$ (1.6g, 2.0 x 10^{-3} mol) was dissolved at room temperature in a solution of hydrazine hydrate (0.95g) and EtOH (40 cm^3). After the solution was refluxed for 5 mins, a mixture of glacial acetic acid (0.9g), distilled water (15 cm^3) and EtOH (8 cm^3) was added. Upon cooling colourless crystals precipitated, which were filtered off, washed with MeOH and dried under vacuum (yield 0.9g, 60%).

trans - $[PtH(SnCl_3)(PPh_3)_2]$

A mixture of trans-$[PtHCl(PPh_3)_2]$ (0.21g, 0.3 x 10^{-3} mol) and $SnCl_2$ (0.06g, 0.3 x 10^{-3} mol) in an N.M.R. tube was dissolved in dry CH_2Cl_2 (2.5 cm^3). The red-orange solution was allowed to stand for 1 hr. before the N.M.R. spectra were recorded.

cis - $[Pt(SnCl_3)Cl(P(p\text{-}X\text{-}C_6H_4)_3)_2]$ (X = CH_3-, CH_3O-)

A mixture of cis-$[PtCl_2(P(p\text{-}X\text{-}C_6H_4)_3)_2]$ (2.7 x 10^{-4} mol) and $SnCl_2$ (0.05g, 2.7 x 10^{-4} mol) was dissolved in CH_2Cl_2 (4 cm^3) and stirred for 20 mins. The solution was then filtered and the volume reduced to 2cm^3 in a stream of dry nitrogen. The solution was then transferred to an N.M.R. tube.

cis-$[Pt(PPh_3)_2(SnPh_2Cl)Ph]$

A mixture of $[Pt(PPh_3)_2(C_2H_4)]$ [2] (0.16g, 2.1 x 10^{-4} mol and $SnPh_3Cl$ (0.08g, 2.1 x 10^{-4} mol) in an N.M.R. tube was dissolved in CH_2Cl_2 (2 cm^3). The mixture was shaken, then allowed to stand for 30 mins. before running the N.M.R. spectra.

A similar method was used to prepare solutions of two other complexes, which are given below with the quantities of reagents used.

cis-[Pt(PPh_3)$_2$($SnPh_2SnPh_3$)Ph]

[Pt(PPh_3)$_2$(C_2H_4)] (0.28g, 3.8 x 10^{-4} mol) plus Sn_2Ph_6 (0.30g, 4.3 x 10^{-4} mol).

cis - [Pt(PPh_3)$_2$($PbPh_3$)Ph]

[Pt(PPh_3)$_2$(C_2H_4)] (0.24g, 3.2 x 10^{-4} mol) plus $PbPh_4$ (0.17g, 3.3 x 10^{-4} mol).

[$Pt_2(\mu\text{-}Cl)_2Cl_2(PEt_3)_2$]

$PtCl_2$ (0.07g, 2.6 x 10^{-4} mol) was added to [$PtCl_2(PEt_3)_2$] (0.13g, 2.6 x 10^{-4} mol) in xylene (5 cm^3). The mixture was refluxed for 3 days. Upon cooling the solution was filtered and the solvent removed under reduced pressure. The residue was washed with hexane, then dissolved in CH_2Cl_2, filtered through silica and the product precipitated by addition of hexane. This was filtered off, washed with hexane and dried under vacuum (yield 0.096g, 48%).

[Et_4N]$_2$[Pt($SnCl_3$)$_4$(PEt_3)]

To a solution of [$Pt_2(\mu\text{-}Cl)_2Cl_2(PEt_3)_2$] (0.14g, 1.8 x 10^{-4} mol) in CH_2Cl_2 (7 cm^3) was added Et_4NCl (0.14g, 8.5 x 10^{-4} mol), then $SnCl_2$ (0.29g, 1.5 x 10^{-5} mol). The solution was stirred for 2 hours, filtered and reduced to 3 cm^3 under reduced pressure. Ethyl acetate (20 cm^3) was carefully added to form a separate layer on top of the solution. This was then left for one week at room temperature, during which red needles precipitated. These were filtered off, washed with ethyl acetate and dried under vacuum. (yield 0.21g, 79%).

[Pt($SnCl_3$)$_3$($P(OEt)_3$)$_2$]

A mixture of cis-[$PtCl_2(P(OEt)_3)_2$] (0.19g, 3.2 x 10^{-4} mol) and $SnCl_2$ (0.18g, 9.5 x 10^{-4} mol) was dissolved in CH_2Cl_2 (2.5 cm^3) and

stirred for 30 mins. The solution was then transferred to an N.M.R. tube.

[Rh(COD)Cl(P(p-$CH_3OC_6H_4)_3$)]

A mixture of $[Rh(COD)Cl]_2$ [3] (0.23g, 4.6 x 10^{-4} mol) and P(p-CH_3O $C_6H_4)_3$ (0.32g, 9.1 x 10^{-4} mol) was dissolved in CH_2Cl_2 (5 cm^3). A yellow precipitate formed upon addition of EtOH. The product was filtered off, washed with EtOH and dried under vacuum. (yield 0.5g, 90%).

[Rh(COD)($SnCl_3$)$_2$(P(p-$CH_3OC_6H_4)_3$][PPh_3CH_2Ph]

A mixture of [Rh(COD)Cl(P(p-$CH_3OC_6H_4)_3$)] (0.5g, 8.3 x 10^{-4} mol) and $SnCl_2$ (0.3g, 1.6 x 10^{-3} mol) was dissolved in acetone (5 cm^3). ($PhCH_2$)Ph_3PCl (0.3g, 8.5 x 10^{-4} mol) was added to solution, which was reduced to 2 cm^3 in a stream of dry nitrogen and then transferred to an N.M.R. tube.

[Pt($SnPh_3$)$_2$($Ph_2PCH_2CH_2PPh_2$)]

[Pt(CO_3)($Ph_2PCH_2CH_2PPh_2$)] [4] (0.17g, 2.6 x 10^{-4} mol) was suspended in benzene (30 cm^3). A large excess of Ph_3SnH (1.6 cm^3) was added to the stirred suspension. The solution was then filtered and the product precipitated by addition of hexane, which was then filtered off washed with hexane and dried under vacuum. (yield 0.20g, 60%).

[Pt_2($Ph_2PCH_2PPh_2$)$_2$($SnCl_3$)$_2$]

A mixture of [Pt_2Cl_2($Ph_2PCH_2PPh_2$)$_2$] [5] (0.2g, 1.6 x 10^{-4} mol) and $SnCl_2$ (0.06g, 3.2 x 10^{-4} mol) in CH_2Cl_2 (2.5 ml) was stirred for 30 mins. The red-orange solution was then transferred to an N.M.R. tube.

[Te($SnPh_3$)$_2$]

A solution of NaHTe was prepared by adding $NaBH_4$ (2.2g, 5.8 x 10^{-2} mol) in H_2O (25 cm^3) to a stirred suspension of Te (3.7g, 2.9 x 10^{-2}

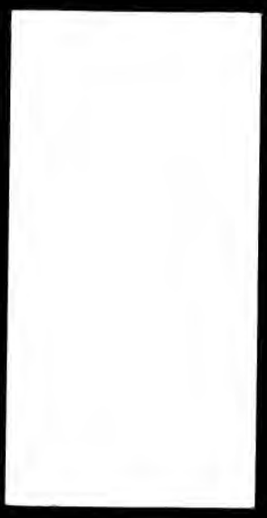

mol) in H_2O (25 cm^3) at room temperature. After 15 mins. the reaction was warmed on a steam bath for 10 mins, then allowed to cool to room temperature. A solution of Ph_3SnCl (11.2g, 2.9 x 10^{-2} mol) in benzene (40 cm^3) was then added dropwise with stirring. After the addition was complete the reaction was stired for a further 30 mins. The benzene layer was then separated off and evaporated to dryness under reduced pressure. The product was then recrystallized from diethyl ether/hexane to give a white, air sensitive product. (Yield 9g, 75%).

5.4 PERFORMANCE OF MULTIPLE RESONANCE EXPERIMENTS

The multiple resonance experiments were performed on specially modified JEOL FX90Q and FX60 N.M.R. spectrometers. A separate frequency generator (Genrad 1061) was used to provide the irradiating radio-frequency field, which was fed via a tunable amplifier and a trap tuned to the decoupler frequency (to prevent loss of proton decoupler power) to either, the doubly tuned decoupler coils (for high frequency irradiation) or to a specially wound separate coil in the probe (for low-frequency irradiation, JEOL FX60 only). This arrangement is summarised in FIG. 5.I.

FIG. 5.I

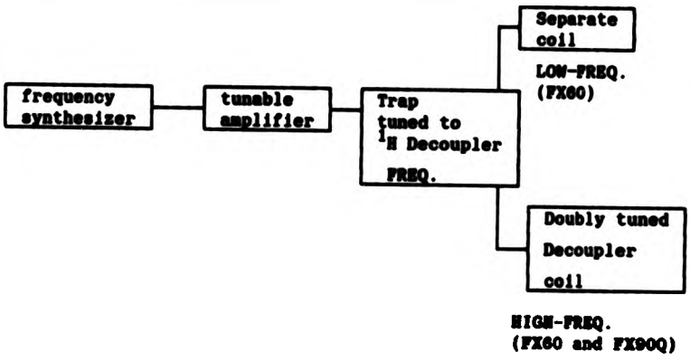

A separate coil could not be installed in the FX90Q probe due to limitations on space.

Using this set up the irradiating radio-frequency field is applied to the sample continuously throughout the pulse sequence. This is quite satisfactory in many multiple resonance experiments. However, under certain conditions the irradiating radio-frequency field will cause electronic interference which will reduce the quality of the spectrum obtained. This is especially important in heteronuclear double resonance experiments, where the sample is subjected to a number of

different radio-frequencies (stimulating field, proton decoupler, irradiating field, etc.). Also interference problems generally get worse the closer the irradiating frequence is to the resonant frequency of the observed nucleus. As mentioned in Chapter II interference can be minimised by reducing the power of the irradiating radio-frequency field, but this may not always be sufficient.

A better way of reducing interference is to "gate" the irradiating radio-frequency field, so that it is not applied continuously to the sample, but only during part(s) of the pulse sequence.

In order to synchronise the switching "on" and "off" of the power of the irradiating radio-frequency field the output of the separate frequency generator is modulated with an output from the spectrometer. In the case of the FX60 this output is taken from the oscillator circuit for the proton decoupler. This has been modified, so that the controls for gating the proton decoupler can be used to provide a gated output, whilst the proton decoupler bypasses the oscillator circuit and provides continuous proton decoupling to the sample. In the FX90Q an output is taken from a spare channel of the computer, which is controlled by the pulse program allowing the irradiation to be synchronised with the pulse sequence. The required modification to the set up given in FIG. 5.I is shown in FIG. 5.II.

FIG. 5.II

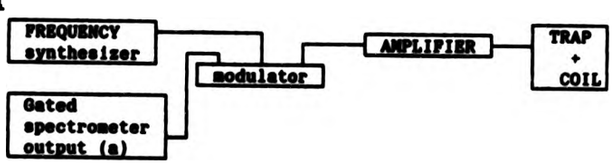

(a) FOR FX60 - oscillator circuit for proton decoupler

FOR FX90Q - pulse programmer

The ways in which the irradiating radio-frequency field is gated are different on the FX60 and the FX90Q spectrometer. This is due to the nature of the output from the spectrometer used in the gating. There are three ways of gating the irradiation on the FX60. The first two consist of either having the irradiation turned off during the accumulation of the F.I.D. and on for the rest of the pulse sequence, or vice versa. This is not of much value for reducing interference, but allows different perturbation effects to be separated as mentioned in Chapter II. The third way of gating the decoupler is to alternately switch the irradiating radio-frequency field and the receiver on and off during the accumulation of F.I.D. as shown in FIG 5.III.

FIG. 5.III

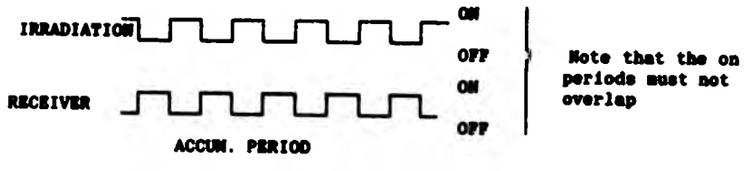

The relative time the receiver is switched on compared to the irradiation can be varied, which effectively changes the power of the irradiation applied. This method does have the disadvantage that the gating is not synchronised with the accumulation of data points in the F.I.D. This can result in some of the data points being missed when the receiver is switched off during accumulation of the F.I.D.

This problem is avoided with the FX90Q. Since the spectrometer output used to gate the irradiation is controlled by the pulse program, the pulse program can be specially written so that irradiating radio-frequency field is switched on during the accumulation of the F.I.D but only in the gaps between the acquisition of each data point.

FIG. 6.IV

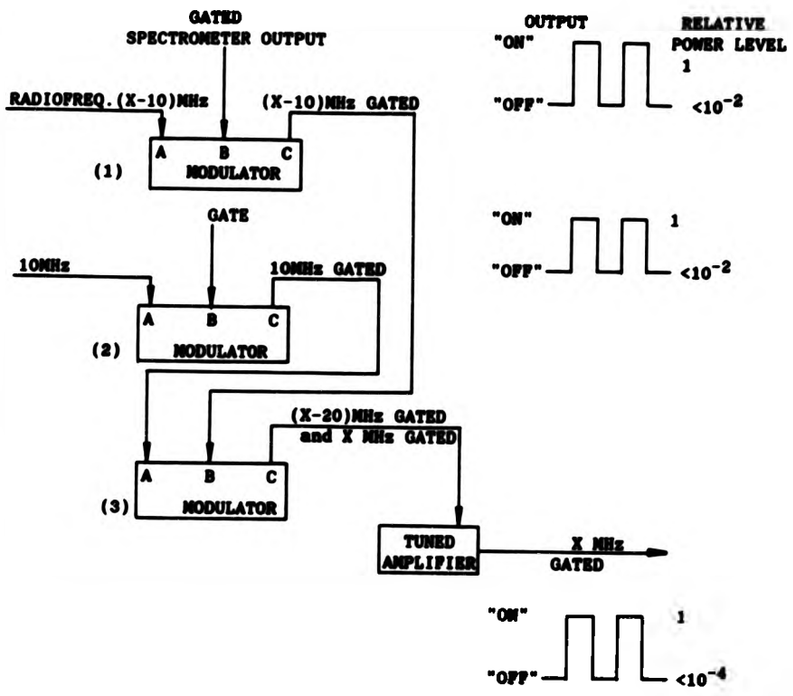

The required radio frequency for the experiment is X MHz. The output of Modulator (3) is the sum and difference of the two inputs; the (X-20) MHz output is removed by the tuned amplifier.

Consequently all data points are acquired and at no time are the receiver and irradiation on at the same time, minimising the interference caused by the irradiating radio-frequency field.

Ideally, the gated output would be reduced to zero during the off periods, but in practice with the arrangement shown in FIG. 5.II some irradiating radio-frequency power does reach the sample. (If the amplitude of the gated irradiation is taken as 1 during the on period, during the off period, it can be as high as 10^{-2}). For many experiments this is sufficient, but where greater power attenuation is necessary, the irradiating radio-frequency field can be doubly gated (this will increase the power attenuation to 1 ("on") : 10^{-4} ("off") using the set up shown in FIG. 5.IV.

Another problem that can occur especially with relative sign determining multiple resonance experiments, where perturbation effects on transitions due to coupling between at least three nuclei (some of which may have low natural abundancies) need to be observed, is sensitivity. Where the observed nucleus is coupled to protons variants of the INEPT pulse sequence can be used to alleviate sensitivity problems (FIG. 5.V).

FIG. 5.V

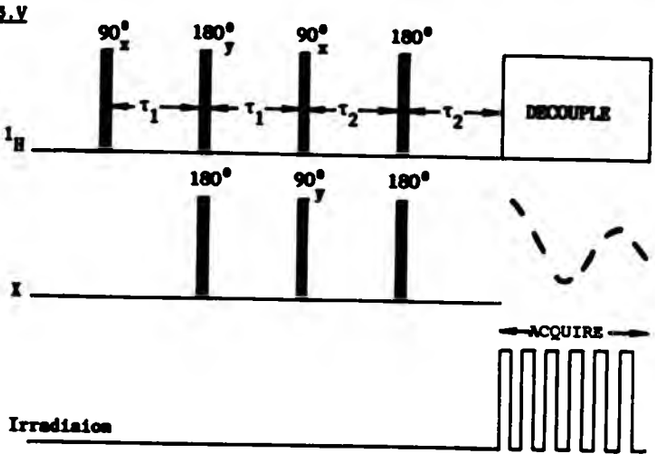

A standard INEPT pulse sequence is used with a modified acquisition phase. An extra output from the spectrometers computer, modulated with the output of a frequency generator, is used to control the gating of the irradiation. The irradiation is applied during the acquisition phase of the pulse sequence. However as described for the FX90Q the irradiation is not applied continuously, but is gated, so that whilst individual points of the F.I.D. are being acquired the irradiation is switched off.

5.5 References

1) J. X. McDermott, J. F. White, G. M. Whitesides, J.A.C.S., 98, 6521, (1976).

2) C.D. Cook, G.S. Jauhal, J.A.C.S., 90, 1464, (1968).

3) J. Chatt, L.M. Venanzi, J.C.S., 4735, (1957).

4) P. J. Hayward, D. M. Blake, G. Wilkinson, C. J. Nyman, J.A.C.S., 92, 5873,(1970).

5) M. P. Brown, R. J. Puddephatt, M. Rashidi, K. R. Seddon, J. C. S. Dalton, 951, (1977).

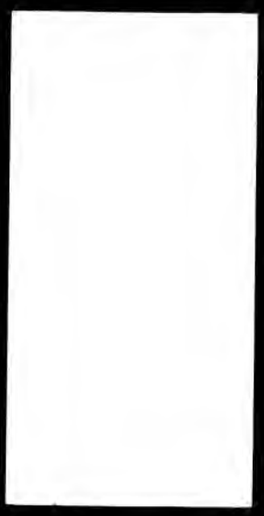

TITLE Nuclear Magnetic Resonance Studies of Organotin and Related Species

AUTHOR N. H. Rees

INSTITUTION and DATE City of London Polytechnic 1988